2016

Study of Resistivity and Shear Wave Velocity as a Predictive Tool of Sediment Type in Levee Foundation Soils, Louisiana Gulf Coast Levee System

Derek Stephen Goff
Louisiana State University and Agricultural and Mechanical College

STUDY OF RESISTIVITY AND SHEAR WAVE VELOCITY AS A PREDICTIVE TOOL OF SEDIMENT TYPE IN LEVEE FOUNDATION SOILS, LOUISIANA GULF COAST LEVEE SYSTEM

A Thesis

Submitted to the Graduate Faculty of the
Louisiana State University and
Agricultural and Mechanical College
in partial fulfillment of the
requirements for the degree of
Master of Science

in

The Department of Geology and Geophysics

by
Derek Stephen Goff
B.A. University of Colorado, 2012
May 2016

ACKNOWLEDGEMENTS

I would like to thank my major advisor, Dr. Juan Lorenzo and my thesis committee members, Dr. Karen Luttrell and Dr. Phil Bart for their input. A special thanks to Koichi Hayashi for assisting me with the collection of electrical resistivity data and producing the resistivity profiles. I would also like to thank the Coastal Protection and Restoration Authority and the Louisiana Sea Grant for funding this research through the Coastal Science Assistantship Program. I would also like to give special thanks to my fiancé, Alianna, for providing constant support.

TABLE OF CONTENTS

ABSTRACT

Geotechnical sediment type of levee foundation soils may be estimated by using cross-plots of shear-wave velocity and electrical resistivity for Louisiana levees. Best-fit polynomial models for estimating soil type in Japanese levees have been created using cross-plots of shear-wave velocity and electrical resistivity. A similar study or model for flood protection structures in the Mississippi River delta plain or other major river delta does not exist. We make the soil-type estimation model more relevant to the foundation soils in the Louisiana Coastal Zone by identifying silt in addition to sand and clay, and eliminating gravel as a dominant soil type. We analyzed seismic data, electrical resistivity data, and the soil type descriptions of 2 boring logs from the London Avenue Canal (LAC) levee in New Orleans, LA. Additional geophysical and Cone Penetration Test data from the "V-line" levee in Marrero is collected and analyzed. We combine the LAC and Marrero data to construct a cross-plot of shear-wave velocity, resistivity, and the dominant soil type with a total of 41 samples. In order to estimate soil types from different depths, we correct shear-wave velocity for overburden pressure. We find that larger grain sizes correlate to larger shear wave velocities and smaller resistivity values. Whereas clay can statistically be distinguished from soils dominated by either sand or silt sediment, sand and silt dominated soils plot with similar shear-wave velocity and electrical resistivity values. A correction for the effects of saturation on resistivity may improve our estimations to distinguish sand and silt dominated soils.

CHAPTER 1: INTRODUCTION

Joint consideration of geophysical and geotechnical data for levee systems in deltaic environments can improve the understanding of levee foundation soils (e.g., Lane et al. 2008, Karl et al., 2011). Levee foundations soils are the subsurface units on which levees are built, and are separate from the soils comprising an earthen levee body. The relationships between geophysical properties and soil types require further understanding before the stratigraphy in the foundation soils can be quantitatively assessed. Studies in other parts of the world (e.g., Inazaki et al., 2011) have shown that resistivity and shear wave velocity correlate to the soil type. However, a similar study of the deltaic sediments from the fluvial, marsh, and swamp depositional environments found throughout the Louisiana Coastal Zone (Figure 1) do not exist. The Louisiana Coastal Zone is a region encompassing all coastal wetlands, delta systems, and over 1,000 miles of levees (CPRA, 2012).

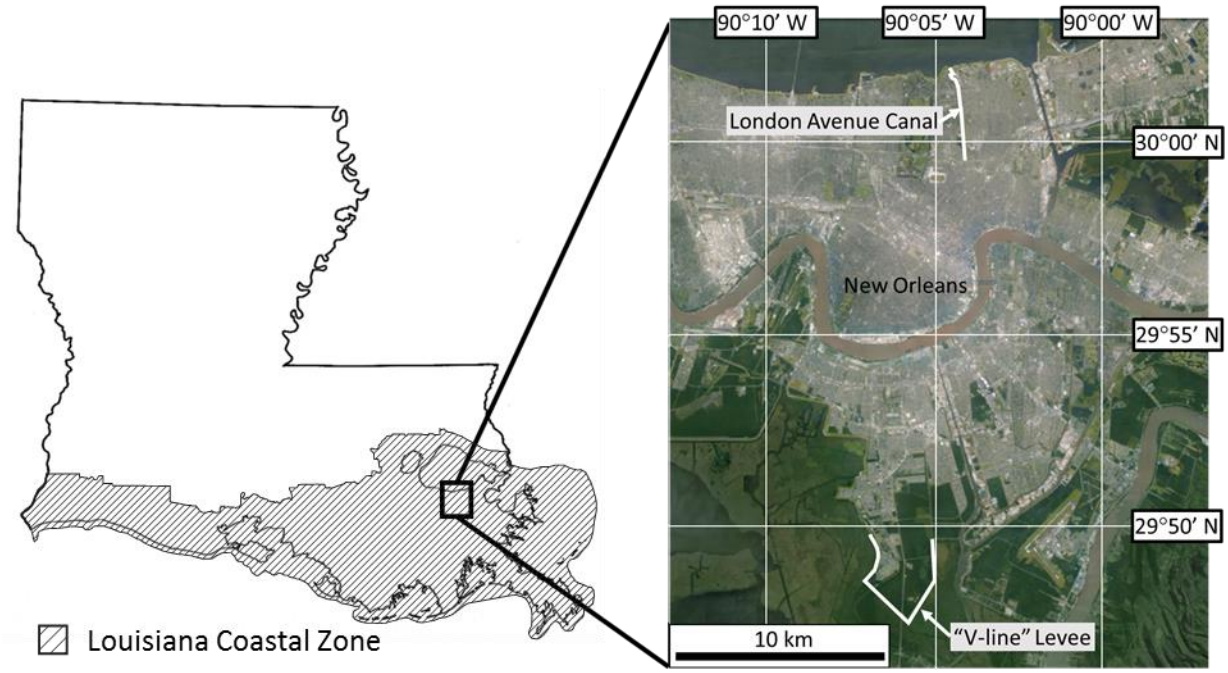

Figure 1: Left: an outline of the state of Louisiana (U.S. Geological Survey, 2006). Right: the greater New Orleans area, with the London Avenue Canal and Marrero "V-line" earthen levee highlighted (Google Earth, 2015).

Two study areas were chosen to test the relationship between resistivity, shear wave velocity, and common deltaic soil types. We collected seismic and resistivity data with streamer acquisition systems because the streamers systems cover more area per day. Seismic data emphasized the collection of surface wave signal, such that surface wave inversion techniques (Xia et al., 1999) could be used to create shear wave velocity profiles along the levee toes.

Analysis of the geophysical data from the study areas provide new correlations for the behavior of levee foundation soils in coastal regions. Cross-plot analysis of geophysical data and soil properties indicates grain size increases as shear wave velocity increases and resistivity decreases in levee foundation soils (Hayashi et al., 2013). Soil identification improves by compensating for overburden pressure and velocity increases with depth. The removal of

overburden effects allow for interpretation of silt dominated layers separate of sand and clay layers.

(1.1) THE RELATIONSHIP OF GEOPHYSICAL PROPERTIES AND SOIL TYPES

In laterally heterogeneous depositional environments, such as the Louisiana Coastal Zone (CPRA, 2012), unaccounted changes in foundation soil types can lead to the failure of flood protection structures (Dunbar et al., 1999, Dunbar and Britsch, 2008, IPET, 2007, Rogers et al., 2008). Geotechnical tests such as soil borings and Cone Penetrating Tests provide near-continuous sampling of soil properties, but lack lateral control between sites (Dunbar et al., 2007). An efficient, non-invasive method is necessary to supplement existing geotechnical work in coastal floodplains between borings and penetrations; this method must provide information to identify decameter size lateral changes in sediment type.

Geophysical properties of different soil types, primarily electrical resistivity and shear wave velocity, provide enough distinction to distinguish soil types (e.g., Inazaki, 2007). Changes in saturation, permeability, and porosity alter the resistance of the path an electrical current follows in the subsurface creating spatial fluctuations of electrical resistivity, such as when going from unconsolidated sands to clays (Archie, 1942). The range for possible electrical resistivity values partly depends on the ionic concentrations present in the saturating fluid (Samouëlian et al., 2005). The spatial fluctuations of shear wave velocity are caused by changes in the compaction of soil over time (Bitri et al., 2013, Whiteley and Caffi, 2014) or contrasts in sediment stiffness between different sediment types (Cercato et al., 2010). The ability to identify changes in the foundation soils can lead to improved site and drilling planning by locating differentially-compacted or stratigraphically heterogeneous zones in the foundation soils that require additional geotechnical testing (Dunbar et al., 2007).

An empirical approach to determining soil type from shear wave velocity and resistivity cross-plots has shown predictive capabilities in Japan (Hayashi et al., 2014b) and the state of Washington (Hayashi et al., 2014a). Hayashi et al. (2013) developed the second order multivariable polynomial equation from a least squares regression to fit the cross-plotted data from Japan. Their model took into account clays, sands, and gravels, but did not distinguish a silt-size clast between clays and sand. Adapting their empirical approach for use in the depositional environments of the Louisiana Coastal Zone requires introducing a separate silt classification in order to cope with the higher amounts of these fine-grained soils expected.

(1.2) STUDY AREAS

Two suitable locations to adapt the cross-plotting soil-identification method (Hayashi et al., 2013) for distinguishing silt from sand and clay were identified in the Greater New Orleans metropolitan region. The sites were chosen for the availability of pre-existing geotechnical boring logs or reports, reports of Cone Penetrating Tests, and well-documented heterogeneous soil types which contribute to hazards for the levees. The two sites are the I-wall levee toe bounding the London Avenue Canal, and an earthen levee, approximately 15 km south of New Orleans (Figure 1). Shear wave velocity models also exist for the earthen levee (Lorenzo et al., 2014), which are readily incorporated into the cross-plots. Relating the shear wave velocity and electrical resistivity measurements with the geotechnical tests allows for new relationships to be established that predict soil type and identify stratigraphic related hazards for levee systems built on the swamps and marshes sediments typical of the Louisiana Coastal Zone.

(1.2.1) London Avenue Canal

The investigation site of the London Avenue canal levee is located in London Park, approximately 500 meters south of the canal outlet into Lake Pontchartrain (Figure 2). The London Avenue Canal provides a well-understood geologic setting with a varied depositional history (Veatch and Martin 2011) that allows for geophysical observations to be made for several sand, silt, and clay soil types. Rapidly changing high water levels in the London Avenue Canal during Hurricane Katrina created two breaches of the levee. High water levels created large uplift pressures in the unconsolidated sands of the Pine Island Beach Trend (Figure 3), inducing piping and deflecting the I-wall levee until failure (IPET, 2007). Low shear strength of the organic clays in the swamp and marsh layers also contributed to failure by not providing adequate resistance to deflection (Dunbar and Britsch, 2008).

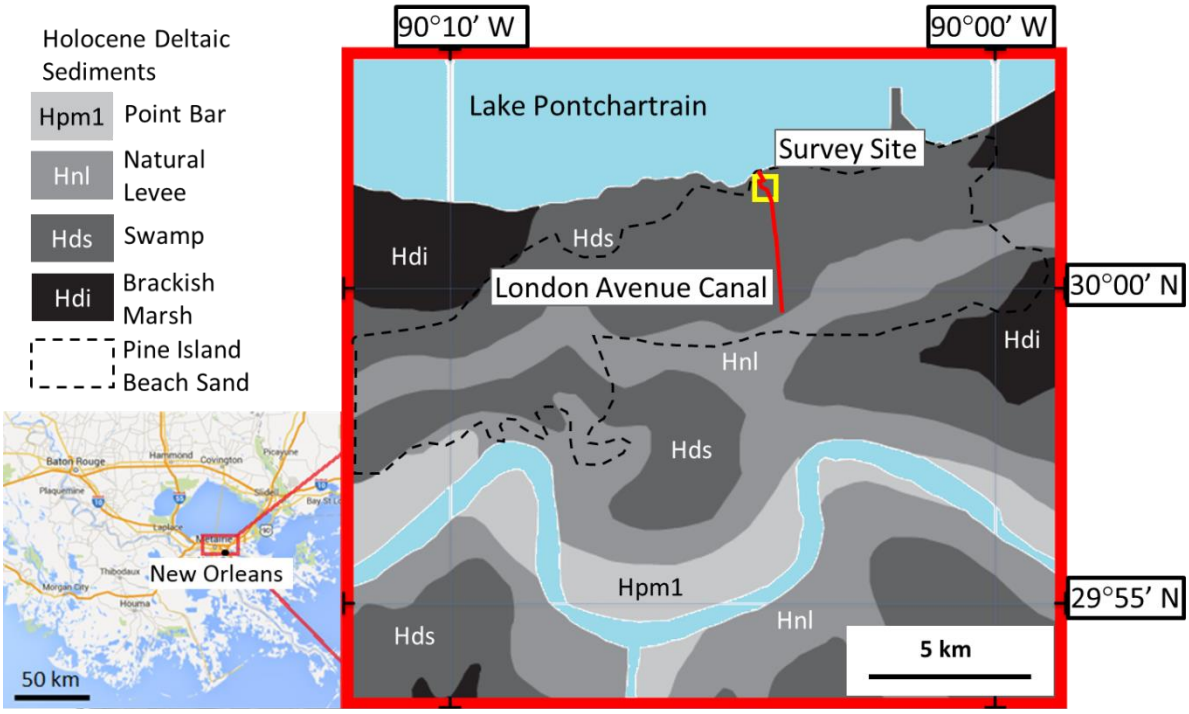

Figure 2: Depositional environment of the surface geology (Saucier, 1994b). The survey site at the London Avenue Canal is located within the depositional extent of the Pine Island Beach Trend. A cross section of the western levee toe (Figure 3) is highlighted in red, and the yellow box of the survey site is the shown in Figure 4.

Lake Pontchartrain is a brackish water environment, and sets the hydraulic head for the soils underlying London Park. Because the elevation difference between the lake and the protected side of the levee toe is approximately 3 meters, the water table is expected to be shallow (USACE, 1989a). Soil saturation with a brackish fluid is a major influence of electrical resistivity, and makes the soils less resistive (Archie, 1942). The low resistivity measurements in London Park are representative of the environments of levees located in other brackish water systems, such as the swamps and marshes commonly found throughout the Louisiana Coastal Zone.

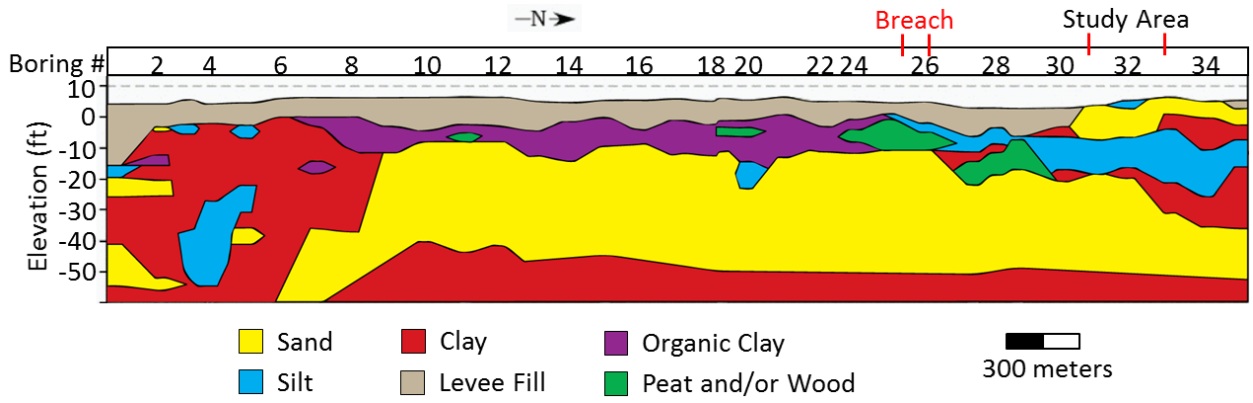

Figure 3: Geological cross-section along the western side of the London Avenue Canal (USACE, 1989a). The area of the northern breach, highlighted in red, possesses a weak organic-rich layer overlying a layer of pervious unconsolidated sand (Dunbar and Britsch, 2008). The Pine Island Beach Trend, extends underneath the breach and the study area and overlies Pleistocene clay.

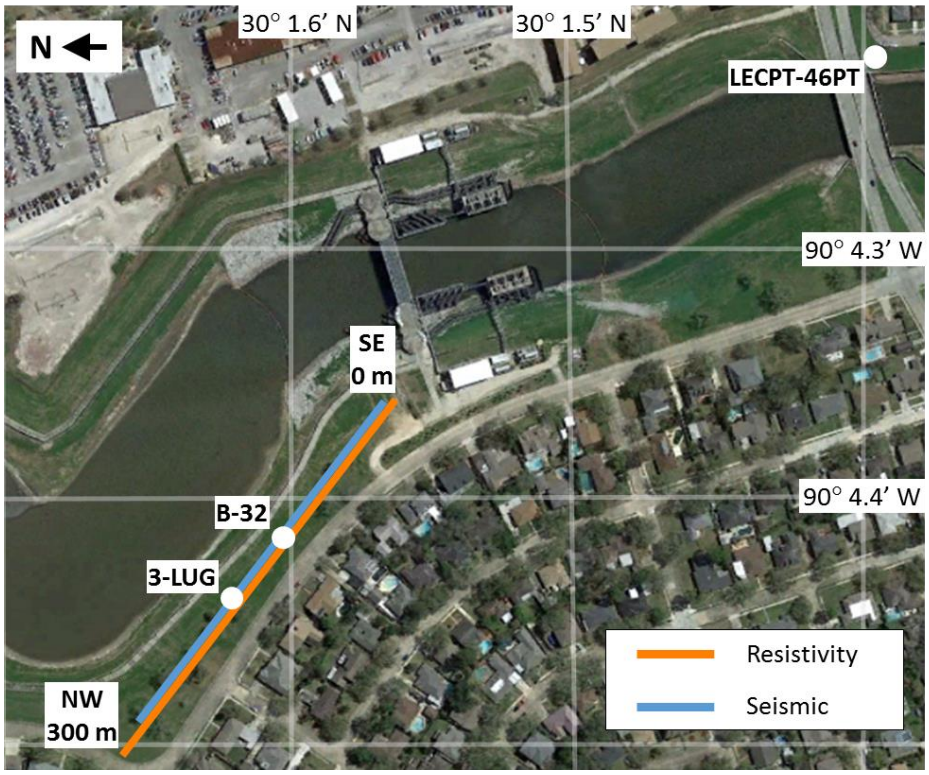

Figure 4: The location of the resistivity and the seismic lines along the London Avenue Canal in London Park. Lake Pontchartrain is located 300 meters from the northern edge of this image. The resistivity and seismic profiles were gathered while occupying the same line, although the seismic line was shorter; the lines are separated here for greater discernment. The lines average 20 meters from the crest of the levee. Boring logs (B-32 and 3-LUG) were taken at 2 sites along the survey lines (USACE, 1989b). The Cone Penetration Test site LECPT-46PT (USACE, 2010), used to estimate the shear wave velocity of the Pine Island Beach Trend, lies ~400 meters from the SE limit of the surveys.

(1.2.2) Marrero "V-Line" Levee

The Marrero "V-line" earthen levee was constructed on an area characterized as a modern swamp and marsh depositional environment (Figure 5). Cone Penetration Tests were made along the "V-line" levee every ~300 m along its crest and toe (Figure 6) (FFEB, 2007). Geotechnical and seismic techniques indicate that differential compaction of the sub-levee foundation soils led to tension cracks forming in the levee body (Lorenzo et al., 2014).

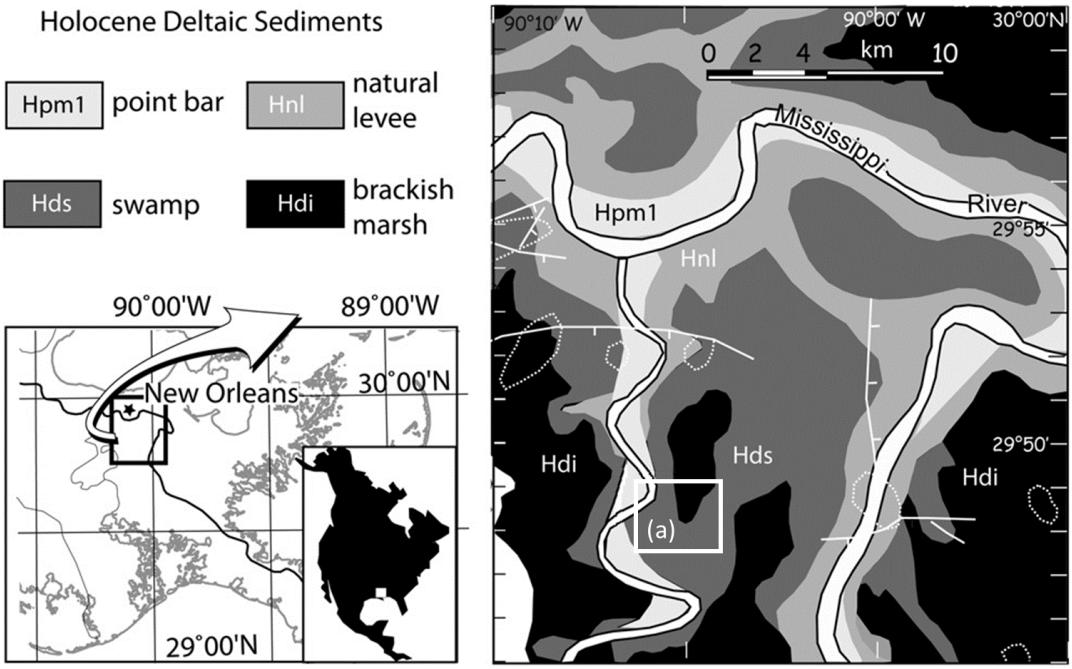

Figure 5: The surface depositional environments around the Mississippi River south of New Orleans, LA (Lorenzo et al., 2014). The site of the Marrero "V-line" levee (a) is approximately 15 km south of New Orleans and 25 km south of the London Avenue Canal levee (Figure 6). Bayou des Familles flows through the northwestern corner of the "V-line" study area.

(1.3) QUATERNARY GEOLOGIC BACKGROUND OF GREATER NEW ORLEANS

Holocene sediment deposits are the primary surface geology exposed throughout the Mississippi delta and the Louisiana Coastal Zone (Saucier, 1994b, CPRA, 2012), and are the main focus of this research. Pleistocene sediments occasionally comprise surface geology (Saucier, 1994b), but do not pose a risk to structural integrity of the levees within the Coastal Zone (Dunbar et al., 1999). The Holocene sediment wedge thickens towards the ocean in a south-easterly direction (Dunbar et al., 1999) and overlies well consolidated Pleistocene clay known as the Prairie formation (Fisk, 1944). The top of the Prairie formation lies at a depth of 15 meters near Lake Pontchartrain (Plate 4), and deepens to 30 meters in the south near the "V-line" levee (Kolb et al. 1975, Plates 4 and 7). The Pleistocene Prairie formation possesses larger shear strength and soil stiffness than the Holocene sediments (Montgomery, 1974), and is not considered a risk to the foundation soils (Dunbar and Britsch, 2008).

The Mississippi avulsions throughout the Holocene shaped the delta complexes and determined the type and location of sediment deposited (Kolb and Van Lopik, 1958). The growth and waning of the St. Bernard and Plaquemines-Balize delta complexes of the Mississippi river (Roberts, 1997) created the depositional environments for the Holocene sediments in the study

Figure 6: The Marrero "V-line" levee with the Cone Penetration Tests along the crest of the levee labeled (Hicks, 2011).

areas (Saucier, 1994b). A river dominated delta is the body of sediment deposited in an area of interaction between a high energy fluvial source and a calmer, large body of water (Scruton, 1960). Deltas are created in a cyclical process, beginning with rapid progradation during regression, followed by a slower transgressive stage as the fluvial source is captured into another delta lobe (Roberts, 1997). The rapid progradation begins with the fine grained prodelta, deposited distally from the delta front. The prodelta of the St. Bernard delta complex deposited a clay layer from 14 to 22 meters deep at the site of the Marrero "V-line" levee (Saucier, 1994b). Progradation of the delta front brings coarser sediments such as silty sands and clayey silts (Frazier, 1967). The delta complexes slowly aggrade after overextending and diminishing the river gradient (Roberts, 1997). The aggradation at the delta mouth and transition into a meandering environment created of the 4 main depositional environments as mapped by Saucier in the greater New Orleans study area that we see today (1994a): Mississippi point bars, swamps, marshes, and natural levees.

(1.3.1) Point Bars

Large sand to silt deposits are concentrated within point bar depositional environments. Point bars form along a meandering river where flow velocity drops as the river changes course, resulting in larger sediment grains being deposited on the inside of a river bend (Hubbard et al., 2011). Point bars contain predictable patterns of grain size as coarse sand grains are deposited on the upstream portion of the sandbar and fine to silt size sediment on in a downstream flow direction (Labrecque et al., 2011). While the LAC study area shows no evidence of point bar deposits in the surface geology, the surveys at the Marrero "V-line" study area lies ~2 km from Bayou des Familles and the associated sand bars. The clean sands identified at the "V-line levee" (FFEB, 2007) may be sourced from point bars formed along similar distributaries.

(1.3.2) Natural Levees

Natural levees tend to form distinct depositional environments in the deltaic plain through discrete flooding events along major rivers and distributaries. Flooding events commonly deposit thin beds less than 20 cm thick, with an abundance of beds thinner than 5 cm inter-mixed (Saucier, 1994b). Natural levees build up over time as overbank floods deposit sediment along the banks of the rivers. These beds are made almost exclusively of clay soils within the modern delta (Coleman and Prior, 1982).

(1.3.3) Backswamps

Swamp deposits typically consist of widespread sequences of clay to silt overbank sediment (Saucier, 1994b). Inland swamps are typically found upriver of the delta mouth around abandoned distributary channels. Occasional breaks in the natural levees lead to the formation of crevasse splays and the input of new sediment into the swamp. Sedimentation following a breach occurs quickly as coarse grains fall out of suspension, especially when the breach fails to sustain a flow (Boggs, 1995). Sediment from minor crevasse splays and small distributaries generally form lenses and ribbons that are too thin to distinguish between events (Saucier, 1994b).

Large amounts of peat and organic clays are also found in the cypress swamps that historically populated the study areas (Dunbar and Britsch, 2008). Borings along the London Avenue Canal (Figure 4) encountered 1-3 meters of organic sediments, deposited in the swamp environment that predated human inhabitation. Cypress swamps are rich in organic plant life, and capture large amounts of cypress pollen (Frazier, 1967). Organic rich layers are generally weaker in terms of elastic rigidity (Dvorkin et al., 1999) and shear strength (Dykes and Warburton, 2008) compared to mineral based sediment.

(1.3.4) Marshes

The area surrounding New Orleans includes large tracts of intratidal fresh-to-brackish water marshes (Kolb and Saucier, 1982). The marshes found on the Mississippi deltaic plain trend to consist of silts and clays with both a high organic content and water saturation (Saucier, 1994b). The salinity of the water effects the organic content in the Louisiana Coastal Zone marshes, as fresh and brackish water environments contain more organic matter and fewer dissolved minerals than saltwater marshes (DeLaune et al., 2002).

(1.3.5) The Pine Island Beach Trend

Prior to the formation of the St. Bernard and Plaquemines-Balize delta complexes, the Pearl River system deposited sand via longshore drift over the present-day northern portion of New Orleans (Figure 2) to form a relict barrier island (Kolb and Saucier, 1982). These

unconsolidated sands formed the Pine Island Beach Trend (PIBT) approximately 5000 to 6000 years B.P., and lie beneath the deposits from the St. Bernard and Plaquemines-Balize delta complexes (Saucier, 1994b).

The PIBT affected the structural integrity of the levee system during Hurricane Katrina. Water levels higher than normal in the London Avenue Canal increased pressure on the I-wall levee. The increase of pressure displaced the I-wall enough to establish a pathway from the canal into the PIBT, which induced piping in the PIBT leading to the I-wall levee failure at the northern breach (Dunbar and Britsch, 2008). Piping occurs when the hydraulic head becomes greater than the overburden pressure, and a large hydraulic conductivity suspends unconsolidated sediment in the flowing water (Seed et al., 2006). Piping from the canal to the protected side of the levee occurred because the I-wall base ended within the PIBT, creating a pathway for the hydraulic head to equalize (IPET, 2007).

(1.4) GEOPHYSICAL SOIL TYPE ESTIMATION

Recently studies (e.g., O'Neill et al. 2008) combine electrical resistivity and seismic methods to improve the interpretation of soil types. Seismic shear velocity can give an indication of the primary mineralogy of the sediment based on the shear modulus (Mavko et al., 2009). Because the shear modulus of quartz based sand and silt is 500% greater than that of unconsolidated clay (Taggart and Kaiser, 1960, Dvorkin et al., 1999) a greater sand and silt content implies a greater shear wave velocity. Larger porosity and less tortuosity trends towards larger grain size with greater permeability, yielding a resistivity nearly equivalent to the saturating fluid (Ghassemi and Pak, 2011).

Hayashi et al. (2013) introduce an empirical soil estimation based on cross-plots of shear wave velocity, V_s, and resistivity data, ρ, from soils common in the Japanese levee system (Figure 7). The empirical relationship indicates increases in grain size yield increases in resistivity and shear wave velocity. A polynomial equation of the form:

$$S = a * V_s^2 + b * V_s + c * \left(log_{10}(\rho)\right)^2 + d * log_{10}(\rho) + e * V_s^2 log_{10}(\rho) + f * V_s \left(log_{10}(\rho)\right)^2 + g * V_s log_{10}(\rho) + h \quad (1.1)$$

is a model optimized by a least-squares regression of the Japanese geophysical data consisting of clay, sand, and gravel data points for levee foundation soils (Hayashi et al., 2013). The least-squares regression determines the values for coefficients 'a' through 'h' (Equation 1.1) (Hayashi et al., 2014b). Hayashi et al. (2013) represent the sediment types as integers according to increasing grain size for the regression, where S=1 is clay, S=2 is sand, and S=3 is gravel. S in Equation 1.1 represents the probability that the dominant sediment type is either clay, sand, or gravel (Hayashi et al., 2014a). Hayashi et al. (2013) also introduce a model for levee bodies, but we do not focus on this model because the levee body model focuses on unsaturated soils in the levee body whereas we are concerned with saturated soils in the levee foundation.

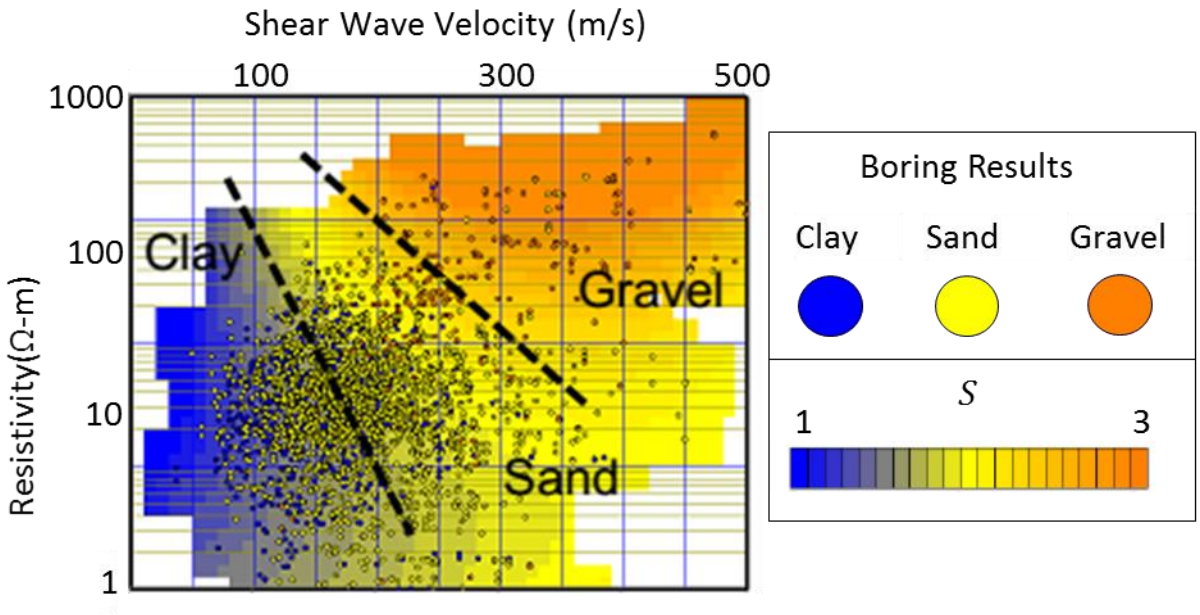

Figure 7: A cross plot of shear-wave velocity, electrical resistivity, and soil type. Hayashi et al. (2013) best fit a surface through this 3-D data set. The best fit surface indicates that a larger grain size corresponds to a larger electrical resistivity and larger shear-wave velocity.

The difference between the depositional environments in the Louisiana Coastal Zone and the environments from which Hayashi et al. (2013) amass soil data requires a new regression to accurately interpret soil typ. Clay, sand, and gravel sediment classes are dominant in an area of high sediment yield and elevation gradient, such as Japan (Milliman and Syvitski, 1992), but the Holocene deposits of the Mississippi delta plain are primarily composed of sand, silts, and clays (Saucier, 1994b). The depositional environments in delta plains typically contain saturated soils. Whereas seismic shear velocity is, nominally, not effected by the saturating fluid (Gassmann, 1951), the resistivity of the saturating fluid impacts the electrical resistivity of soil. The impact either increases or decreases the subsurface resistivity based on whether the fluid resistivity is greater than or less than the natural resistivity of the soil. A new cross-plot analysis and least-squares regression using geophysical data from the study areas changes the coefficients of Equation 1.1 to account for the lower resistivity values of the deltaic environment and to identify silt in addition to sand and clay.

(1.5) SURFACE WAVE INVERSION

The propagation of a Rayleigh wave through a heterogeneous medium provides enough information to construct a shear-wave velocity profile of the subsurface. The plane wave wave propagation of a Rayleigh only exhibits dispersive behavior in heterogeneous environments. Dispersion is the property where velocity varies with the frequency, such that phase velocity and group velocity are different (Ikelle and Amundsen, 2005).Whereas in-situ electrical resistivity acquisition systems and processing methods are mature and numerous (e.g., Maillet, 1947, Kuras et al., 2006), new methods of collecting and extracting in-situ shear wave velocity are still developing. Surface wave inversion can generate shear wave velocity profiles using dispersion calculations of the Rayleigh wave.

Seismic surface waves propagate along the boundary between two differing elastic media. Rayleigh waves can be generated at the interface between ground and air (Strutt, 1885). Constructive and destructive interference of compressional and vertically polarized shear waves along a free surface boundary create Rayleigh waves under special conditions (Scholte, 1947). Rayleigh waves are essentially the superposition of several plane waves with different frequencies and wavelengths traveling together at a rate known as a group velocity (Ikelle and Amundsen, 2005). Aki and Richards (2002) represent the Rayleigh wave as a harmonic plane wave by in Cartesian coordinates:

$$\vec{u}(x_1, x_3, t) = U_i(x_3)e^{i(kx_1 - \omega t)} \ (i = 1,3) \tag{1.2}$$

where u is the displacement vector, U_i are depth-dependent eigenfunctions in the direction of motion ($i = 1$) where in the vertical direction $i = 3$ (Figure 8), t is time, ω is the angular frequency, and k is the wavenumber. The wavenumber relates to the wavelength, λ, of a propagating wave by:

$$k = \frac{2\pi}{\lambda} = \frac{\omega}{c} \tag{1.3}$$

where the phase velocity, c, is the apparent frequency-dependent velocity for a portion of the wave with frequency ω. The boundary conditions indicate no traction across the surface boundary, setting the initial conditions for the stresses, σ_{ij} at the surface as:

$$\sigma_{13}|_{x_3=0} = \sigma_{23}|_{x_3=0} = \sigma_{33}|_{x_3=0} = 0 \tag{1.4}$$

These boundary conditions make it possible to solve the eigenfunctions, U_i, given that the solution to (1.2) also satisfies Navier's equation for 2D-Rayleigh wave motion (Malischewsky and Scherbaum, 2004):

$$\rho\ddot{u}_i = \mu\frac{\partial^2 u_i}{\partial x_j \partial x_j} + (\Lambda + \mu)\frac{\partial^2 u_j}{\partial x_i \partial x_j} \tag{1.5}$$

where Λ and μ are Lamé's parameters, and ρ is density. These elastic parameters of the subsurface directly control the velocity of the Rayleigh wave. Lay and Wallace (1995) solve (1.2) describing the displacement for a Rayleigh wave in a homogeneous half space as:

$$u_1(x_1, x_3, t) = A\left[e^{kS_\alpha x_3} - \left(1 - \frac{1}{2}\frac{c^2}{\beta^2}\right)e^{kS_\beta x_3}\right]e^{i\omega(t-k)} \tag{1.6}$$

$$u_3(x_1, x_3, t) = -iA\left[-S_\alpha e^{kS_\alpha x_3} + \frac{1}{S_\beta}\left(1 - \frac{1}{2}\frac{c^2}{\beta^2}\right)e^{kS_\beta x_3}\right]e^{i\omega(t-\frac{x_1}{c})} \tag{1.7}$$

where S_α and S_β represent the abbreviated relationship between phase velocity and group velocity:

$$S_\beta = \sqrt{1 - \frac{c^2}{\beta^2}} \tag{1.8}$$

$$S_\alpha = \sqrt{1 - \frac{c^2}{\alpha^2}} \tag{1.9}$$

For a body wave propagating in an elastic medium, α denotes the group velocity for compressional waves and β denotes the group velocity for vertically polarized shear waves. The displacement potentials are out of phase by $\pi/2$, such that u_3 leads u_1 and produces the elliptical motion (Figure 8) characteristic of Rayleigh wave propagation (Lay and Wallace, 1995).

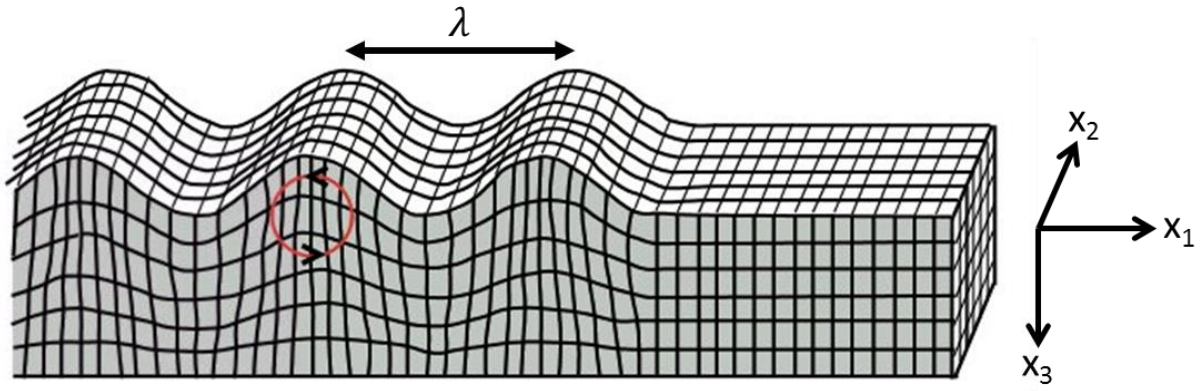

Figure 8: A Rayleigh wave travels with retrograde elliptical particle motion as it propagates through a homogeneous medium, eventually transitioning to prograde motion at greater depths. In the 2D case with plane strain in the x_1-x_2 plane, the Rayleigh wave moves in the x_1 direction, but creates displacements in the x_1-x_3 plane (Ikelle and Amundsen, 2005).

Rayleigh waves propagate at a single velocity in a homogeneous half-space. The velocity of a Rayleigh waves depends on frequency only in a layered earth. The velocity of a Rayleigh wave is invariant to the frequency of the wave, depending only upon the elastic properties which determine shear and compressional wave velocities (Equations 1.8 and 1.9).

Rayleigh waves disperse within a layered earth because Rayleigh waves decay in strength by $\sim e^{\frac{x_3}{\lambda}}$, allowing geophones to only detect longer wavelength surface waves propagating with a velocity relative to the sediments at x_3 (Aki and Richards, 2002). The longer wavelength components of a Rayleigh wave are influenced primarily by the elastic properties of deeper sediments than the shorter wavelength components (Rix and Leipski, 1991); if deeper layers support faster travel of Rayleigh waves, longer wavelengths travel faster than the shorter wavelength Rayleigh wave contributions.

The dispersive property of surface waves (Nazarian et al., 1983) is used to extract shear wave velocity models of the subsurface by direct search inversions (Xia et al. 1999; Haskell 1953). The use of surface waves to understand foundation soils started with the Spectral Analysis of Surface Waves, or SASW (Heisey et al., 1981). SASW uses two geophones to determine the phase velocity of ground roll with different wavelengths by varying receiver spacing (Nazarian et al., 1983). However, SASW provides estimation of the elastic moduli (Stokoe et al., 1994) at a single site position, which lends itself to higher vertical accuracy at the expense of lateral data acquisition (Heisey et al., 1982).

Multi-channel Analysis of Surface Waves (MASW) is a method using a geophone array to capture the seismic signal of a propagating surface wave. The seismic data from a surface wave can be transformed into the frequency domain, and displayed as a function of its phase velocity in a plot called a dispersion image (Park et al., 1999). The fundamental and higher order modes can be distinguished in a dispersion image. Due to the nonlinear complex nature of Rayleigh wave displacement in a layered elastic medium, inversions are typically performed numerically instead of analytically (e.g., Xia et al., 1999). A direct search inversion attempting to match the fundamental mode of a dispersion curve can yield a subsurface model for shear wave velocity (Wathelet, 2008).

Addition of an initial cross-correlation step to the MASW processing scheme improves the lateral resolution of the shear wave velocity model by locating the changes of a surface wave to the midpoint between the two cross-correlated receivers instead of the midpoint between the receiver and the shot location (Hayashi and Suzuki, 2004). Hayashi and Suzuki (2004) name the point between the two receivers a Common Mid-Point (CMP). The cross-correlated signals with the same CMP and spacing between receivers are stacked, and then combined with the other stacked signals from the same CMP, but with different spacing, to create a new gather (Hayashi and Suzuki, 2004). The original MASW processing scheme is applied to these new gathers to generate a dispersion image and invert for shear wave velocity.

CHAPTER 2: FIELD METHODS

Seismic and electrical resistivity methods make near-continuous non-invasive measurements that are used for the calculation of physical properties of the subsurface. Considering both seismic and electrical measurements for the upper 20 meters of the near-surface aids the accurate interpretations of the levee foundation sediments. In comparison, well logging for resource exploration uses integrated petrophysical measurements (i.e. sonic and electrical resistivity) to determine lithology and fluid properties (Asquith et al. 2004). Similar measurements applied to the near surface improve upon geophysical soil identification by jointly using geotechnical soil data, seismic, and electrical resistivity from study areas in the greater New Orleans area.

(2.1) TOOLS

(2.1.1) Capacitively Coupled Resistivity

Capacitively Coupled Resistivity (CCR) generates apparent resistivity measurements of the subsurface in a method similar to dc resistivity, except that the galvanic electrodes are replaced with sensors capacitvely coupled with the earth (Timofeev et al., 1994). The Geometrics OhmMapper (Geometrics, 2001) CCR system used in this study couples to the subsurface with a capacitive-line antenna sensor, where the earth and antenna act as the two plates of a capacitor, separated by the insulating antenna cover (Kuras et al., 2006). The capacitance allows an AC current from the transmitter to create a time-dependent electric field in the earth (Figure 9), ultimately producing an AC current in the earth (Yamashita et al., 2004). The voltage, U, across a receiver's capacitvely coupled antennas responds to the AC current, allowing for determination of apparent resistivity, ρ_a:

$$\rho_a \cong \frac{\mathrm{Re(U)}}{\hat{I}} \times K^{dc} \tag{2.1}$$

where $\hat{I}$ denotes the magnitude and direction of current flow, and the term

$$K^{dc} = \frac{2\pi}{\frac{1}{r_{11}} + \frac{1}{r_{22}} - \frac{1}{r_{12}} - \frac{1}{r_{21}}} \tag{2.2}$$

represents the direct current geometric factor (Kuras et al., 2006). The geometric factor simplifies to a scalar in a 2D system. An increase in distance between the dipoles decreases the potential across the receiving antenna for a CCR array, such that $Re(U) \propto r_{12}$ (Yamashita et al., 2004). The geometric factor changes with the distances between the dipoles from each portion of the antenna, and whether they repel or attract (Figure 10).

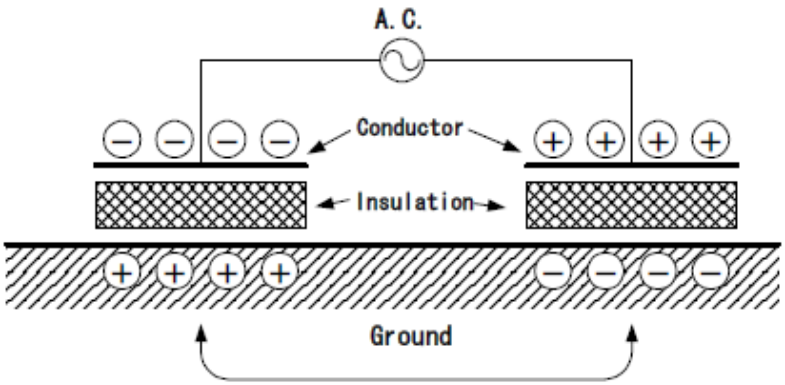

Figure 9: This conceptual model of a CCR transmitter shows the buildup of an electrical field in the ground by coupled capacitance on either side of the dipole antenna at a single moment in time. As the AC current fluctuates, the electric field in the earth will change as well, allowing the AC current to flow in the earth coupling. Similarly, a CCR receiver can measure the voltage across the antenna due to the coupled current. Yamashita et al. (2004).

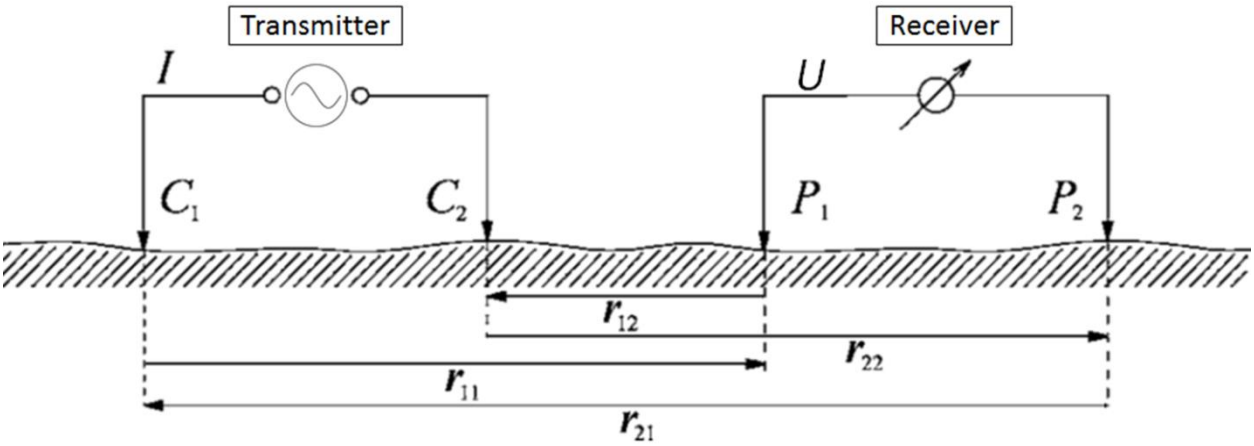

Figure 10: The geometric arrangement of the transmitter and receiver dipole (antenna) length and antenna separation affect the observed potential at the receiver. Greater spacing between the transmitter and receiver (r_{12}) leads to smaller potential drop across the receiver. Increases in dipole length will similarly decrease the observed potential drop and due to increasing the geometric factor. Figure modified from Kuras et al., (2006).

The Geometrics OhmMapper towable streamer system allows for fast, economic, and virtually continuous lateral acquisition of apparent resistivity data that can be used to understand the resistivity structure of the near surface. The OhmMapper generates a current through the transmitting antenna twice every second, effectively making an apparent resistivity measurement. An android tablet compiles measurements and position data simultaneously. Coupling the capacitors with the earth to generate an AC current causes the current strength to degrade with depth. The skin depth, δ, for the OhmMapper is considered the depth of penetration (Timofeev et al., 1994):

$$\delta = 503 * \sqrt{\rho / f} \quad (2.3)$$

where ρ is the resisitivity of the earth and f =16,500 Hz is the operating frequency of the OhmMapper. For example, an approximate average resistivity of 10 ohm-m indicates that a 12 meter penetration depth before the AC current drops to 1/e its original strength.

(2.1.2) Cone Penetration Test

The Cone Penetrometer uses a hydraulic system (Figure 11) to push a piezometric cone into the ground to determine, among other important geotechnical properties, stratigraphy. Multiple sensors on the cone measure the resistance to movement against the tip and the friction along the sleeve in what is known as a Cone Penetration Test, or CPT. The tip resistance (q_c) and sleeve friction (f_s) estimate Soil Behavior Type (SBT) (Robertson et al., 1986). The SBT classification system is based on global empirical relationships of q_c, f_s, and CPT measurements of known soil types, with 12 classifications to predict the soil type and grain size in the subsurface (Lunne et al., 1997). The original Robertson et al. (1986) chart is commonly used by civil engineers to predict the Soil Behavior Type. The chart bases soil type classes on the tip resistance and friction ratio (R_f), where $R_f = {f_s}/{q_c} \times 100\%$.

Advanced piezometer cones may also record pore pressure at the tip, behind the cone, and along the friction sleeve to correct for pore pressure and overburden (Robertson, 1990). Corrections for pore pressure enhance determination of SBT (Robertson, 2009). Positive pore pressures weaken the sediment by decreasing the measured tip resistance, such that silt possesses similar resistance as sand and clay appears to be silt (Lorenzo et al., 2014). We do not have access to pore pressure data, and therefore rely on the original Robertson et al. (1986) chart.

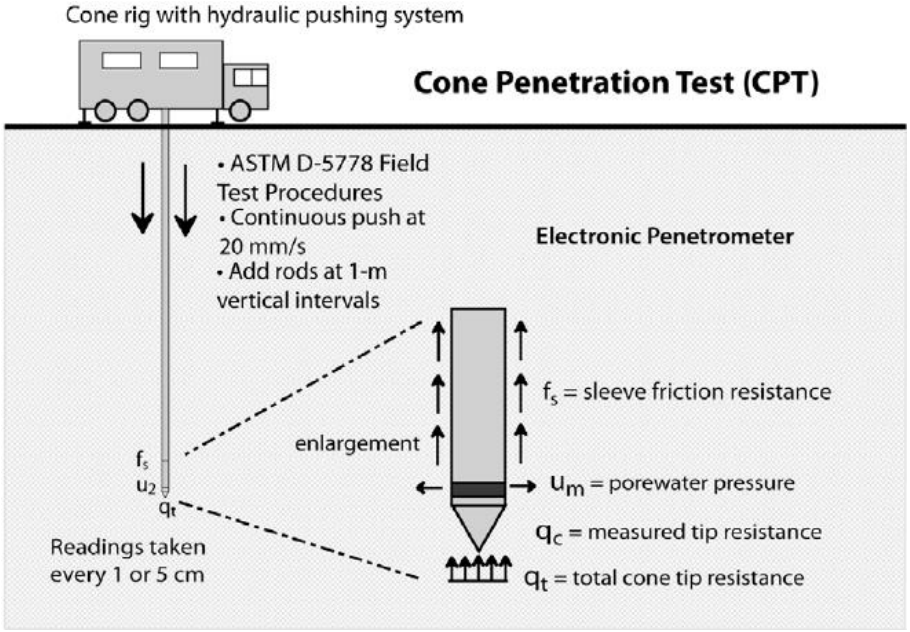

Figure 11: Diagram of an advanced Cone Penetrometer (Lunne et al., 1997).

(2.2) FIELD TECHNIQUES

(2.2.1) MASW Seismic Data Acquisition

A seismic survey along the London Avenue Canal (LAC) collected seismic data with the specific focus of recording surface waves. The survey acquired Rayleigh wave data along a 274 m line next to the protected toe of the western LAC levee in London Park (Figure 4). Approximately 20 meters separate the survey line from the crest of the levee, which runs roughly parallel to the levee. A sledgehammer source and a towable land-streamer array of 23 vertical component geophones possessing a resonant frequency of 4.5 Hz collected the data (Table 1). Five 26 second long gathers collected at each shot-point increase the signal-to-noise ratio by allowing for an average of ~10 separate strikes per gather. By gathering more hammer strikes, we obtain an increase in signal-to-noise ratio when we cross correlate and stack each gather during data processing.

Table 1. Seismic Acquisition Parameters for LAC Seismic Survey

Seismic Acquisition	
Acquisition date	Jun-1-2012
Source-receiver offset	12 -78 m
Shot-point advancement	12 m
Number of shot-points	16
Geophone separation	3 m
Datum, Coordinate system	WGS84, UTM
First shot-point location	15 R, 782245.00 m E, 3325342.00 m N
Last shot-point location	15 R, 782097.00 m E, 3325443.00 m N
Geophones	23, Mark Products L-10B 4.5 Hz Vertical Sensor
Seismograph	24-Channel, 24-bit resolution, R24 Geometrics Strataview
Sample rate, Record length	2000 Samples/s, 26 s
Gathers	5 gathers/shotpoint
Seismic source	7-13 vertical blows: ~15.25 cm x ~15.25 cm x ~2.5 cm (6 x 6 x 1 in) aluminum plate; using ~4.5 kg (10 lb) sledgehammer

(2.2.2) Electrical Resistivity Acquisition

We collect apparent resistivity data next to the protected toe of the LAC I-wall levee (Figure 4) and the unprotected and protected toes and crest of the Marrero "V-line" earthen levee (Figure 12). The CCR system acquired each line twice using two separation geometries (Table 2) between the transmitter and receivers. The acquisition of two geometries is only necessary because of the low electrical resistivity values encountered at the survey areas. Kuras et al. (2006) show an increase in diploe separation, such as for the long geometry, reduces the chance of overestimating resistivity when surveying low resistivity areas, and also increases the depth sensitivity for an apparent resistivity measurement. However, the longer array allows for current to spread deeper and lose potential strength (Timofeev et al., 1994) thus the short acquisition geometry is necessary to fill in for shorter shallower apparent resistivity measurements.

Towing of the CCR streamer system stopped when consecutive apparent resistivity measurements varied by more than an order of magnitude. Acquisition of apparent resistivity continued uninhibited throughout the extent of the stop. The survey halt allowed multiple apparent resistivity measurements to be gathered at a single position. The multiple measurements at a single location improve signal-to-noise by eliminating systematic noise related to movement, and providing enough samples that spikes in apparent resistivity appear as outliers. Poor coupling of the antennas with the surface and a high background noise level relative to the apparent resistivity values contribute to an uncertainty of 20-30% for the true resistivity values from the profiles (K. Hayashi, pers. Com., 2014). Towing continues once consecutive apparent resistivity measurements are within the same order of magnitude.

Figure 12: The site of the Marrero "V-line" levee with the approximate start and end points of the resistivity survey marked by the tip of the arrows. We gathered CCR data along the crest and protected and unprotected toes of the levee (Table 2). The resistivity lines along the toes run parallel to the crest of the levee, approximately 30 m from the crest on the protected side and 15 m from the crest on the unprotected side.

A least-squares inversion of the resistivity data, run in the program OhmImager (Geometrics, 2013), determines the true resistivity values for the profiles from the London Avenue Canal (Figure 4) and Marrero "V-line" study areas (Figure 12) (K. Hayashi, pers. com.,

2014). The inversion uses the apparent resistivity from both the short and long CCR acquisition geometries. We exclude outlier apparent resistivity values at a single location, and invert the remaining data for a true resistivity profile.

Table 2. Resistivity Acquisition Parameters for London Avenue Canal and "V-line" levee

Resistivity Acquisition	
Acquisition Date	Dec-17 -2013 (LAC) and Dec-18-2013 (V-line)
System	Geometrics CCR OhmMapper 5 receivers, 1 transmitter Towed by Ford E-series van
Operating Frequency	16.5 kHz
Array Style	Dipole-Dipole
Sample Rate	2 S/s
Transmitter-Receiver offset	Short Separation Geometry: 10-20 m Long Separation Geometry: 20-40 m
Receiver Spacing	Short Separation Geometry: 2.5 m Long Separation Geometry: 5 m
Dipole Length (Short, Long)	5, 10 m
Datum, Coordinate system	WGS84, UTM
LAC Survey Locations	
Start of line	15 R 782323.00 m E, 3325276.00 m N
End of line	15 R 782082.00 m E, 3325442.00 m N
"V-line" Survey Locations	
Start of protected toe	15 R 780724.00 m E, 3299297.00 m N
End of protected toe	15 R 781523.00 m E, 3300573.00 m N
Start of center line (crest)	15 R 780727.00 m E, 3299242.00 m N
End of center line (crest)	15 R 781522.00 m E, 3300507.00 m N
Start of unprotected toe	15 R 780721.00 m E, 3299209.00 m N
End of unprotected toe	15 R 781524.00 m E, 3300493.00 m N

CHAPTER 3: DATA

(3.1) LONDON AVENUE CANAL SEISMIC DATA

The seismic data collected from the London Avenue Canal study area includes arrivals interpreted as surface waves, direct waves, and refractions. Assuming increasing velocity with depth the surface waves should disperse with increasing offset, where low frequency waves arrive earlier than high frequency waves (Stokoe et al., 1994). However, dispersion effects cannot be observed in the time domain because body waves constructively and destructively interfere with the signal (Figure 13). Frequency analysis of the shot gather indicate the seismic energy possesses a frequency content predominantly ranging from 3 to 60 Hz.

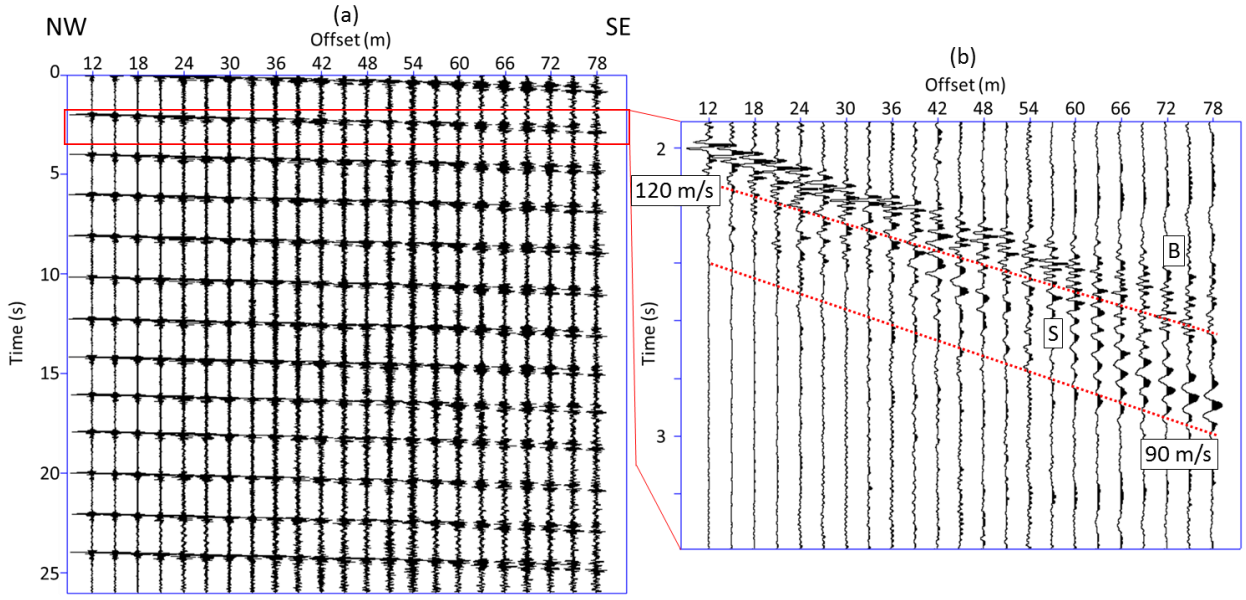

Figure 13: The first shot gather from the shot-point at 45 m (a) of the LAC survey contains the data from 23 geophones. We balance trace amplitudes by dividing the entire trace by the RMS value using the SeismicUnix "pbal" function (Stockwell, 1999). The gather (a) consists of seismic waves generated by 13 hammer blows over 26 seconds. The seismic energy from a single hammer blow outlined in red (inset b) shows the seismic waves. Body waves typically arrive first, especially at far offsets (B). Surface waves propagate slower (S), but separate from body waves at far offsets. Constructive and destructive interference increases with decreasing offset from the source.

(3.2) ELECTRICAL RESISTIVITY

The inversion of the OhmMapper CCR meter apparent resistivity data at the London Avenue Canal and Marrero "V-line" study areas create 2D electrical resistivity profiles (Figures 14, 15). A general trend of a resistive top layer overlying a conductive layer is found at both sites. However, the low resistivity values present in the foundation soils limit the skin depth of inverted 2D profiles to 10 meters.

We extract true resistivity values from the 2D profiles (Geometrics, 2014) for the location of each CPT and boring log to coincide with the 1D shear wave velocity profiles. Even though the true resistivity models from the least squares inversions possess higher resolution, the 1 meter resolution of the shear wave velocity profiles limits the depth-interval for extracting

electrical resistivity data to 1 meter. We use the minimum extraction interval to compile electrical resistivity data for cross plot analysis. However, both study areas contain electrical resistivity values that exceed the operational limits of the OhmMapper system. We expect inaccurate resistivity values below 1 Ω-m, because the instrument is not designed for such low resistivity (Yamashita et al., 2004). We do not analyze resistivity values smaller than 1 ohm-m in order to avoid expected inaccuracies.

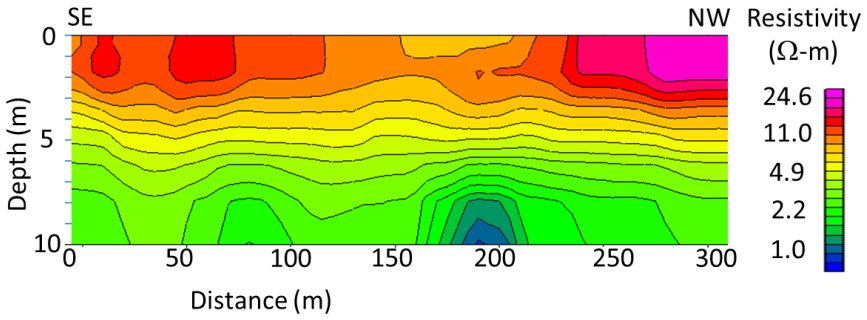

Figure 14: The 2D resistivity profile generated by the least squares inversion of the apparent resistivity data collected in London Park approximately 20 m SW of the London Avenue Canal levee crest (Figure 4). Resistivity decreases with depth, with the greatest resistivity occurring near the road in the shallow NW part of the survey.

(3.3) RECONCILIATION OF PRIOR STUDIES WITH NEW STUDIES

We use publicly available data to identify and classify the soil types in the vicinity of geophysical measurements. Borings and cone penetrometer data provide the soil identification data required to build a geophysical cross plot. We use the single most northern CPT of the 164 Cone Penetration Tests made along the east and west sides of the canal following Hurricane Katrina in 2005 (Veatch and Martin 2011). Of the 82 boring logs made for the redesign of the London Avenue Canal in the late 1980s, only 2 borings originate near the survey (USACE, 1989b). We use only 3 of the results from the Cone Penetration Tests at the "V-line" levee (FFEB, 2007). We only use CPTs and boring logs that either spatially overlap, or can be projected onto the geophysical survey lines. Additionally, seismic surveys conducted along the V-line levee provide velocity profiles (Lorenzo et al., 2014) from which Vs and resistivity can be related to soil type.

(3.3.1) London Avenue Canal Boring Logs

Two boring locations corresponding to boring logs B-32 and 3-LUG (USACE, 1989a) lie on the geophysical survey lines at the London Avenue Canal study area (Figure 4). Boring logs are sediment descriptions made at discrete depth intervals corresponding to changes in sediment type. The boring log for B-32 (Figure 16) contains sediment descriptions made by visual classification, and for select samples, wet and dry density, water content, and unconfined compressive strength (USACE, 1989b). Boring log 3-LUG (Figure 16) provides soil classification consistent with the Unified Soil Classification System (ASTM D2487). The log includes the Atterberg limits (ASTM D4318), water content, void ratio, saturation, and dry density values for each sample. However, 3-LUG does not include grain size distribution required for USCS, but we assume the engineers performed the sieve analysis in order to name each soil according the Unified Soil Classification System (ASTM D2487).

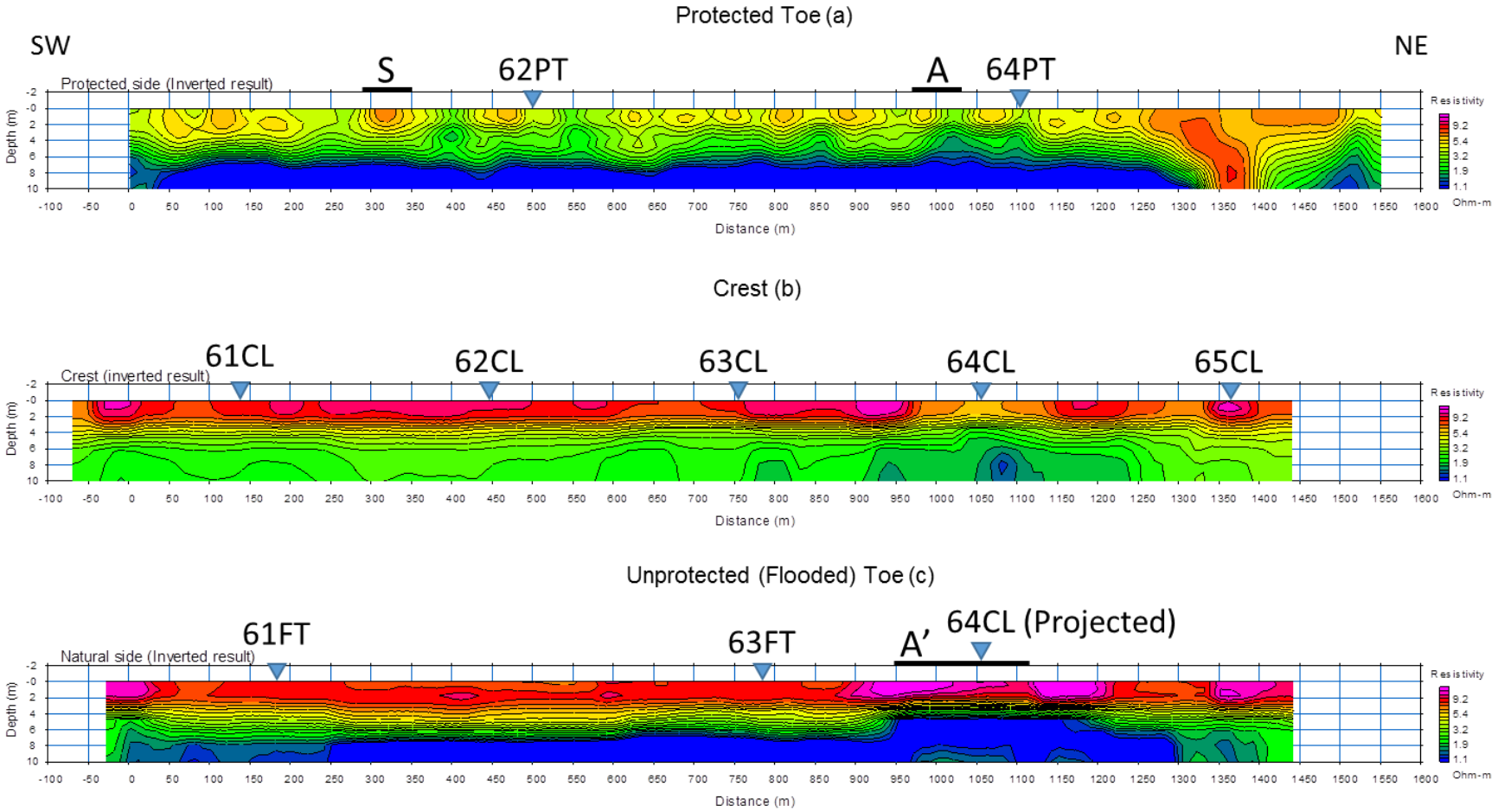

Figure 15: Resistivity data were collected using an OhmMapper CCR system along the protected toe (a), crest (b), and unprotected toe (c) of the Marrero "V-line" levee. The CPTs made along the levee (Figure 12) are shown for the protected toe (PT), flooded toe (FT), and crest of levee (CL) (FFEB, 2007). The extent of the three seismic surveys A, A', and S (Lorenzo et al., 2014) are shown marked above the profile.

The soil descriptions available from visual inspection and laboratory tests require a unifying system of soil classes in order to distinguish soil type using geophysical data. We define the dominant soil type by the main sediment in the soil description, effectively homogenizing the soil for each sample in the boring logs. We interpret each sample using the dominant sediment into clay, silt, or sand homogenous soil classes. For example, the dominant soil type for a 'silty clay with sand' or a 'sandy silt' under the Unified Soil Classification System are clay and silt, respectively. Additionally, the visual description from B-32 classify several meters as "sandy silt", which we simplify to silt.

Using sand and clay as soil classes allow us to match the soil classes from Hayashi et al. (2013). However, Hayashi et al. (2013) do not incorporate the next most common soil type mentioned in the boring logs, silt, into their soil classes. A three soil type classification system matches the prevalent soil types in the coastal region, while testing if these soil classifications are distinguishable by geophysical methods.

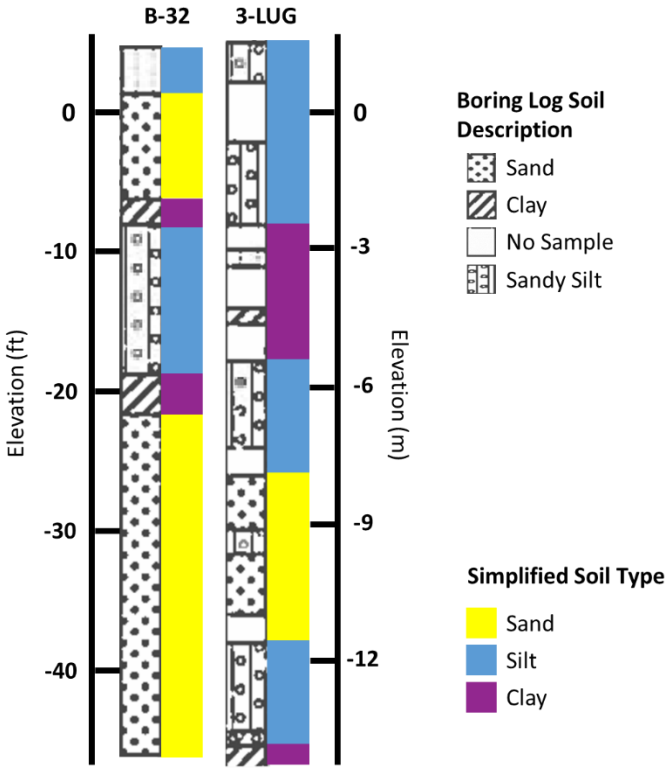

Figure 16: The borings for boring logs B-32 and 3-LUG lie 128 and 159 m, respectively, from the start of the LAC survey lines (Figure 4). The soil descriptions from B-32 and 3-LUG compose the left column for each boring (USACE, 1989b). The color classifications to the right of each boring log represent our interpretation of the dominant soil type for the corresponding sample. "Simplified Soil Type" refers to our use of the dominant soil type as a classification scheme. The discrete sampling for boring log descriptions create gaps in the 3-LUG log, corresponding to depths with no analyzed samples. We fill the gaps by extending the zones with analyzed samples.

(3.3.2) London Avenue Canal CPT Data and V_s Estimation

The test site for the Cone Penetration Test (CPT) LECPT-46PT (USACE, 2010), the closest CPT made to the London Avenue Canal study area, lies ~400m from the SE limit of the survey lines (Figure 4). The remaining CPTs along the Canal levees lie further south of the study area (Figure 2). LECPT-46PT penetrates through the PIBT, providing us with data to estimate velocity and soil structure of the area (Figure 17).

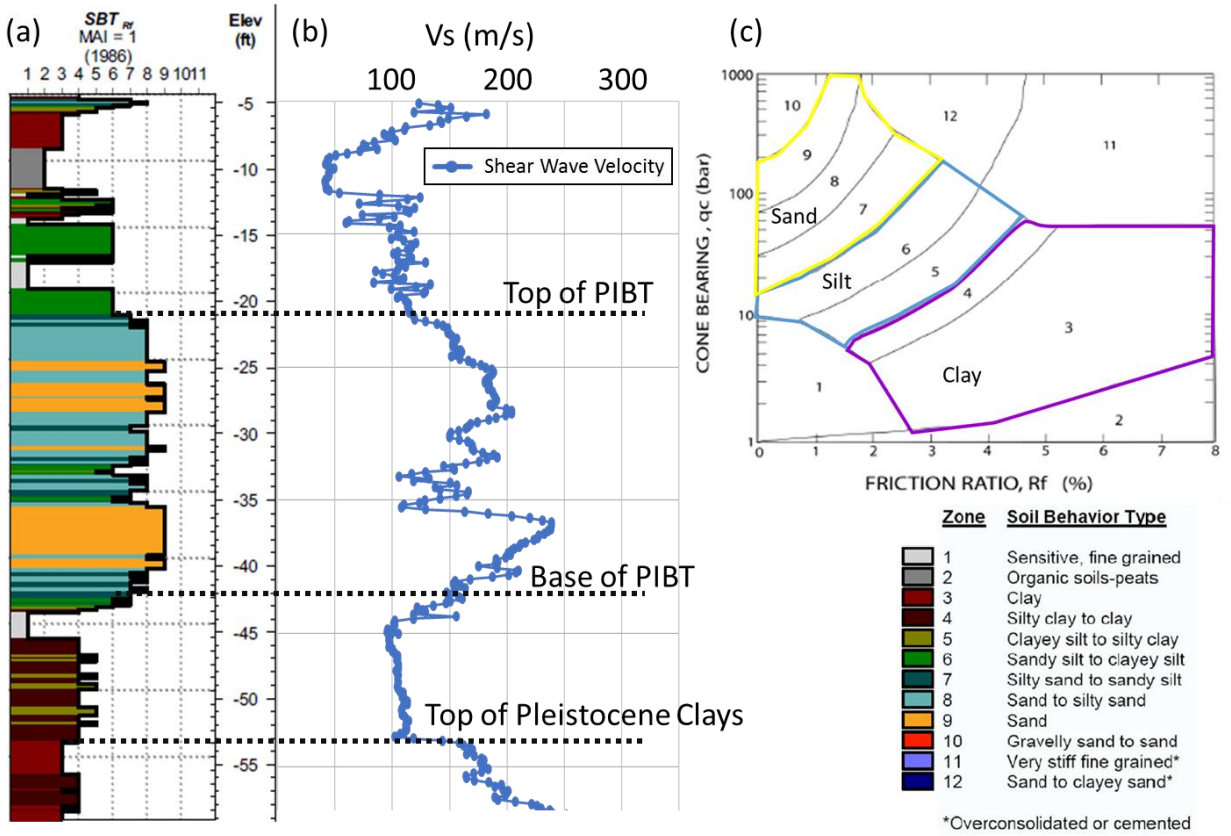

Figure 17: We use the Robertson et al. (1986) Soil Behavior Type (SBT) chart for LECPT-46PT (USACE, 2010) (a) to interpret the stratigraphy near the LAC study area (Figure 4). A sand layer, interpreted as the PIBT, lies at ~6 meters depth (20 feet). Estimates of shear wave velocity (b) come from empirical relationships (3.1, 3.2), and compensate for soil type. The dominant soil listed in the SBT (a) determines the empirical relationship to use. A modified SBT classification (Lorenzo et al., 2014) segments soil type (c) into sand, silt, or clay classes. Figure modified from (USACE, 2010).

Existing empirical formulas define relationships between shear wave velocity and values of q_c and f_s for different sediment types (Robertson, 2009). We use the empirical relationships introduced by Hegazy and Mayne (1995) and Mayne and Rix (1995) because they are specific to sand and clay, respectively, and do not require pore pressure measurements to predict V_s. Mayne and Rix (1995) introduce an empirical estimation for shear wave velocity designed from data collected in predominantly clay soils:

$$V_s = 1.75 q_c^{0.627} \tag{3.1}$$

CPT-derived V_s values (3.1) for sound in clay work well when the SBT corresponds to clay soils, providing shear-wave velocity estimates similar to the shear-wave velocity values for clay from Lorenzo et al. (2014). Also as expected, (3.1) over-estimates shear wave velocity in sands, such that they are an order of magnitude greater than the V_s values observed in unconsolidated sands at the "V-line" levee (Lorenzo et al., 2014). The empirical estimation of V_s built for sands by Hegazy and Mayne (1995) applies more appropriately when the Soil Behavior Type (SBT) indicates the presence of sand.

$$V_s = 12.02 q_c^{0.319} f_s^{-o.0466} \tag{3.2}$$

Assuming differences between silt and sand are grain size and not mineralogical, the two soil types should possess similar shear wave velocities; silt dominated soils are included with sand.

(3.3.3) Marrero CPT and Seismic Surveys and Analysis

Hicks (2011) analyzed the CPTs from the Marrero "V-line" levee (FFEB, 2007) to determine SBT (Figure 18) and several other geotechnical properties.

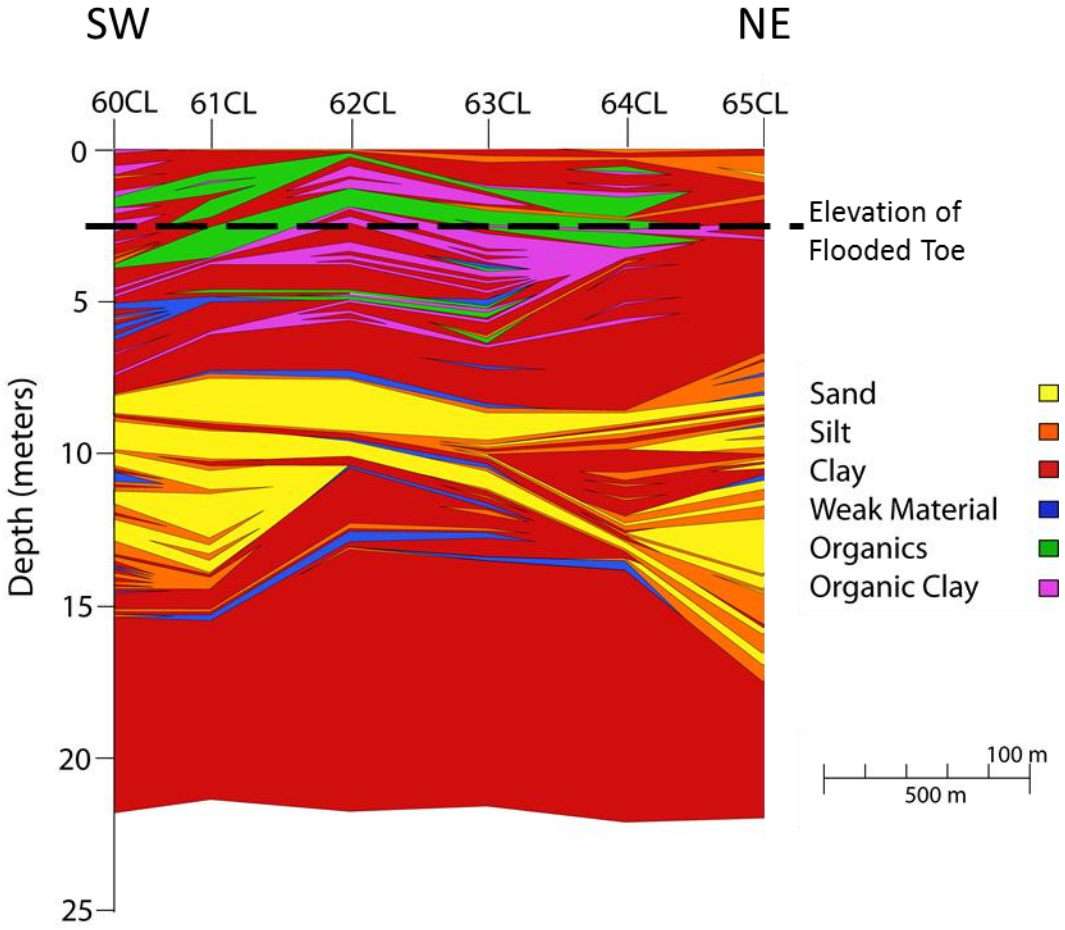

Figure 18: A profile of SBT underneath the Marrero 'V-line' levee (Hicks, 2011) constructed from the CPTs along the crest of the levee (Figure 15b). The crest of the levee resides 2.5 m above the elevation the flooded toe, which is the elevation difference between the projection of CPT 64CL onto seismic survey line A'.

We group SBT for the Marrero "V-line" levee the same as for LECPT-46PT (Figure 17c). Simplifying SBT into sand, silt, and clay groups reconciles SBT with the simplified soil classifications for the LAC boring logs. Even though the cone penetrometer responds to in-situ mechanical properties of the soil instead of grain size distribution (Robertson, 2009), the CPT-based SBT is often consistent with the Unified Soil Classification System (e.g., Molle, 2005). Based on the Robertson et al. (1986) classification system, a "3" and "4" are taken as a clay, "5" or "6" as a silt, and "7" to "9" as a sand (Figure 17), with several modifications for organics and weak materials too (Lorenzo et al., 2014).

We combine three 1D shear-wave velocity structures of the subsurface from the Marrero study area with nearby CPTs into a new data set for cross plot analysis. Lorenzo et al. (2014) derive the 1D V_s profiles through forward-ray-trace modeling of refracted and reflected shear wave arrivals. We pair profile "S" and profile "A" from the protected side of the levee with the two nearest CPTs from the protected toe of the levee, 62PT and 64PT, respectively. We pair a third profile from the unprotected flooded side of the levee, "A'", with the closest adjacent CPT on the crest of the levee, 64CL, because 64CL and profile A' lie on the same low resistivity anomaly ranging from 950 to 1100 meters (Figure 15). We use the CPT data from 64CL starting at a depth equal to the surface of the flooded toe, 2.5 meters deep (Lorenzo et al., 2014), because 64CL lies on the crest of the levee 2.5 meters above the elevation of the seismic profile A'.

Cross-plot analysis requires matching the CPT and V_s data with a corresponding location for resistivity values. The location of 62PT and 64 PT determine the location for extracting the resistivity values (Figure 15a). The projection of 64CL on the flooded toe resistivity profile (Figure 15c) determines the location for the resistivity to use with A'.

CHAPTER 4: ANALYTICAL TECHNIQUES

(4.1) SEISMIC PROCESSING FOR DISPERSION CURVE

Seismic processing of data follows six steps (Figure 19) to create a dispersion image and invert for shear wave velocity. Cross-correlations of the raw seismic data are calculated for every pair of traces in each shot gather in order to locate where changes in the subsurface occur laterally (Hayashi and Suzuki, 2004). The five gathers generated from the same shot point are cross-correlated independently. The cross-correlation pairs from every shot-point and every gather are re-arranged into new gathers according to the mid-point between the pair of traces. These new gathers are termed Common Mid-Point Cross Correlation (CMPCC) gathers (Hayashi and Suzuki, 2004). Applying a frequency-domain wave-field transformation (Park et al., 1999) to each CMPCC gather creates dispersion images, which are representative of the velocity structure of the subsurface. Finally, the interpreted fundamental mode from the dispersion images are inverted using a direct search algorithm to determine the shear wave velocity structure of the subsurface as described in the following sections.

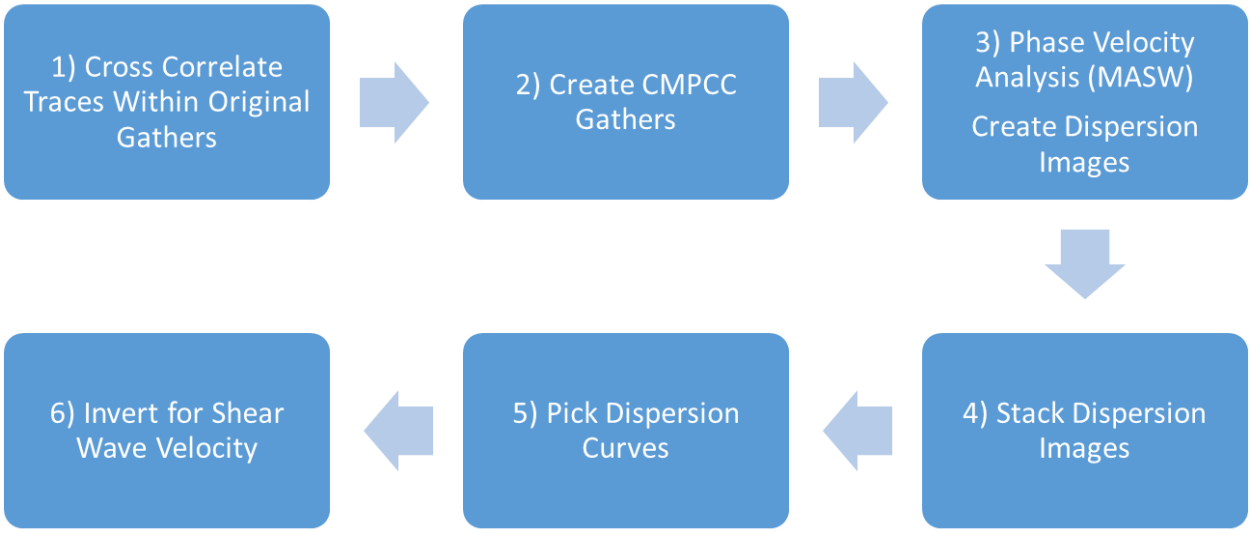

Figure 19: A flowchart of the processing scheme used to generate the dispersion curves from the raw seismic data, ending with the inversion for a 1D shear wave velocity profile. The inversion is covered in detail in section 4.2.

Seismic Unix (Stockwell, 1999) is open source software used to process seismic data to generate dispersion images (Liner, 2013). Seismic Unix (SU) was adapted using a Perl wrapper (Appendix A) to run the cross correlations and create the dispersion images. The dispersion curves were picked by hand to generate ASCII files containing points in the frequency-phase velocity domain. Several imaging, picking, and processing (i.e. gaining, header manipulation, etc.) SU programs were used, and multiple Perl wrappers were incorporated to have them function together (Appendix A).

(4.1.1) Common Mid-Point Cross Correlation

The cross correlation of the two seismic traces, $X(t)$ and $Y(t)$, containing signal from surface waves provides a measure of similarity, $m_{X,Y}(\tau)$, over all recorded times (Ikelle and Amundsen, 2005):

$$m_{X,Y}(\tau) = \sum_{t=-\infty}^{+\infty} X(t)Y(t-\tau) \tag{4.1}$$

where time lag, τ, is a set time difference between the filter trace, $Y(t)$, and a sample trace, $X(t)$, such that no time lag, $\tau = 0$s, calculates the similarity between the traces exactly as recorded. For a given seismic arrival, $m_{X,Y}(\tau)$ peaks when τ equals the time required for the seismic wave to propagate from $X(t)$ and arrive at $Y(t)$. $X(t)$ represents the trace from the receiver closest to the source. A positive time lag indicates the physically real scenario of the seismic wave propagating from $X(t)$ first to $Y(t)$. Correlation calculations use all 26 seconds of original data for time, t, and calculate $m_{X,Y}(\tau)$ for τ = -26s to $\tau = 26$s. We cross-correlate the data from each receiver with the data from every other receiver in a gather for a total of $N(N-1)/2$ possible cross-correlations, where N is the number of receivers in an array. A 23 geophone array yields a total of 253 cross-correlation pairs per gather.

Cross-correlating every trace across all times and possible time lags yields the similarity, $m_{X,Y}(\tau)$, as a seismic wave propagates from $X(t)$ to $Y(t)$, but also produces the side effect of $m_{X,Y}(\tau)$ calculations between seismic arrivals with different sources (Figure 20). For small time lags ($0 < \tau <$ ~3s), the cross-correlation between $X(t)$ and $Y(t)$ eliminates the need to separate the seismic data associated with different hammer strikes by only calculating (4.1) for seismic data associated with the same hammer strikes (e.g., Figure 13a), reducing overall processing time. However, at larger time lags the cross-correlation of the entire trace introduces what we call "cross-correlation noise". The uneven timing between hammer strikes forces seismic data associated with different hammer strikes to require different time lags in order for (4.1) to peak. Additionally, non-uniform source waveforms contribute to the mismatch, culminating in error prone $m_{X,Y}(\tau)$ values that are no better than noise.

Windowing time lag, τ, to values which only calculate (4.1) for seismic data associated with the same hammer strike excludes the cross-correlation noise, while retaining sufficient data to calculate a dispersion curve. We set the beginning of the window at $\tau = 0$s (Figure 20), because the moment of no lag aligns and sums both traces exactly as recorded, making $\tau = 0$s equivalent to $t = 0$s. When $\tau = t = 0$s the positive progression of lag and time are equivalent. We set the maximum extent for the window of usable cross-correlation data at 2s, because the hammer strikes always occur at an interval greater than 2s.

We reorganize and stack the windowed cross-correlation pairs to create Common Mid-Point Cross Correlation (CMPCC) gathers. We organize cross-correlation pairs using two properties: spacing and the common mid-point (CMP). We define spacing as the distance between two receivers that make a cross correlation pair, and the CMP is located equidistant between both receivers (Hayashi and Suzuki, 2004). A CMP can lie between two neighboring receivers or share the same position of a receiver. Cross-correlation pairs with the same spacing and CMP are summed horizontally in the time domain. We concatenate the stacked cross-correlation pairs with the same CMP into a single file known as a CMPCC gather, with traces organized by increasing spacing (Figure 21) (Hayashi and Suzuki, 2004).

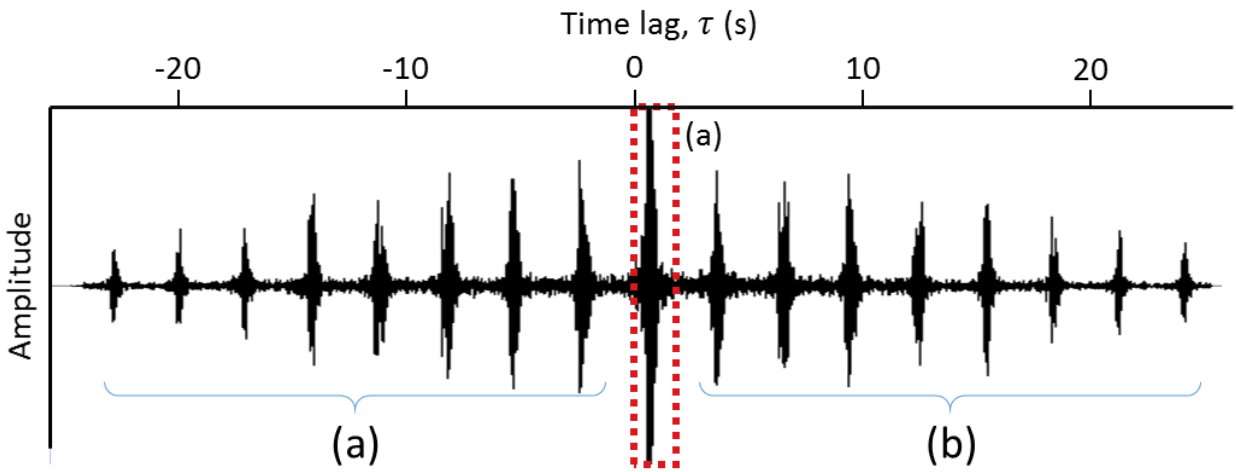

Figure 20: A typical cross-correlation from offsets 36 and 39 m, at shot point 45 m (Figure 13a) when using multiple hammer strikes per gather. The outline (a) depicts the 2s time lag window used to construct the CMPCC gathers, from $\tau = 0 - 2$s. The correlation between different hammer-strike-induced seismic waves generate "correlation noise" (b), represented by the amplitude spikes.

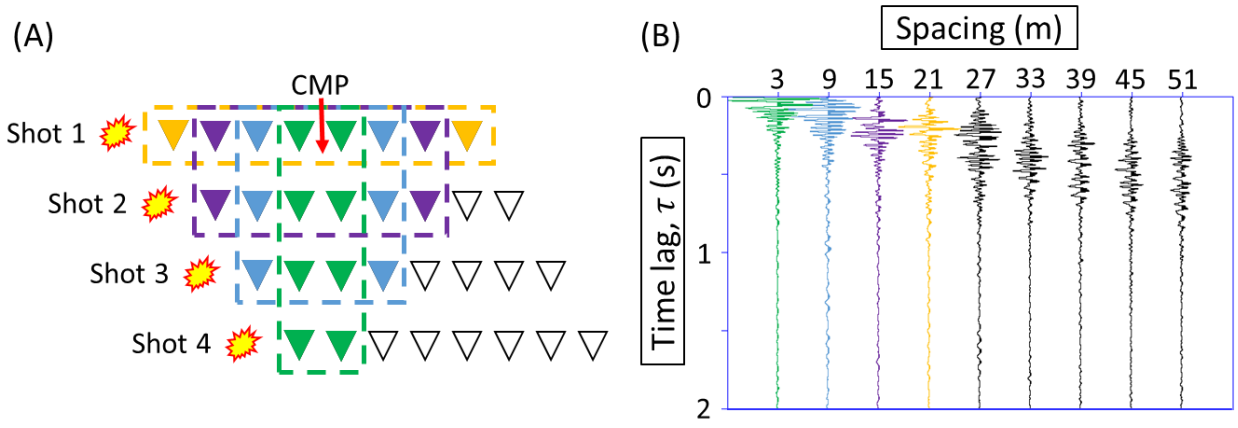

Figure 21: The concept of the CMPCC gather relies on the array geometry and a common mid-point between two receivers (A). Each color denotes a receiver pair with the same spacing and CMP, regardless of shot point. Note that a CMP sharing the same position with a receiver will produce a CMPCC with different spacing values. The CMPCC gather (B) lists the stacked and windowed cross-correlations by increasing spacing versus the time lag, τ. The color of each trace coordinates to the receiver pairs with the same spacing and CMP that create the trace.

Signal-to-noise increases with an increase in the number of cross-correlation pairs horizontally summed (Ikeda et al., 2013). The greatest number of cross-correlation pairs occur between 45 and 200 meters at the London Avenue Canal site (Figure 22). The number of cross correlation pairs are low at the beginning and end of the line because of the fixed site for the first and last geophone. CMPCC gathers closer to the flank of the survey line contain smaller receiver spacings and have lower signal-to-noise content.

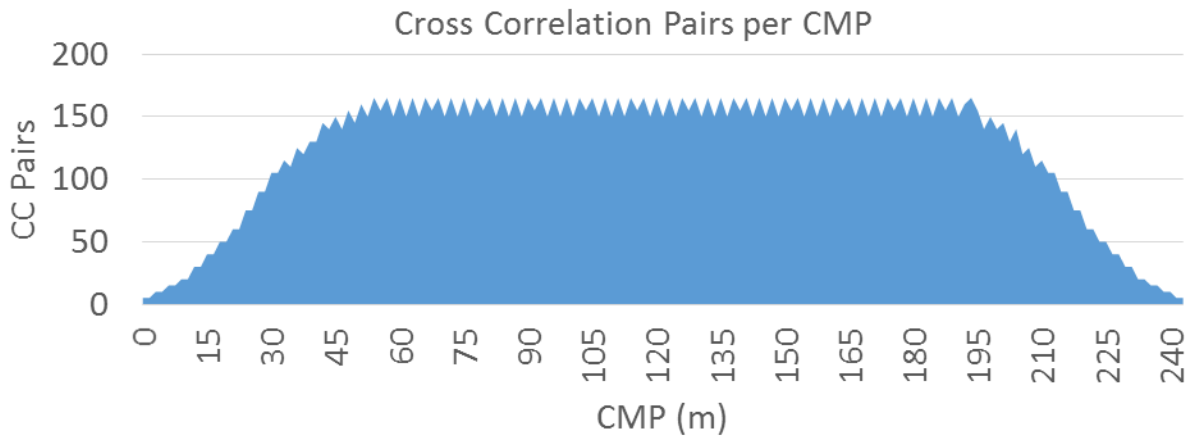

Figure 22: The number of cross correlation pairs available for each CMP for the London Avenue Canal study area acquisition line (Figure 4). By collecting 5 gathers at each shot point, we increase the amount of cross correlation pairs at each CMP five-fold.

(4.1.2) Calculation of Dispersion

We generate dispersion images using a wavefield transformation of the CMPCC gathers using the following steps from Park et al. (1998), as implemented in the program "suphasevel" (Liner, 2013). First, a Fourier transform converts the CMPCC gather from the offset-time domain, $u(x,t)$, into the offset-frequency domain, $U(x,\omega)$:

$$U(x,\omega) = \int u(x,t)e^{i\omega t}\,dt \tag{4.2}$$

Offset (x) in the offset-time domain is equivalent to spacing (x) in the spacing-time-lag domain that is used to construct the CMPCC gathers (Hayashi and Suzuki, 2004). $U(x,\omega)$ can be described by the product of the phase, $P(x,\omega)$, and amplitude $A(x,\omega)$ spectra:

$$U(x,\omega) = P(x,\omega)A(x,\omega) \tag{4.3}$$

where $P(x,\omega)$ contains time-lag information within the real and imaginary parts of each frequency component. Whereas $P(x,\omega)$ contains all phase information, $A(x,\omega)$ encapsulates the information related to amplitude, such as attenuation and spherical divergence (Park et al., 1999). Park et al. (1998) rewrites (Equation 4.3) as:

$$U(x,\omega) = e^{-iK_\omega x}A(x,\omega) \tag{4.4}$$

where the angular wavenumber, K_ω, is the ratio of angular frequency, ω, to phase velocity, c_ω:

$$K_\omega = \frac{\omega}{c_\omega} \tag{4.5}$$

Using an assumed phase velocity to calculate an assumed angular wavenumber, k, a new integral transformation applied to $U(x,\omega)$ (Equation 4.4) creates a dispersion image in the wavenumber-frequency domain (Park et al., 1998):

$$V(\omega,k) = \int e^{-ikx}\,[U(x,\omega)/|U(x,\omega)|]dx = \int e^{-i(K_\omega - k)x}\,[A(x,\omega)/|A(x,\omega)|]dx \tag{4.6}$$

where the transformation equally weights the wavefields from different spacings by normalizing the amplitude portion of $U(x,\omega)$ in (4.6) with respect to the spacings by $A(x,\omega)/|A(x,\omega)|$. Normalizing amplitudes compensates for geometrical signal losses like attenuation and spherical divergence. Additionally, the phase portion of (4.4) combines with the complex exponential of the integral transformation. We assume phase velocities ranging from 60 to 400 m/s and limit the frequencies examined to less than 60 Hz.

For a given velocity the integral transformation essentially sums the wavefield contribution from each trace, over the spacing of all traces, for each frequency. Substituting (4.4) into (4.6) creates the dispersion image, $V(\omega,k)$, which will have a maximum for a given ω if

$$k = K_\omega \tag{4.7}$$

because $A(x,\omega)$ is always both both real and positive. Therefore, whenever the assumed phase velocity generates the condition (4.7), it means the seismic wave traveled with that frequency and phase velocity over the spacing. Complete dispersion plots are calculated for all possible phase velocities, c, and frequencies by substituting (4.5) and (4.7) into (4.6):

$$I(\omega,c) = \int e^{-i\omega\left(\frac{1}{c_\omega}-\frac{1}{c}\right)x}[A(x,\omega)/|A(x,\omega)|]dx \tag{4.8}$$

where $I(\omega,c)$ is a function that defines the dispersion of the surface wave in the frequency-phase velocity domain. The spacing-dependent phase shift of the wavenumber allows for the inclusion of a multichannel array data to create the dispersion curves (Park et al., 1998). Several independent-amplitude peaks for $I(\omega,c)$ can form for a single phase velocity when higher order modes follow the fundamental mode of a surface wave, resonating at higher frequencies (Xia et al., 2003). An interpretation of the dispersion images of $I(\omega,c)$ for each CMPCC yields a dispersion curve that can be inverted for shear-wave velocity.

(4.1.3) Stacking Dispersion Images

Two different CMPCC gather spacing patterns can be created from the same acquisition geometry depending on the defined location of the midpoint (Figure 23). The first spacing pattern forms when the CMP is located between two neighboring receivers. The initial spacing between the nearest receivers is 3 m, with cross-correlation pair spacing incrementally increasing by 6. The second spacing pattern forms when the midpoint and a receiver occupy the same position. Whereas this second spacing pattern maintains the incremental increase of 6 m, the initial spacing between the first cross correlation pair is 6 m.

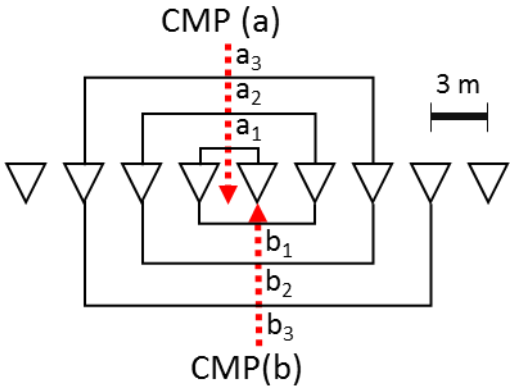

Figure 23: A CMPCC gather can possess two different spacing patterns depending on whether the center of a CMPCC gather occupies the space between receivers or the same location of a receiver. For the first spacing pattern (a), the spacing between traces are 3, 9, and 15 meters for a_1, a_2, and a_3, respectively, such that $a_n = 6n-3$. The spacing between traces for the second spacing pattern (b) are 6, 12, and 18 meters for b_1, b_2, and b_3 respectively, such that $b_n = 6n$ meters.

Combining the different CMPCC gather geometries into a single dispersion image increases the signal-to-noise ratio. The increase occurs because the combination of the two gather geometries is effectively a decrease in receiver spacing for a traditional MASW data acquisition. A decrease in receiver spacing for a fixed length improves the resolution of the dispersion plot by narrowing the width of the curves Park et al. (2001). Since different spacing between receivers sample different wavelengths and frequencies (Rix and Leipski, 1991), combining the two CMPCC gather geometries into a single dispersion plot improves the curves at a greater frequency density.

We calculate dispersion plots for neighboring CMPCC gathers, each with different spacing patterns and horizontally sum them (Figure 24). Stacking the dispersion images results in a new 3 m spacing between stacked CMPCC gathers. The decrease in lateral resolution improves the dispersion images, allowing for easier interpretations of the fundamental mode of the dispersion curve.

(4.1.4) Picking Dispersion Curves

An interpretation of a dispersion plot (Equation 4.8) distinguishes the fundamental mode from higher order modes (Figure 25). The fundamental mode of a Rayleigh wave is the smallest frequency able to propagate in a layered earth (Scholte, 1947). Higher order modes resonate at greater frequencies than the fundamental mode, and generally exhibit the weaker peaks (Xia et al., 2003). The picks of the fundamental mode are made using an interactive program (Appendix A). Picks are saved as an ASCII file containing frequency-phase velocity coordinates. The ASCII file is exported into the *Geopsy* inversion program, *Dinver* (Wathelet, 2008) (Appendix B). Curves are saved as a *Geopsy*-specific "*.target*" file. The inversion software requires the binary "*.target*" files to operate properly.

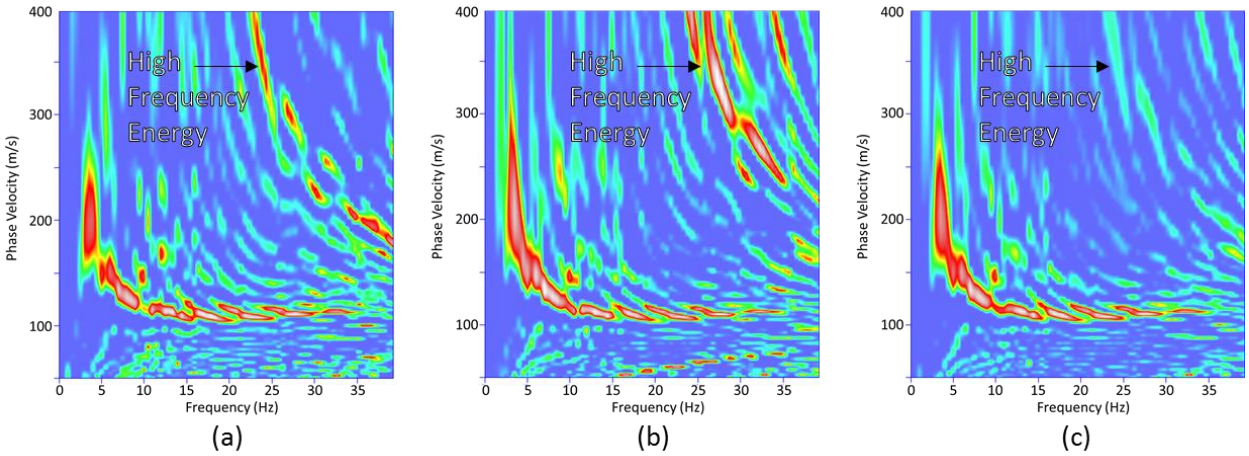

Figure 24: Dispersion images for the CMPCC gathers centered at 67.5m (a) and at 69m (b). In both images, the high frequency energy unassociated with the fundamental mode in the upper right are clearly visible. Stacking (summing) the two dispersion images (c) yields greater signal at 10 Hz, and eliminates much of the non-fundamental mode noise. Stacking more than 2 dispersion curves produced no interpretable difference.

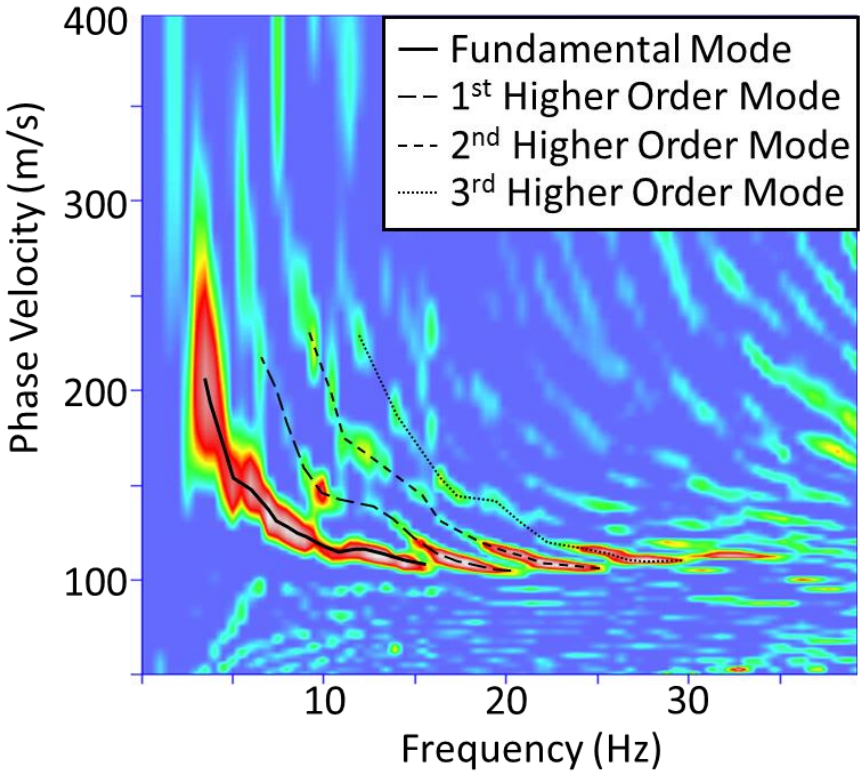

Figure 25: The fundamental mode of the stacked dispersion plot (Figure 24 [c]) is stronger than those of the higher order modes. The higher order modes are typically harmonic multiples of the fundamental mode. Mis-interpretation of a higher order mode as the fundamental mode introduces errors into the inversion for shear wave velocity by suggesting higher velocities at a given depth than the fundamental mode indicates (Xia et al., 2003).

(4.2) INVERSION OF DISPERSION CURVE FOR VS

We invert the dispersion curve files for 1D shear wave velocity profiles using the inversion package, *Dinver* in the open-source software, *Geopsy* (Wathelet, 2008). *Dinver* conducts a direct search inversion, generating models of the subsurface that could produce the dispersion curves picked from surface wave seismic data. A walkthrough of the Perl wrappers used to analyze dispersion curves in bulk and automatically output 1D shear wave velocity models is detailed in Appendix B.

A direct search inversion of parameter space determines the lowest misfit dispersion curve, from which a shear wave velocity model of the subsurface is constructed. A neighborhood algorithm (Sambridge, 1999) guides the inversion to conduct a global search of the following parameters that influence the dispersion curve: Vs, layer thickness, Vp, Poisson's ratio, and density. The neighborhood algorithm varies a single parameter and calculates the misfit of each tested model. If a change in the parameter reduces misfit, the new model becomes a starting point to test another parameter. If the misfit increases, the new model is dropped, and the original starting model is used to vary a different parameter instead (Sambridge, 1999).

The misfit function is a calculation of the difference between the experimental data and the calculated dispersion based on the tested model. The Dinver inversion program defines misfit based on Wathelet et al. (2004):

$$misfit(\omega) = \sqrt{\sum_{i=0}^{n_f} \frac{(c_{di} - c_{ci})^2}{\sigma_i^2 n_F}} \tag{4.9}$$

where the interpreted phase velocity of the stacked dispersion curve, c_{di}, is used for each frequency, ω_i. The phase velocity of the calculated dispersion curve, c_{ci}, corresponds to the same frequency, ω_i. The uncertainty of the frequency samples considered is σ_i, and n_F is total the number of frequency samples considered. If no uncertainty is provided, σ_i is replaced by c_{di} in (Equation 4.9) (Wathelet et al., 2004).

(4.2.1) Inversion Constraints from Prior Site Knowledge

The geophysical parameters that influence the dispersion of a surface wave are shear wave velocity, layer thickness, density, Poisson's ratio, and compressional wave velocity. The parameter limits for each tested model remain constant during the direct search inversion (Table 3). Each CMPCC uses the same parameter limits. Shear wave velocity of the subsurface dominates the dispersive effect of surface waves (Wathelet, 2008); therefore the optimal thickness for shear wave velocity that minimizes misfit determines the thickness of each model layer. Linking thickness parameters reduces the number of testable models for the direct search inversion, thereby increasing inversion speed.

The limits for compressional wave velocity (Table 3) do not guarantee an accurate fit of the dispersion curve. Xia et al. (1999) show that a 25% change in Vp yields a 3% change in phase velocities in a dispersion curve. A similar 25% change in Vs and density yield ~40% and 10% changes, respectively. Vp contributes negligible effect on calculated phase velocities in unconsolidated soil environments, allowing for a large range (Table 3) of permissible Vp values

(Wathelet, 2008). The relationship between Vs and Vp from Poisson's ratio determines acceptable extrema for Vp.

Table 3. Parameter Ranges for Models of Calculated Dispersion Curves

Parameter	Minimum	Maximum	Thickness Linked to:
Compressional Wave Velocity	100 m/s	2200 m/s	Vs
Poisson's Ratio	.33	.49	Vs
Shear Wave Velocity	50 m/s	250 m/s	Not linked
Density	1600 kg/m^3	1800 kg/m^3	Vs
Thickness	2 m	See Table 4	N/A

We constrain the range of values for Poisson's ratio by examining Vp-Vs ratios. Seismic evidence from the Marrero study area constrains the range for Vp-Vs ratios from 4 to 9 in the mixed soil conditions of the swamp and marsh depositional environments (Lorenzo et al., 2014). The range of values for the Vp-Vs ratio agree with laboratory tests of saturated and unsaturated sands (Zimmer et al., 2002). The consolidated Pleistocene clays require consideration, because their shallow burial depth at the LAC study area could affect the velocity of the half-space. The Pleistocene Prairie formation possesses a greater shear modulus and shear wave velocity than the overlying Holocene sediments (IPET, 2007). The higher shear wave velocity could lower Vp-Vs ratios (Mavko et al., 2009), assuming any increase in Vs contributes a larger influence on the Vp-Vs ratio than an increase in Vp. We assume a lower limit of 2 for Vp-Vs ratios for the Pleistocene clay. The values of the constrained Vp-Vs ratio range correspond to a Poisson's ratio of .33 to .49 (Mavko et al., 2009).

Geotechnical data from the London Avenue Canal study area provide maximum and minimum constraints for the density and velocities values used in the inversion process. Wet density values collected from boring logs B-32 and LUG-3 (USACE, 1989b) indicate in-situ densities of 1600-1800 kg/m^3. The cone penetration test nearest to the London Avenue Canal study area, LECPT-46PT (Figure 17) provides an in-situ maximum shear wave velocity of 250 m/s and a minimum of 50 m/s.

(4.2.2) Layer Thickness Calculation

The wavelength of a Rayleigh wave influences the Rayleigh wave's penetration depth, thereby affecting the resolvable thickness of the first layer (Stokoe et al., 1994). The penetration depth of a Rayleigh wave equals its wavelength (Park et al., 1999), but reasonable calculations for Vs commonly range to depths between half (Stokoe et al., 1994) and a third (Heisey et al., 1981) of the observed wavelength. Attempts to calculate shear wave velocity above or below this depth lead to higher variance in layer thickness models (Rix and Leipski, 1991). Stokoe et al. (1994) built upon the depth-wavelength approximation by showing that the minimum observed wavelength, λ_{min} determines the minimum calculable Vs layer thickness for the first layer, H_{min}. Applying the lower bound wavelength-depth relation from Heisey et al. (1981), H_{min} is approximated as:

$$H_{min} = {}^{1}/_{3}\,\lambda_{min} = {}^{1}/_{3}\,{}^{c_{min}}/_{f_{max}} \tag{4.10}$$

where c_{min} is the minimum corresponding phase velocity for the maximum observed frequency of the fundamental mode (Park et al., 1999). H_{min} represents the smallest possible layer thickness of the first layer; we assume that deeper layers thinner than H_{min} cannot be resolved.

Near-field effects, such as interference with body waves, limit the ability for a Rayleigh wave to begin propagating as a plane-wave (Park et al., 1999). Surface waves begin plane-wave propagation when the source-to-first-receiver offset, x_1, exceeds half the largest desired wavelength, λ_{max}, (Stokoe et al., 1994):

$$x_1 \geq \frac{1}{2}\lambda_{max} \tag{4.11}$$

The criteria of (Equation 4.11) suggests that the maximum observable wavelength of a surface wave exhibiting plane-wave propagation is double the source-to-first-receiver offset, which for our study is 24 meters.

(4.2.3) Layer Thickness of Velocity Models

Interpretation of the fundamental mode dispersion curve decides the minimum phase velocity and maximum frequency of the Rayleigh wave, thereby determining the minimum resolvable thickness of the first layer, H_{min}. We use an interpreted stacked dispersion curve representative of the LAC dispersion images (Figure 25) to determine a minimum phase velocity of ~100 m/s and maximum frequency of ~15 Hz. Applying (Equation 4.10) to these values approximates H_{min} as ~2m. We limit the direct search inversion to a minimum thickness of 2m for all layers with the assumption that deeper layers thinner than H_{min} cannot be resolved.

We estimate the range of penetration depths to be 12-25 meters. The penetration depth of the Rayleigh wave determines the calculable depth for shear-wave velocity. A Rayleigh wave travels 12m (Table 1) from the shot location to the nearest-offset geophone for the LAC survey. Applying (Equation 4.11) suggests a maximum wavelength of 24 m, which limits calculable depth for shear-wave velocity to 12 m (4.11). However, the geophones at far offsets do not experience the body wave interference and only detect Rayleigh waves propagating as plane-waves (Park et al., 2001). The smallest frequency and largest shear-wave velocity observable on a typical dispersion image (Figure 25) are ~3 Hz and ~225 m/s, respectively. Therefore the maximum observable wavelength from the data is 75m, which makes a depth of 25 m the maximum calculable depth for shear-wave velocity (Heisey et al., 1982).

The assumed minimum layer thickness and maximum penetration depth limit possible layer thicknesses between 2 and 7 meters for the models created by the direct search inversion. We use a five-layer model over a half-space as the base model. The inversion optimizes all parameters for each layer in the base model in order to match the interpreted dispersion curve. A five layer model allows for the algorithm to generate a model—with minimum thickness of 2 m for each layer—to match the 10 m of available resistivity data from the CCR experiment. However, we expect some thicker layers. We increase the maximum thickness of each layer for each deeper layer (Table 4) in order to reach the maximum calculable depth of 25 m, while

forcing most layers to focus on optimizing parameter space in the upper 10 meters. Ultimately, constraining the maximum thickness of any model layer does not matter, because if the true layer is thicker, then the underlying model layer will possess the same properties, effectively creating one large layer (Xia et al., 1999).

Table 4. Inversion Model Layer Thickness Constraints

Layer	Minimum	Maximum	Measurement
Initial (H_0)	2 m	3 m	Bottom Depth
H_1	2 m	4 m	Thickness
H_2	2 m	5 m	Thickness
H_3	2 m	6 m	Thickness
H_4	2 m	7 m	Thickness
Half-Space (H_5)			

(4.2.4) Neighborhood Inversion through Parameter Space

We standardize the direct search inversion process for all interpreted dispersion curves in order to determine the model that best matches the interpreted curve. The inversion creates 5000 initial models based on a Markov-Chain (Smith and Roberts, 1993) random walk (Figure 26) using the first valid model created as a seed for the remaining models (Wathelet, 2008). Voronoi cells are created around each starting model, such that the number of models sampled, known as the sampling density, is constant in each cell (Sambridge, 1999). Multiple iterations of the Markov-Chain walk improve upon the existing models.

The misfit between the calculated dispersion curve and the interpreted dispersion curve quantifies the validity of each test model, with the inversion minimizing the misfit (Equation 4.9). The 500 models with the lowest misfit are allowed to explore parameter space under the neighborhood algorithm (Wathelet, 2008), testing each parameter to find a lower misfit. The neighborhood algorithm tests each parameter within the original Voronoi cells until a smaller misfit is found (Sambridge, 1999). When a lower misfit is found, a new Voronoi cell is established and the boundaries redrawn.

Each iteration of the inversion creates 500 new models, which the predetermined areas of misfit minima. A new, random, and valid model acts as an initial seed to create an additional 500 models, totaling 1,000 models per iteration. The even split between exploration of local minima and new models better suits the search for a global minimum in the parameter space of a five layer model (Sambridge, 1999). Voronoi cell density increases in areas with the greatest probability of finding the global misfit minimum. Wathelet (2008) recommends 10^4 valid test models for a 4 layer inversion. In our case, improvements to misfit per model approach a near negligible level around $2x10^5$ valid models. Therefore we assume $2x10^5$ valid test models to be sufficient for the additional layer. We run 200 iterations with 1,000 models per iteration for the inversion to generate $2x10^5$ models within parameter space for each original stacked CMP, not including the initial models.

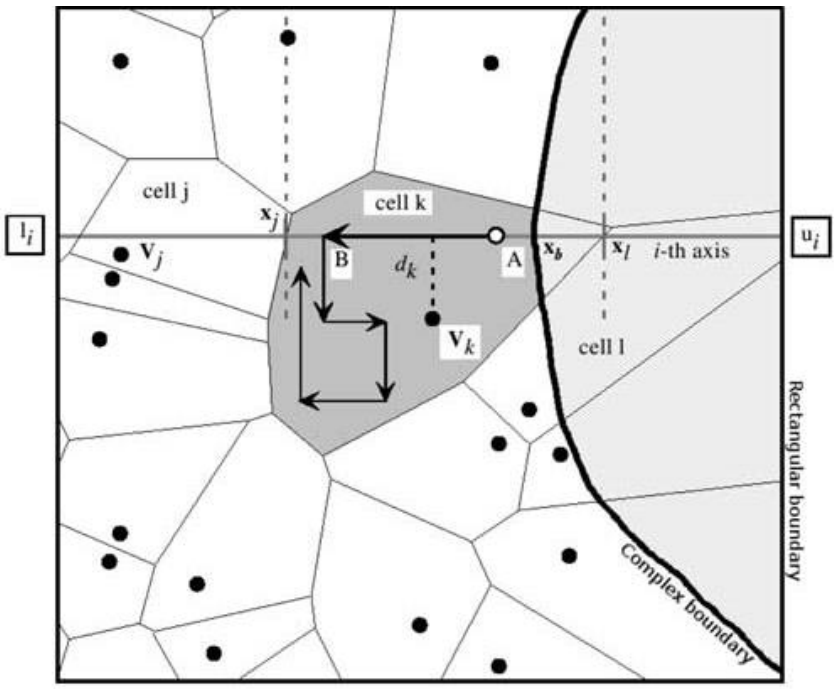

Figure 26: The image depicts the Markov-Chain random walk confined within a Voronoi cell and two other boundaries. The rectangular boundary has limits for each parameter (Table 3), where l_i and u_i represent the lower and upper limits, respectively, for the parameter on the i-th axis. The complex boundary (x_b) results from linking different parameters (i.e. V_p and V_s via Poisson's ratio). Voronoi cells establish the region around the valid test models (black dots) from which the Markov-Chain walk begins. The cell limits (e.g. the boundaries with cell j and cell l: x_j and x_l) ensure that the new test model will form within a known area of low misfit. The neighborhood algorithm tests each parameter at least once before the random walk ends and can return a new valid model (Wathelet, 2008).

The low-misfit models converge on a single velocity structure when representative of the true velocity structure (Wathelet, 2008). The best 1000 models with the lowest misfit are extracted from the inversion report in order to generate a representative velocity structure for the CMPCC gather (Figure 27). A 1-meter reporting interval of velocity values allows for the identification of changes in the velocity structure, whereas larger reporting intervals may miss the actual depth at which velocity increases. The uncertainty of the depth range for which a reported velocity applies increases with increases in reporting interval. Smaller intervals do not provide additional information of the velocity structure when deviations are considered due to the 2 m minimum thickness in the inversion parameters.

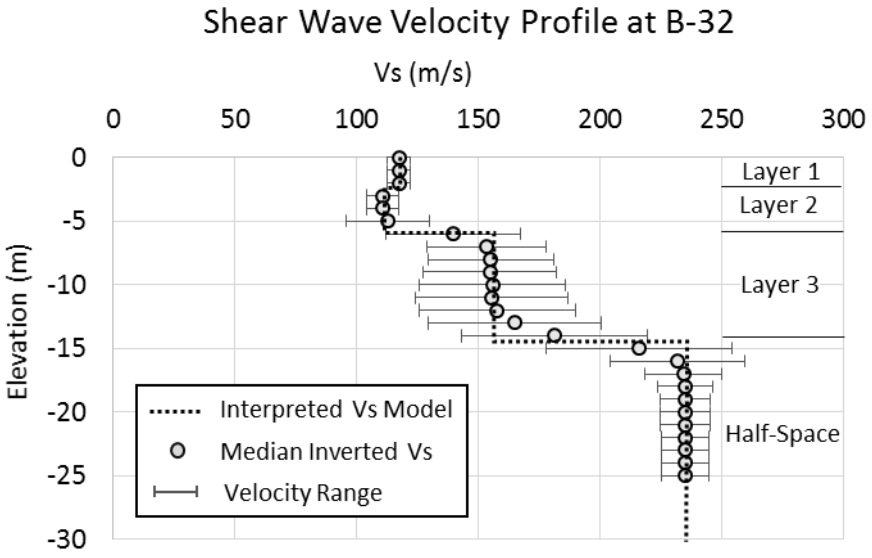

Figure 27: The inversion of the dispersion curve interpretation generates a shear wave velocity profile for the drill site of boring B-32. *Dinver* computes the median velocity for every meter between the surface and 25 m depth (Wathelet, 2008). The bars through each point represent the range of velocities from the best 1000 models comprising the 1D velocity profile. This three-layer model exhibits a velocity reversal at 3-5 meters, where the high velocity layer (1) overlies a lower velocity layer (2). Layer 3 comprises the remaining parameter layers, creating a single 10 meter velocity layer of ~150 m/s. We interpret the high velocity half-space below 15 meters as the Pleistocene clay.

(4.3) SHEAR-WAVE VELOCITY PROFILES (INTERPOLATION)

The inversion process generates outlier 1D shear wave velocity profiles for several of the CMPCC gather dispersion curves. The velocities of outlier profiles vary by over 50 m/s compared to neighboring profiles, and do not make geological sense typically because discontinuous low-velocity zones at the depth of the Pleistocene clays should not exist. A pseudo-2D shear wave velocity profile (Figure 28a) allows for easy visual identification of lateral discontinuities and large velocity reversals from the outlier models. We form data files containing position, depth, velocity, and velocity ranges by exporting profiles from *Geopsy* and concatenate profiles in Excel. The plotting program Surfer (Golden Software, 2013) uses the file to interpolate velocities between each CMPCC.

Multiple interpolation methods can generate pseudo-2D shear wave velocity profiles, but kriging (Cressie, 1990) and inverse distance weighting (IDW) (Zimmerman et al., 1999) interpolations provide the only geologically sound profiles. The kriging interpolation method preserves the local heterogeneities and velocity reversals of each profile, while still creating an interpretable profile. The IDW interpolation smooths neighboring profiles together, averaging out heterogeneities in the process. The IDW interpolations lose too much of the original 1D profiles, making the kriging interpolation preferable. The kriging based interpolation uses a sampling grid of 3 meters in the horizontal direction to match spacing between stacked CMPs, and the 1 meter sampling grid in the vertical direction to match the shear wave velocity profiles.

Applying the same kriging interpolation to the velocity ranges (Figure 27) for each profile generates a 2D profile. The velocity range profile aids in the identification of outlier 1D

velocity profiles to exclude from the interpolated 2D velocity profile. The two main areas containing the largest velocity ranges (Figure 28 [b]) exist on the edges of the survey. These areas contain low numbers of cross-correlation pairs (Figure 22). A new velocity profile (Figure 29) results from the exclusion of low cross-correlation pair areas and the removal of several anomalous profiles with large deviations outlined in Figure 28 [b]. The new 2D pseudo velocity profile exhibits a general 3-layer model.

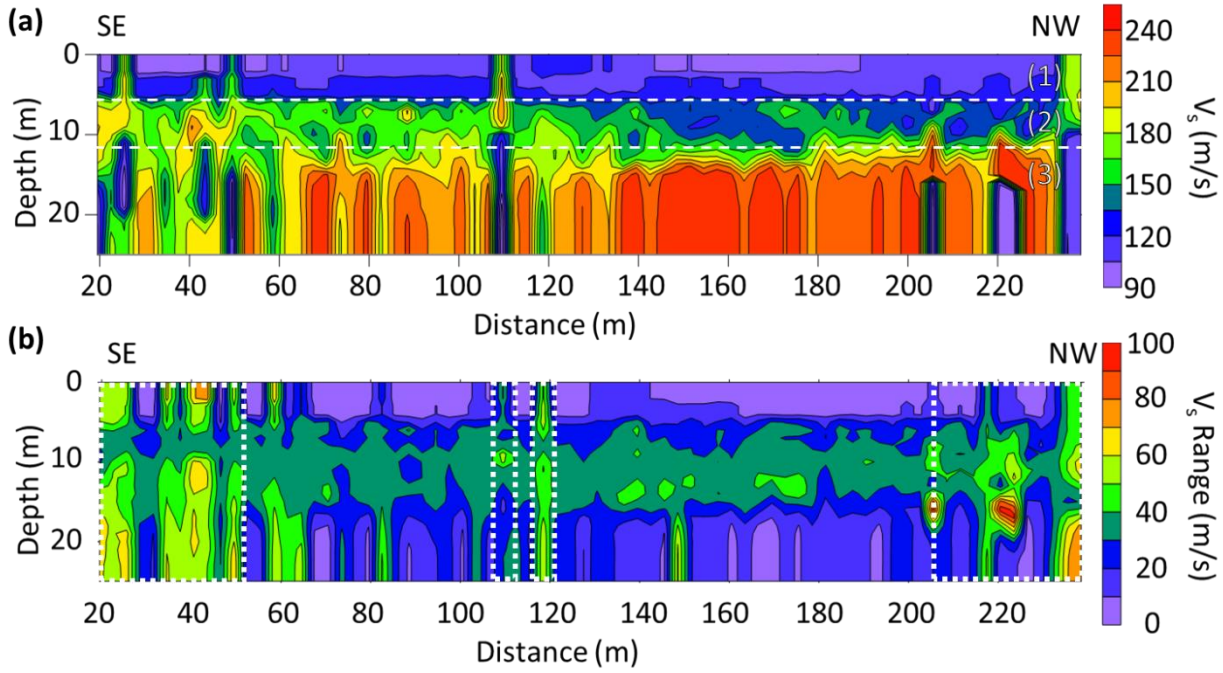

Figure 28: The kriging based interpolation of the shear wave velocity profiles from *Geopsy* (Wathelet, 2008). The pseudo-2D shear wave velocity profile (a) exhibits a general 3-layer trend, with velocity increasing with depth. The largest ranges of shear wave velocity (b) are contained in two areas on the periphery of the survey. Additionally, several outlier profiles with anomalously large velocity ranges in the upper 5 meters exist centered at approximately 106 and 120 meters.

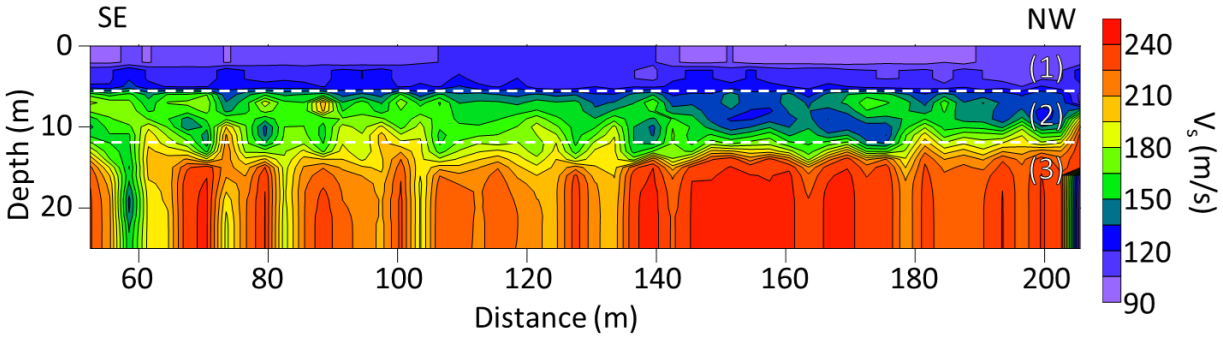

Figure 29: Eliminating the 1D profiles that show large velocity ranges or possess less than 150 cross correlation pairs (Figure 22) improves the pseudo 2D shear wave velocity. The improved profile and original pseudo 2D profile exhibit the same 3 layers. Layer 2 contains a low velocity zone from 140 to 180 m along the profile.

(4.4) SOIL TYPE ESTIMATION

The empirical model developed by Hayashi et al. (2013) for levee foundations relates soil type to resistivity and shear wave velocity in saturated conditions (1.1). Henceforth, the term "Hayashi model" refers to the Hayashi et al. (2013) empirical model for estimating soil type of foundation soils from resistivity and shear wave velocity. We interpret the LAC data using the Hayashi model, with the assumption that the underlying soils are saturated. The resistivity survey provides data down to only 10 meters. Although shallow, this depth of penetration ensures that the bottom layer reached is the Pine Island Beach Trend, but the underlying high velocity Pleistocene clays are not sampled. The Hayashi model indicates that grain size coarsens with depth (Figure 30).

The Hayashi model does not distinguish silt from clay or sand. However, the dominant sediment type identified by boring logs (USACE, 1989b) at the LAC site is silt. The Hayashi model requires modification to be useful in the Louisiana Coastal Zone, where silt is a significant soil type. A new model should be generated by running a similar least squares regression using geophysical and geotechnical data available along the New Orleans levees.

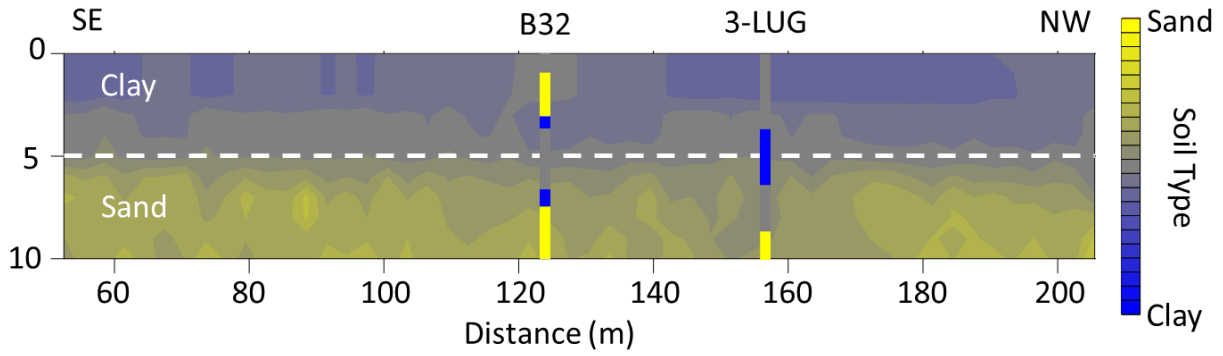

Figure 30: The Hayashi model applied to the resistivity and shear wave velocity data from the London Avenue Canal study area estimates the soil type. Two distinct layers are identifiable. A predominantly shallow clay layer transitions to a predominantly sand layer at 5 meters.

(4.5) CROSS-PLOT ANALYSIS

The data from the LAC study area provides the larger set of geophysical data and boring logs to use for identifying the link between resistivity, shear wave velocity, and soil type. The 1-meter depth sampling from the 1D shear wave velocity profiles is the coarsest sampling interval, and therefore acts as a guide to match with resistivity and soil type. The 1-meter-sampling interval produces 11 data points each for the boring log B-32 and 3-LUG, from the surface to the bottom of the resistivity profile at 10 meters.

A cross-plot of the LAC data for all sediment types (Figure 31) shows that grain size increases as resistivity decreases and shear wave velocity increases. The original soil type descriptions based on the Unified Soil Classification System (ASTM, 2011) are re-interpreted based on the dominant soil type present (Figure 16). We use 3 soil types to classify clay, silt, and sand. The LAC data show a possible initial trend in contradiction with the Hayashi model, where grain size decreases as resistivity increases. Unfortunately, only 4 of the 22 data points at the LAC site were recorded as sand. More examples of sand and clay are necessary to definitively identify any trends.

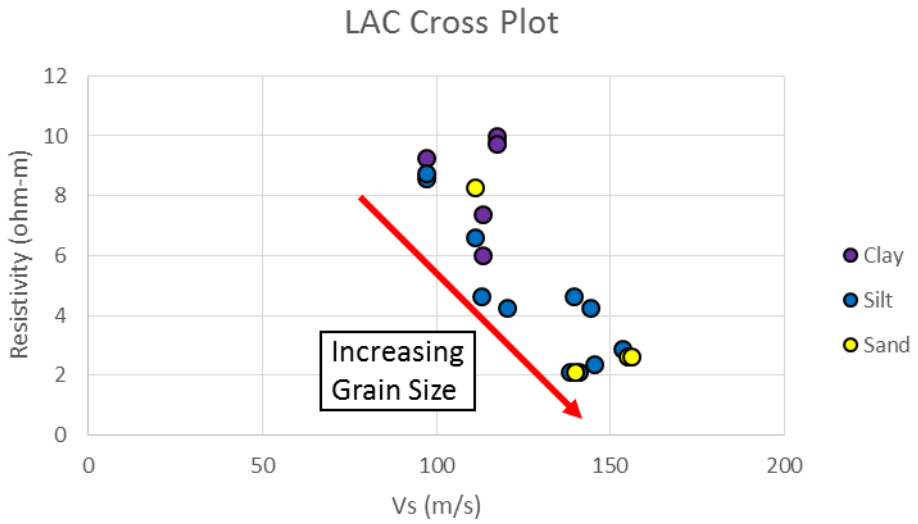

Figure 31: A cross plot of the geophysical data from the toe of the London Avenue Canal levee shows a possible trend of increasing grain size from resistive, low shear wave velocity clays to low resistivity, high shear wave silts and sands.

The Marrero "V-line" levee provides another location to analyze readily available geophysical and geotechnical data to test the relationship between electrical resistivity, shear wave velocity, and soil type. We compile the shear wave velocity profiles from Lorenzo et al. (2014) and the capacitvely coupled resistivity profiles with the simplified soil behavior types from CPT data (FFEB, 2007) into a cross plot (Figure 32). The "V-line" data indicate a possible trend of grain size decreasing with increasing resistivity. The trend is similar to the LAC trend, but less dependent on resistivity and heavily influenced by shear-wave velocity.

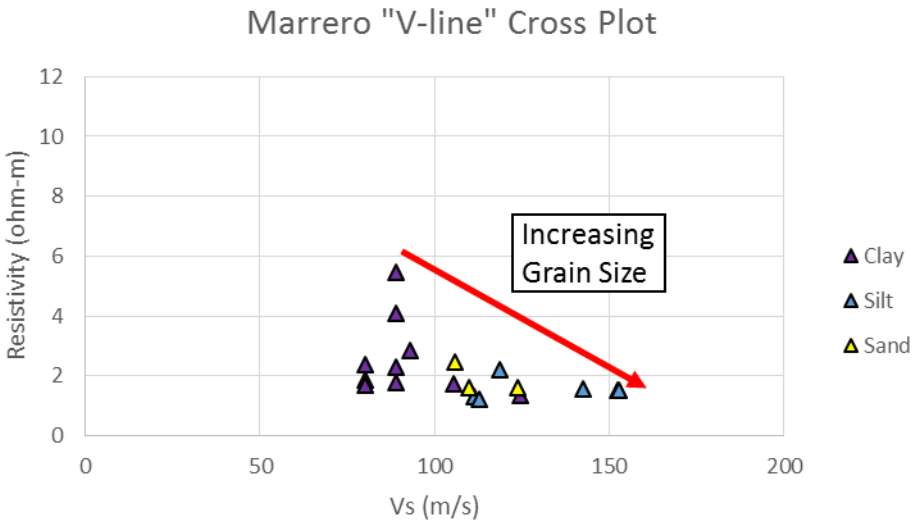

Figure 32: A cross plot of the geophysical data from the Marrero "V-line" levee indicates shear waves propagate faster in silts and sands than clays. Similar to the cross plot of LAC data, a trend of decreasing resistivity with increasing grain size is noticeable, but not as emphasized. However, the resistivity of the LAC surpasses the resistivity values for the Marrero study area.

(4.6) MODIFIED SOIL TYPE APPROXIMATION FROM GEOPHYSICAL METHODS

We create a new polynomial expression, based on the Hayashi model, to fit the geophysical and soil samples from the LAC and Marrero "V-line" levee study sites. We preserve the form of the polynomial expression (4.12) from the Hayashi model. We modify the soil type integers in the polynomial expression, S, from 2 to 3 for sand and introduce 2 as silt. Clay remains as 1.

$$S = av_s^2 + bv_s + c\left(log_{10}(\rho)\right)^2 + dlog_{10}(\rho) + ev_s^2 log_{10}(\rho) + fv_s\left(log_{10}(\rho)\right)^2 + gv_s log_{10}(\rho) + h \quad (4.12)$$

A least-squares regression through the data from LAC and the Marrero "V-line" study areas determines new coefficients, a through h, for (4.12). We conduct a least-squares regression using the Data Analysis program within Microsoft Excel (2013). We run regression analyses on the LAC data, the Marrero data as well as on a combined dataset from both survey sites (Table 5). The resultant surface approximates the likelihood of encountering a given soil type based on a set of Vs-resistivity coordinates.

The least-square regressions show a weak correlation ($R^2 \cong .5$) between shear wave velocity, electrical resistivity, and soil type. The cross-plot of the combined dataset from both sites (Figure 33) suggests shear wave velocity increases as grain size increases. Even though most sands exhibit lower resistivity values than clays, the abundance of silt across many resistivity values at the same velocity weakens the correlation between soil type and resistivity. The coefficient in the regression supporting resistivity, 'd', changes from positive to negative depending on whether we use the Marrero data set or one of the others (Table 5). If a change in saturation influences the resistivity data, then a correlation between depth and resistivity should be observed (albeit weak), assuming saturation changes with depth.

Table 5. Optimized Coefficients of (4.12) for LAC, Marrero, and a Combined Dataset

Dataset	LAC	Marrero	Both
a	-0.00018	-0.00111	-0.0001229
b	0.044573	0.193288	0.00253185
c	9.142055	33.00619	27.8777762
d	-11.7488	3.981299	-38.224711
e	-0.00031	0.003906	-0.0009707
f	-0.09955	-0.32978	-0.265452
g	0.154217	-0.43991	0.46281306
h	-0.99241	-6.26332	3.04140512
R^2	0.425966	0.54277	0.47923997

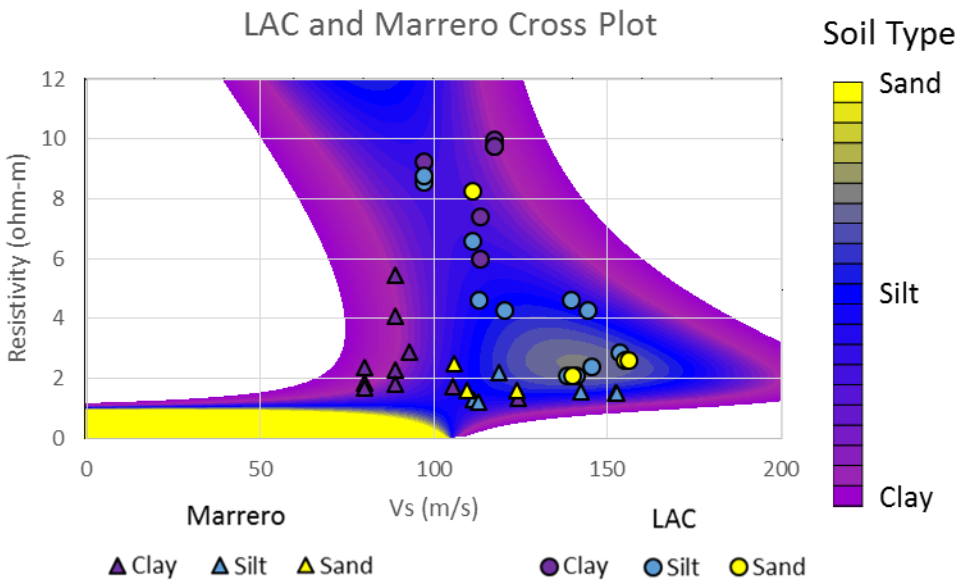

Figure 33: A cross plot using geophysical data from the Marrero (Figure 32) and LAC (Figure 31) study sites represented as triangles and circles, respectively. A best-fit polynomial surface to both data sets (Table 5) to (4.12) generates the contoured surface of soil type. An outlier zone is predicted from the best-fit polynomial surface within the low-velocity, low-resistivity sand zone (lower left corner of the graph) straddling the region between the origin to 100 m/s and 1 ohm-m, However, this outlier zone does not match any of the physical data or model.

(4.7) EFFECTS OF DEPTH ON RESISTIVITY

Resistivity is driven by the electrical properties of the sediment grains, the packing arrangement, and most importantly, the saturating fluid (Archie, 1942). The effect of the saturating fluid on the resistivity of the soil depends on the air-to-fluid ratio in the pore spaces and the pore fluid composition (Samouëlian et al., 2005). Since electrical current flows along ionic pathways, the amount of dissolved ions in the pore fluid determines the resistivity of the fluid. If saturation increases with depth, then the amount of dissolved ions in the soil increases, which decreases the overall resistivity.

Soil types on a depth-resistivity cross-plot indicate a general trend of decreasing resistivity with greater depth (Figure 34). Below a depth of 3 meters, clay soils are less resistive than the silt and sand soils when compared at equal depths. Below 3 m, sand and and silt soils tend to show a similar resistivity. Regardless of the depth of the comparison, the magnitude of resistivity values from the Marrero study site are smaller than the values from the LAC study area.

The relationship between soil type and resistivity may depend on the environmental conditions of the survey area. For instance, the protected toe of the LAC levee resides 3 meters above the water level in the canal, which is the same depth at which resistivity values decrease. Soil saturation may increase with depth as a result of the shallow hydraulic head.

The change in water content between soil types with depth, 28% for sand compared to 56% for clay, could contribute to the observed differences in resistivity. The measured water content from LUG-3 and B-32 for sand averages 28.2$\pm$3.2% across depths of 2.4-13.4 meters,

whereas clay averages 56.2±6.2% across depths of 3.4-15.8 meters (USACE, 1989b). The boring logs record the maximum water content for clay as 66.4% at 3.4 m depth. Unfortunately, no information exists detailing the water level in the canal. Water content increases with depth in sand, which conflicts with the Hayashi et al. (2013) assumption of a fully saturated foundation soils. However, water content does not equate to saturation. The effect of saturation on the resistivity of a soil type can be calculated assuming tortuosity and grain composition if saturation and porosity measurements are takenduring the resistivity survey.

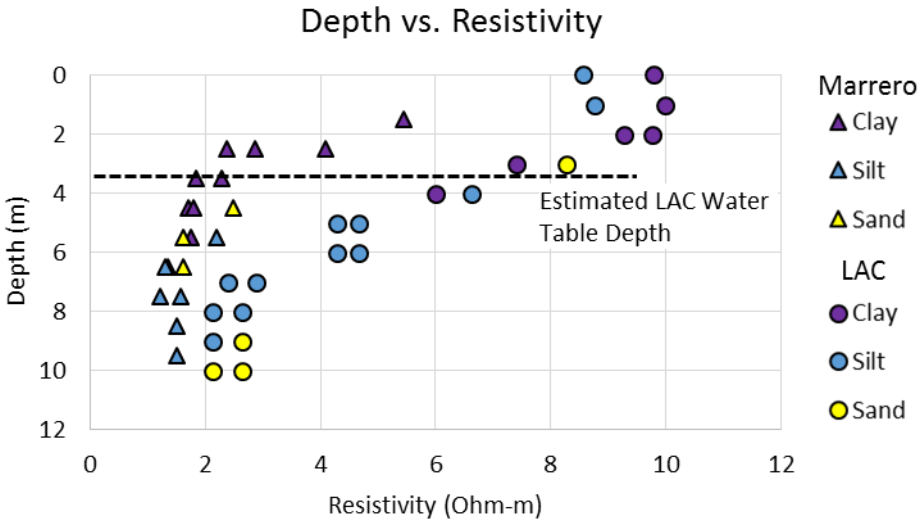

Figure 34: Resistivity values from the Marrero V-line and London Avenue Canal study sites, are represented by triangles and circles, respectively. Silt and sand samples are generally more resistive than clays when sampled at the same depth, especially below the expected water table. By assuming the water depth in the canal sets the water table elevation at London Avenue Canal study area, the water table should exist at a depth of ~3 meters.

(4.8) EFFECTS OF DEPTH ON SHEAR WAVE VELOCITY

Seismic velocities generally increase with increasing depth, but unlike resistivity, the shear modulus should be relatively invariant during changes in saturation (Gassmann, 1951, Biot, 1956); another factor must contribute to the positive correlation between velocity and depth. For the Hertz-Mindlin model, increases in the hydrostatic confining pressure, P, can increase effective rigidity, G_{eff}, (Mavko et al., 2009):

$$G_{eff} = \frac{5-4\nu}{5(2-\nu)} \sqrt[3]{\frac{3C^2(1-\phi)^2G^2}{2\pi^2(1-\nu)^2}P} \tag{4.13}$$

where ν represents Poisson's ratio, C represents the average number of grain contacts, G represents the shear modulus of the grains, and ϕ represents the porosity. An increase in G_{eff} generates an increase in Vs by the relationship:

$$V_s = \sqrt{\frac{G_{eff}}{\rho}} \tag{4.14}$$

where ρ is the bulk effective density of the medium. Assuming all other factors remain constant, shear wave velocity increases as a power function of pressure:

$$V_s \propto \sqrt[6]{P} \tag{4.15}$$

Between two given depths, shear wave velocity should increase with the overburden pressure (4.15). We calculate the increase in shear wave velocity using a mean density of 1700 kg/m^3 (Table 3), showing that the pressure change is 1.7 kPa/m, and compare the expected velocities to the velocity data. The ratio between velocities at a depth of 1 m compared to a depth of 10 m is 0.7:1 due to change in overburden pressure. A useful ratio requires the use of a non-zero starting depth and pressure, therefore we start at 1 meter. For the two LAC velocity values available for a depth of 1 meter (Figure 35), the pressure gradient indicates that the silt sample would display an increase in velocity from 97 m/s to 139 m/s, and the clay sample would increase from 117 m/s to 167 m/s at a depth of 10 meters. Values of the velocity from samples (142 and 156 m/s) at a depth of 10 meters. fall within the predicted range.

I also attempt to remove the pressure effect on shear wave velocity by a simple, empirical approach. A linear regression through shear-wave velocity-vs.-depth data from LAC and Marrero (Figure 35) shows an average increase of 6.4 m/s for each meter below the surface. I subtract the product of the rate of velocity change (6.4 m/s) and depth for each sample from the original velocity value. The product of velocity change and depth corrects each velocity back to an expected velocity at the surface. By using the expected surface velocity, comparisons between clay, silt, and sand do not include the issue of higher velocities simply because one sample lies deeper than another sample.

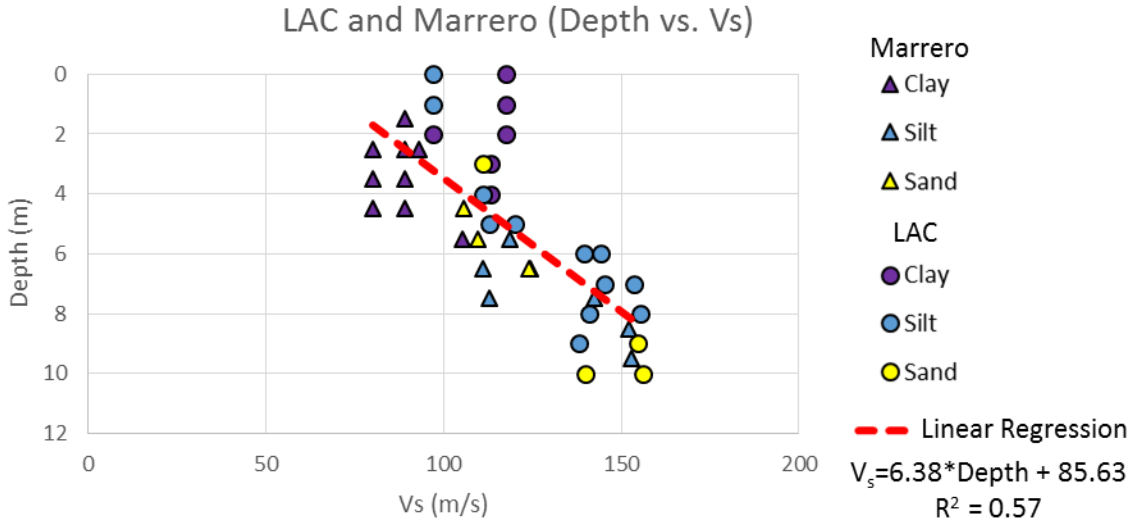

Figure 35: Shear wave velocity versus depth for the velocities from the London Avenue Canal (LAC) and Marrero study areas. A general trend of increasing shear wave velocity versus depth occurs for both the LAC and Marrero datasets, and remains when observing a combined dataset. A linear regression shows velocity increasing ~6.4 m/s per meter in depth.

The depth-corrected velocity values form a new data set, creating an opportunity for a new best-fit model for soil type based on resistivity and depth-corrected shear-wave velocity.

The new model uses (Equation 4.1) as the basis of the model, and optimizes the coefficients "a" through "h" (Table 6) using the same least squares regression that created Table 5. We call this new best-fit model the "depth-corrected model". The depth-corrected model (Figure 36 [b]) exhibits a similar trend that shows coarser grains with a lower resistivity and a higher shear-wave velocity, as also expressed in our first model (Figure 33). We create the new depth-corrected model because it allows for the determination of soil type from shear-wave velocity unaffected by overburden pressure.

Table 6. Optimized Coefficients for (4.12) for Depth Corrected Datasets

Dataset	Both Depth-Corrected	Simplified
a	-0.000637	0
b	0.079239	019574
c	-1.303017	0
d	-29.34369	-0.11859[1]
e	-0.002667	0
f	-0.021209	0
g	0.598012	0
h	-0.266438	0.574068
R^2	0.412221	.148562

From the new, depth-corrected data I also create a simplified model that relates coarse grain sizes (S) with resistivity and shear-wave velocity:

$$S = a * v_s + d * \rho + h \tag{4.16}$$

where v_s is shear-wave velocity, ρ is electrical resistivity , and $a, d,$ and h are coefficients. The best-fit contour surface on the simplified depth-corrected cross-plot (Figure 36 [d]) uses the original resistivity value in place of the base 10 logarithmic value. The least square regression applied to the depth-corrected data and simplified model (Equation 4.16) substantiates similar trends identified within the more complex polynomial models, but does not provide a clustering of silt or sand (Figure 36 [d]).

Soil type determination from the regression analysis only distinguishes between silt and clay, but incorrectly identifies all sand samples as other soil types (Figure 36). The best fit model based on the depth-corrected data and equation 4.12 correctly estimates only clay samples as clays (Figure 36 [a]), whereas 18% of the soil samples predicted as clay by the simplified model are truly silt dominated soils. The polynomial model correctly estimates only clay dominated soils as clay, but at the expense of estimating higher shear-wave-velocity clays as other soil types. However, the inability to predict the likelihood of any sand from the geophysical data collected ([a] and [c] in Figure 36) suggests we require a more robust method of analysis.

The low R^2 values for all of our best fit models ($R^2 < .55$) indicate that either regression modeling for soil type is not a viable first step option for identification of soils in the Louisiana Coastal Zone or our data is of quality. The depth-corrected polynomial approximation model of

[1] The coefficient is directly multiplied by the resistivity value, not a $\log_{10}(\rho)$ value.

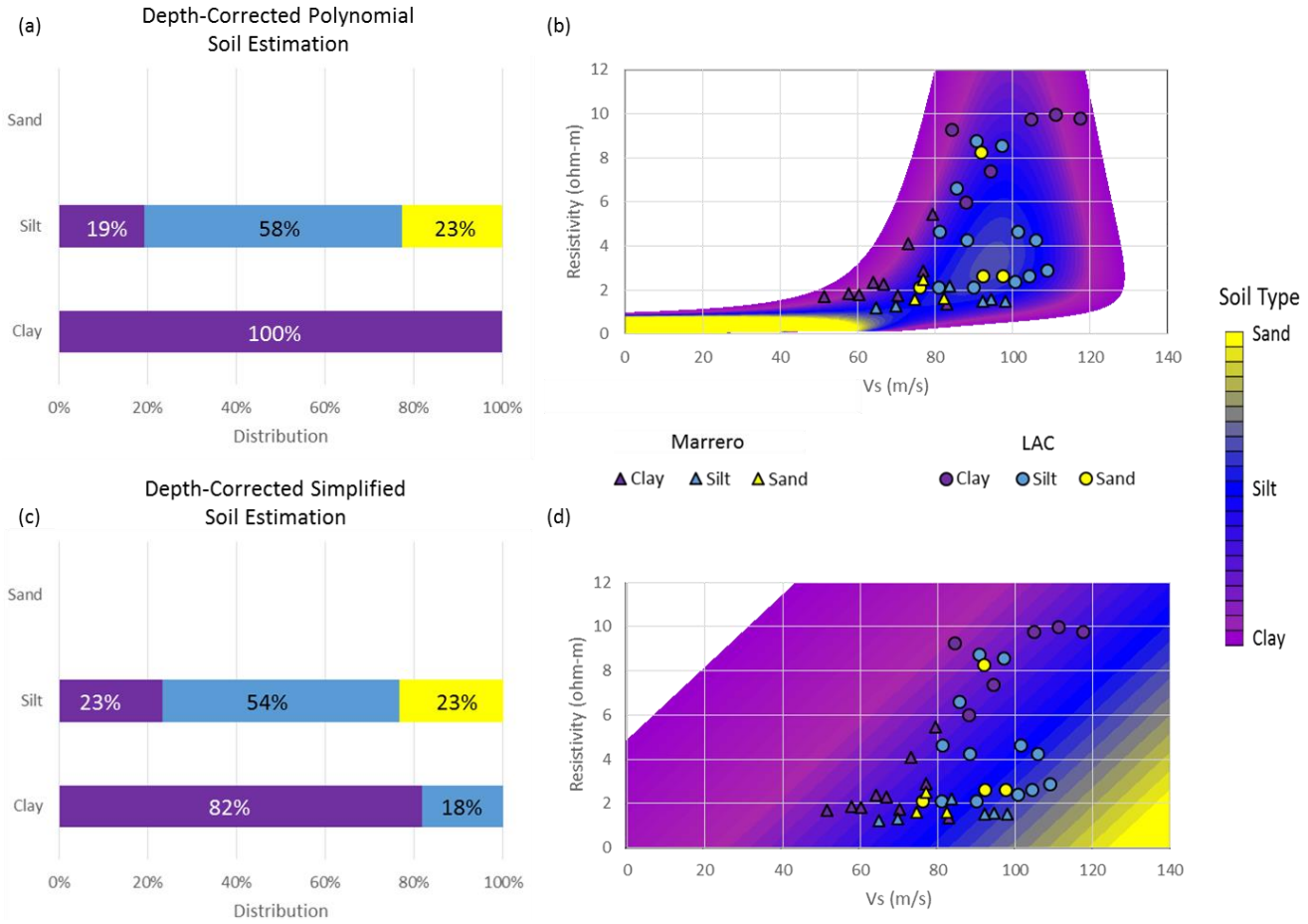

Figure 36: Cross-plots of the overburden-corrected data. The depth-corrected polynomial identifies only clay dominated soil samples as clay [a], where the cutoff between silt/clay is S =1.5, and the cutoff between silt/sand is S =2.5. The contoured surface [b] represents a best fitting surface to all the depth-corrected data (Equation 4.12). The depth-corrected data indicate clay existing at lower shear-wave velocity values for most resistivity values. The prediction of sand [b] at shear wave velocity <60 m/s and resistivity <1 Ω-m is an artifact of the model and not supported by any data. The simplified model [c] uses only resistivity and V_s terms (Equation 4.16) on the same depth-corrected data and uses the same S value distinction between clay, silt, and sand as the polynomial model. The simplified model [d] indicates the same general trend of increasing grain size with decreasing resistivity and increasing shear-wave velocity, but fits the data poorly (R^2 = 0.15).

soil type using shear-wave velocity and resistivity optimized for data from the Louisiana Coastal Zone separate clay into a single class, but fail to clearly distinguish silt from sand. The inability to identify silt and sand separately stems from the similar geophysical values determined for each soil type.

The overburden-corrected data (Figure 36 [b]) provides the basis for interpreting zones for a visual cluster analysis of soil type estimation from shear-wave velocity and electrical resistivity. We start by interpreting a distinct boundary between clay and the other soil types (Figure 37) where clay comprises 70% of samples at higher resistivity and lower shear-wave velocity. An interpreted zone for sand encapsulates the cluster of sand samples at low resistivity (~2 Ω-m) and between shear wave velocity of 70-100 m/s. The remaining zone only contains silt samples, which dominate at higher shear wave velocities and low resistivity.

A soil prediction system based on a visual cluster analysis possesses the main advantage of distinguishing sand samples from silt and clay using the same cutoffs as the models from the regression analysis. Identifying sand dominated soils as primarily exhibiting low resistivity values coincides with the expectation that sand possesses greater permeability and allows for a greater current flow. Coincidently, when silt dominated soils fill in, resistivity increases as the current path increases in tortuosity with the drop in permeability. Finally, we justify the interpretation of a clay zone at low shear wave velocity because clay inherently possesses a lower shear modulus than quartz dominated sand and silts.

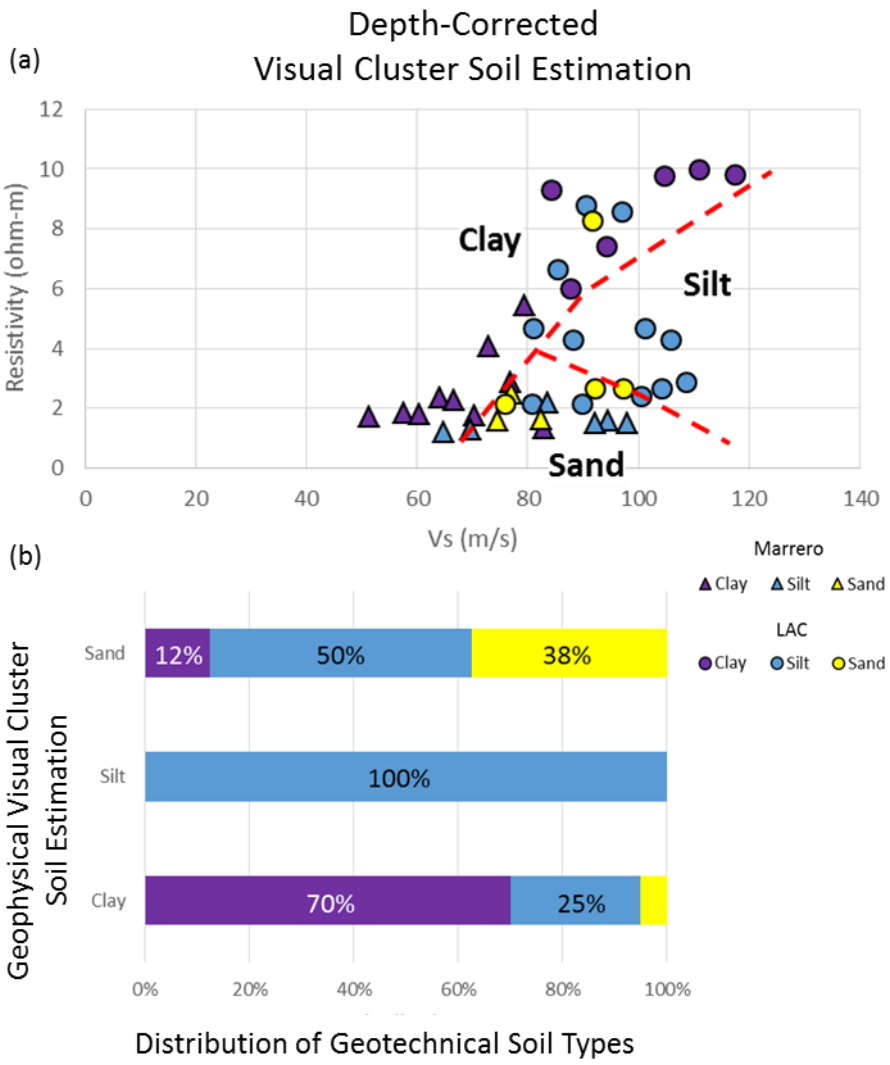

Figure 37: An interpretation of soil type based on depth-corrected shear wave velocity and electrical resistivity. For a given set of shear-wave velocity and electrical resistivity values, the zones depict the most likely soil type to encounter if drilled. The clay boundary follows the slope from the simplified model, bending at higher resistivity to accommodate the remaining clay samples. The clay zone contains 14 clays samples out of 20 total samples. The sand zone encloses 7 of the 8 sand samples from both study areas, but only 38% total samples are sand. Silt samples plot in all 3 zones. The silt zone contains only 5 silt samples, but 70% of silt samples plot in the sand and silt zones. The cross-plot requires more samples to refine the clay-silt boundary.

CHAPTER 5: DISCUSSION

(5.1) THE CONTRIBUTION OF SATURATION TO RESISTIVITY

The electrical resistivity of saturating fluid in soils greatly influences the resistivity of soil. Above the water table, the fraction of water saturated pore space is the determining factor for the change in resistivity assuming large ion concentrations (Archie, 1942):

$$R = aR_w\phi^{-m}S_w^n \tag{5.1}$$

where R is the resistivity of the saturated soil, R_w is the resistivity of the saturating fluid, a is tortuosity, ϕ is porosity, m is the cementation exponent, S_w is the saturation of water, and n is the saturation exponent. Since porosity and water saturation exist on a scale from 0 to 1, R_w determines the magnitude of the soil resistivity. An increase in the porosity reduces the resistivity further. The shallow water tables expected throughout the Louisiana Coastal Zone suggest that the negative resistivity vs. depth gradient (Figure 34) is created by the transition from partially saturated soils at the surface to fully saturated soils at the water table. Assuming electrical resistivity settles on a single value in fully saturated soils, the depth at which resistivity changes cease could indicate the depth of the water table. Only porosity and other physical parameters related to soil type effect resistivity.

Hayashi et al. (2013) use two different models for the levee body and the levee foundation to predict soil types, representing unsaturated and saturated soils, respectively. For complete saturation below the water table, resistivity values vary between different soil types by tortuosity and porosity. However, their assumption for a binary soil property of saturated vs. unsaturated neglects the effect of saturation change (Equation 5.1) over electrical resistivity. If saturation changes within the foundation soils, then the model needs to compensate for the effect before relating resistivity to soil type.

Hayashi et al. (2013) use only two models based on saturation, but it appears that partially saturated foundation soils above the water table require a separate model. Their unsaturated-levee-body model does not work, because applying their unsaturated-levee-body model to the geophysical data from our study returns clay soils at all depths, where $S < 1$ (Equation 4.12). Additionally, we expect the resistivity values for the same soil type above the water table to increase proportionally with depth as saturation increases, which neither the unsaturated-levee-body model nor saturated-levee-foundation model (Hayashi et al., 2013) takes into account. The resistivity values for the same soil type should remain static below the water table. Any changes in resistivity below the water table should be the result of changes in porosity, tortuosity, or the natural resistivity of the mineral composition in the soils.

Separating changes in saturation from factors directly linked to the soil content is essential to properly identify soil type. However, the resistivity of the saturating fluid must be accurately known for each site. At low resistivity the saturating fluid dominates the resistivity of the soil (Archie, 1942), and if the resistivity of the saturating fluid varies site to site then soil type interpretations will vary as well. For example, the resistivity values identified at the Marrero "V-line" levee site are lower than the values from the LAC site for every depth, regardless of soil type. A shallower water table from the Marrero "V-line" levee site could cause the lower resistivity values, but increased salinity could also contribute to the observed decrease in

resistivity. These site specific variations suggest environmental corrections for saturation and salinity be made at each study area.

(5.2) IDENTIFYING SOIL TYPES BY SHEAR-WAVE VELOCITY

Mineralogy differences between sand, silt, and clay contribute to shear-wave velocity variations. Silt and sand possess larger shear moduli than clay. The dominant clay type present in Holocene-aged Mississippi valley sediments is montmorillonite (Taggart and Kaiser, 1960) with a shear modulus that ranges from 16.4 GPa to 26.2 GPa (Wang et al., 2001). We expect larger shear-wave velocity in the quartz dominated sand and silt soils because quartz possesses a shear modulus of 45 GPa (Mavko et al., 2009). Correcting for overburden pressure differentiates clay from silt and sand by their low shear-wave velocity. However, little variation in shear velocity exists between sand and silt. Differentiating between sand and silt soils requires more information than shear-wave velocity provides.

(5.3) SOIL TYPE INTERPRETATION BY CROSS PLOT ANALYSIS OF V_S AND RESISTIVITY

Interpreting clay from both sand and silt require shear-wave velocity and resistivity measurements, because clay appears more often when V_s decreases and resistivity increases (Figure 37). We calculate a 70% chance of encountering a clay layer when resistivity and shear-wave velocity measurements fall within the interpreted zone for clay, given that 14 of the 20 samples in the interpreted zone are clay (Figure 37). We expect the lower shear-wave velocity values for clay compared to silt or sand, because of the mineralogical differences in shear moduli.

We explain the slope of the clay boundary (Figure 37) as the influence of either differential compaction between the clay samples, or differences in saturation. If we compact a clay sample, the shear modulus would increase, thereby increasing shear-wave velocity (Bitri et al., 2013). Tortuosity would likely increase from the compaction, resulting in a larger electrical resistivity (5.1). Alternatively, the shear moduli could remain constant, and the increase to resistivity and shear-wave velocity could be the result of difference in saturation. The resistivity of a wet clay sample would increase if the samples dries and saturation decreases (5.1). The loss of saturation decreases the water content, which decreases the density of the sample. The shear wave velocity increases as a result of the smaller density (4.14). We could determine the valid hypothesis by measuring saturation for the samples at the same time we collect electrical resistivity and seismic data.

Data which represent sand and silt dominated soils plot within the same region on the cross-plot, inhibiting the interpretation of exclusive zones for silt and sand. We interpret a sand zone with relatively low resistivity because six of the seven sand layers encountered at the study areas exhibit relatively low resistivity values (Figure 37). Our interpretation places the 6 sand samples in a zone with 10 other samples, making the likelihood of encountering a sand layer ~40% in the sand zone. Statistically, we have a greater chance of detecting a silt layer for resistivity and V_s values that plot in the sand zone than to detect a sand layer. However, a ~40% probability of detecting a sand layer in the sand zone exceeds the 1 in 25 chance of detecting sand outside of the sand zone (Figure 37). Differentiating between sand and silt does not appear possible with current data, therefore interpretations should distinguish between clay and silt/sand.

(5.4) ERROR AND UNCERTAINTY

Classifying soil types using different soil classification systems requires us to assume consistency across the different soil types and that the geotechnical reports are correct. The visual inspection interprets grain size in order to report soil type in boring log B-32 (USACE, 1989b). The visual inspection benefits our use of B-32, because the continuous soil descriptions for all depths allow us to match the dominant soil type with geophysical measurements. However, we cannot quantify the errors associated with visual inspection and interpretation of the soil type. The standardized measurements from the Unified Soil Classification System (ASTM D2487) that classify soil types in the 3-LUG report provide greater certainty for the dominant soil type. Molle (2005) shows the same soils classified by the USCS and the Soil Behavior Type from CPTs match, therefore leading us to expect soils identified at the Marrero study area by CPT would produce the same results if identified using the USCS such as for LUG-3, and vice versa.

The discontinuous nature of the geotechnical boring log for LUG-3 requires us to interpolate the dominant soil type at those depths where no samples were taken. Only two 1-meter intervals from 3-LUG do not contain samples. The shallow silt (Figure 16) at 1 meter depth plots with a resistivity value of 8.7 Ω-m in the clay zone, and the clay at 5 meter depth plots along the clay/silt boundary with a resistivity value of ~6 Ω-m. The removal of either sample would not change our interpretation of the soil type zones (Figure 37).

We simplify soil types into 3 classes based on the dominant soil type, which neglects the fact that most soil descriptions from the boring logs and SBT in our study areas contain a mix of soils. We plot seemingly homogeneous materials against shear-wave velocity and resistivity, but in reality the chosen data are heterogeneous. The likelihood of misinterpreting the dominant soil type increases when the percent content for each soil type approaches an equal value, which could propagate and affect the final interpretations for soil type zones (Figure 37).

The collection of resistivity data using capacitvely-coupled sensors in the low resistivity soils present under the greater New Orleans area approaches the operational limits of the Geometrics OhmMapper CCR system (Geometrics, 2001). Resistivity measurements from a CCR system often over-estimate resistivity when surveying a low resistivity area (Kuras et al., 2006). Yamashita et al. (2004) argue that the lower limit of the operational range for the CCR system is 3 Ω-m. However, increasing the dipole separation, such as with our longer CCR meter geometry, decreases the likelihood of over-estimating resistivity, assuming the system detects the low voltage signal (Kuras et al., 2006). If the system detects noise instead of the low system signal, then resistivity values less than 3 Ω-m (Yamashita et al., 2004) may be overestimated, effecting over 60% of the samples. Eliminating data less than 3 Ω-m would eliminate all but a single sand sample, and make the study statistically insignificant. Without the samples with less than 3 Ω-m, the depth-corrected data display a much weaker correlation between increasing grain size with a decrease in resistivity and an increase in shear-wave velocity. However our interpretation maintains the same clay/silt boundary, because the clay samples still trend along the same slope as before, and only silt samples plot within the silt zone. Eliminating values below 3 Ω-m would inhibit the interpretation of a sand zone, thus we require that values below 3 Ω-m remain in the analysis.

Since most of the low resistivity measurements can be attributed to depths below 5 meters, it is important to know the skin depth. At the London Avenue Canal study area, the

resistivity averages ~6 Ω-m in the upper ten meters, which corresponds to a skin depth of 10 m (Equation 2.3). Similarly, the resistivity averages ~5 Ω-m in the upper ten meters at the Marrero study area, corresponding to a skin depth of only 9 meters. Eliminating data taken below this depth does not significantly change our interpretation of soil classification based on shear-wave velocity and resistivity (Figure 37). In fact, we remove all data below 9 meters anyways, because those resistivity values are all less than 1 Ω-m, which is the lower limit we accept in order to avoid over-estimated resistivity values. Using galvanic coupling to collect electrical resistivity data could improve data quality, such as for an electrical resistivity tomography survey (e.g., Daily et al. 1992), but it would mean sacrificing the quick data collection through the use of a towed land-streamer.

The uncertainty of the shear-wave velocity data derives mainly from the inversion of the interpreted dispersion curves for shear wave velocity. During the inversion process we generate a large number of 5-layer models to avoid local misfit minima. We assume the 1000 models with the lowest misfit converge on the global minimum. However, the models converge on a velocity for the upper two layers and half-space with greater certainty than they converge on the middle layers (Figure 27). For the typical 1D Vs profile we create from each CMPCC gather, the upper 2 layers and half-space converge on a median velocity with a ~5% deviation (Figure 28). We interpret the convergence of the 3 middle layers from the inversion model on a single median velocity as a single layer (e.g. "Layer 3" in Figure 27). We interpret this single layer as the PIBT, which accounts for the widespread extent under the survey area (Saucier, 1994b). The PIBT exhibits a 25 m/s (~16%) deviation from the median velocity. The 25 m/s uncertainty could affect the shape and extent of the soil zones (Figure 37), but would only affect the lower resistivity values from the LAC study area.

(5.5) FUTURE WORK

The cross-plotting method should also distinguish organic clay and peat, which accumulate in the marsh and swamp depositional environments prevalent in the Louisiana Coastal Zone. Neither set of soil and geophysical data from the study areas contain information on organic-dominated layers. The common worry over the weak shear strength of organic rich layers in the foundation soils (e.g., Dunbar and Britsch, 2008) suggests future surveys target organic rich soils.

Future surveys should focus on gathering MASW-style seismic data and DC electrical resistivity from both saturated and unsaturated soils. Seismic surveys focused on surface collect data quickly with a land streamer and offer horizontally dense 2D velocity models. CCR acquires data quickly, but the capacitive coupling with the surface allowing for a towable system also makes the method susceptible to a quickly decaying voltage in the presence of low resistivity soils. Instead, direct current electrical resistivity imaging can avoid low voltage measurements by increasing the current injected without having to adjust any frequencies, allowing for a greater depth of investigation and greater accuracy. Testing soils with known variable saturation can improve the understanding of resistivity changing with depth, and ways to negate the effect when identifying soil types from geophysical data.

We suggest collecting geotechnical data from Cone Penetration Tests because of the existing integer-based soil description systems and access to pore pressure data to incorporate with geophysical surveys. The pore pressure tools on a CPTu correct for the effect of overburden and pore pressure on penetration resistance (Lunne et al., 1997). Robertson (1990) suggests a

correction to cone resistance based on pore pressure, and introduces a new Soil Behavior Type chart based on pressure-corrected values of CPT measurements. If we use pressure-corrected SBT as the soil type data on Vs and resistivity cross-plots, then we correct all necessary values for the effect of overburden pressure. We can improve regression analysis by only using SBT geotechnical data, and replacing our values of S (Equation 4.12) for clay, silt, and sand with the existing integer system from the Robertson (1990) chart.

Identifying soil type can be further complicated by changes to shear-wave velocity and resistivity values as a result of temporal fluctuations in water saturation. For instance, river levels rising and falling can cause saturation changes for levee foundation soils on the protected side of a river levee. Temporal changes such as a drop in shear-wave velocity or change in resistivity could indicate developing weaknesses in the levee system. Geophysical surveys conducted several times over the same location could help to monitor for hazards like piping, which can occur as water levels rise during seasonal floods (Dunbar et al., 2007). Time-lapse-monitoring geophysical surveys can also detect compaction and consolidation of sediments in areas where the shear modulus of the foundation soils increases (Bitri et al., 2013). Since we collect different data types over the span of several years, temporal changes in the physical properties at the study areas could also affect our geophysical data.

CHAPTER 6: CONCLUSIONS

Interpretations of soil type between traditional geotechnical borings may be improved by collection and analysis of electrical resistivity and shear-wave velocity data. Linear interpolations of soil type between geotechnical sites may miss lateral changes in soil type, which geophysical surveys may detect. The lateral data density of geophysical investigations from our surveys ($\leq$ 3 m/site) compliments geotechnical surveys, which, normally, conduct tests at ~100 m spacings. At the London Avenue Canal study area, shear wave velocity values change by 25% (30 m/s) across soil boundaries. Additionally, as resistivity decreases with depth, we interpret a change from clays and silts from the delta complexes to the deeper Pine Island Beach Trend sands. A cross plot of shear-wave velocity, electrical resistivity, and soil types from the Louisiana Coastal Zone indicate that lower resistivity values exist for all soil types compared to the original models introduced by Hayashi et al. (2013). Through analysis of geophysical data from the Louisiana Coastal Zone, we can begin to quantitatively show that greater shear-wave velocity and smaller resistivity is an indicator of increasing grain size.

We generate a new soil interpretation chart using depth-corrected shear wave velocity and electrical resistivity. Overburden pressure causes the shear-wave velocity of acoustic waves in similar soil types to vary proportionally with depth. Removing the overburden effect from shear-wave velocity improves our interpretations for clay, but does not improve the ability to distinguish silt and sand from one another. Resistivity data requires knowledge of soil saturation during acquisition, and careful attention to the skin depth from CCR surveys in order to be useful for soil type interpretations in low resistivity environments. The data indicates a relative invariance of soil type to electrical resistivity at resistivity values ~3 Ω-m, which we interpret as the resistivity of the saturating fluid dominating the resistivity of the soil.

REFERENCES

Aki, K., and P. G. Richards, 2002, Quantitative seismology. 2nd ed.: University Science Books.

Archie, G. E., 1942, The electrical resistivity log as an aid in determining some reservoir characteristics. Society of Petroleum Engineers. doi: 10.2118/942054-G.

Asquith, G. B., D. Krygowski, and C. R. Gibson, 2004, Basic well log analysis. **16**: American Association of Petroleum Geologists.

ASTM D2487, 2011, standard practice for classification of soils for engineering purposes (Unified Soil Classification System). ASTM International.

ASTM D4318, 2014, Standard test methods for liquid limit, plastic limit, and plasticity index of soils. ASTM International.

Biot, M. A., 1956, Theory of propagation of elastic waves in fluid saturated porous solid. I low frequency range. Journal of the Acoustical Society of America, **28**, 168-191.

Bitri, A., K. Samyn, S. Brulé, and E. Javelaud, 2013, Assessment of ground compaction using multi-channel analysis of surface wave data and cone penetration tests. Near Surface Geophysics, **11**, no. 6, 683-690.

Boggs, S., 1995, Principles of sedimentology and stratigraphy. 4 ed: Prentice Hall.

Cercato, M., F. Cara, E. Cardarelli, G. Di Filippo, G. Di Giulio, and G. Milana, 2010, Shear-wave velocity profiling at sites with high stiffness contrasts: a comparison between invasive and non-invasive methods. Near Surface Geophysics, **8**, no. 1, 75-94.

Coleman, J. M., and D. B. Prior, 1982, Deltaic environments of deposition, Coastal Studies Institute Technical Report: no. 359: Louisiana State University.

CPRA, 2012, Louisiana's comprehensive master plan for a sustainable coast. 114-164.

Cressie, N, 1990, The origins of kriging. Mathematical Geology, **22**, no. 3, 239-252. doi: 10.1007/BF00889887.

Daily, W., A. Ramirez, D. LaBrecque, and J. Nitao, 1992, Electrical resistivity tomography of vadose water movement. Water Resources Research, **28**, no. 5, 1429-1442.

DeLaune, R. D., I. Devai, C. R. Crozier, and P. Kelle, 2002, Sulfate reduction in Louisiana marsh soils of varying salinities. Communications in Soil Science & Plant Analysis, **33**, no. 1, 79.

Dunbar, J. B., and L. D. Britsch, 2008, Geology of the New Orleans area and the canal levee failures. Journal of Geotechnical & Geoenvironmental Engineering, **134**, no. 5, 566-582.

Dunbar, J. B., J. L. Llopis, G. L. Sills, E. W. Smith, R. D. Miller, J. Ivanov, and R. F. Corwin, 2007, Condition assessment of levees, U.S. section of the international boundary and water commission: Flood simulation study of retamal levee, lower Rio Grande valley, Texas, using seismic and electrical geophysical models. US Army Corps of Engineers, Engineer Research and Development Center.

Dunbar, J. B., V. H. Torrey III, and L. D. Wakeley, 1999, A case history of embankment failure: Geological and geotechnical aspects of the Celotex levee failure, New Orleans, Louisiana. US Army Corps of Engineers Engineer Research and Development Center.

Dvorkin, J., M. Prasad, A. Sakai, and D. Lavoie, 1999, Elasticity of marine sediments: Rock physics modeling. Geophysical Research Letters, **26**, no. 12, 1781-1784. doi: 10.1029/1999GL900332.

Dykes, A. P., and J. Warburton, 2008, Failure of peat-covered hillslopes at Dooncarton Mountain, Co. Mayo, Ireland: Analysis of topographic and geotechnical factors. CATENA, **72**, no. 1,129-145. doi: 10.1016/j.catena.2007.04.008.

FFEB JV, 2007, Task order 0008 geotechnical design report V-line levee (East of vertex) and Harvey Canal levee. Department of the Army, New Orleans District, Corps of Engineers New Orleans, Louisiana.

Fisk, H. N., 1944, Geological investigation of the alluvial valley of the lower Mississippi River, Mississippi River Commission: War Dept.

Frazier, D. E., 1967, Recent deltaic deposits of the Mississippi River: Their Development and Chronology. Gulf Coast Association of Geological Societies, **17**, 287-315.

Gassmann, F., 1951, Elastic waves through a packing of spheres. Geophysics, **16**, no. 4, 673-685. doi: doi:10.1190/1.1437718.

Geometrics, 2001, OhmMapper TR1 Operation Manual rev. F: Geometrics, Inc.

Geometrics, 2013, OhmImager 1.0.1., Inc., San Jose, CA.

Geometrics, 2014, GeoPlot 10.0.1.2., Inc, San Jose, CA.

Ghassemi, A., and A. Pak, 2011, Pore scale study of permeability and tortuosity for flow through particulate media using Lattice Boltzmann method. International Journal for Numerical and Analytical Methods in Geomechanics, **35**, no. 8,886-901. doi: 10.1002/nag.932.

Golden Software, Surfer 11 11.5. Golden Software, LLC, Golden, CO.

Haskell, N. A., 1953, The dispersion of surface waves on multilayered media. Bulletin of the Seismological Society of America, **43**, no. 1, 17-34.

Hayashi, K., R. Cakir, T. Walsh, and J. LaVassar, 2014a, Safety evaluation of dams using integrated geophyical method: A case study in Washington State, Symposium on the Application of Geophysics to Engineering and Environmental Problems 2014. 224-232.

Hayashi, K., T. Inazaki, K. Kitao, and T. Kita, 2013, Statistical estimation of geotechnical soil parameters in terms of cross-plots of S-save velocity and resistivity in Japanese levees. 2013 SEG Annual Meeting.

Hayashi, K., T. Inazaki, K. Kitao, and T. Kita, 2014b, Statistical soil type estimation using cross-plots of S-wave velocity and resistivity in Japanese levees. Geo-Congress 2014 Technical Papers: Geo-characterization and Modeling for Sustainability, at Atlanta, Georgia.

Hayashi, K., and H. Suzuki, 2004, CMP cross-correlation analysis of multi-channel surface-wave data. Exploration Geophysics, **35**, no. 1, 7-13.

Hegazy, Y. A., and P. W. Mayne, 1995, Statistical correlations between Vs and cone penetration data for different soil types. International symposium on cone penetration testing, Oct. 4-5, 1995, at Linkoping, Sweden.

Heisey, J., I. Stokoe, and A. Meyer, 1982, Moduli of pavement systems from spectral analysis of surface waves. Transportation research record, no. 852.

Heisey, J. S., K. Stokoe, W. R. Hudson, and A. Meyer, 1981, Determination of in situ shear wave velocities from spectral analysis of surface waves, University of Texas at Austin.

Hicks, J. 2011, Investigation into the cause of earthen embankment instability along the "V-line" artificial levee in marrero, Louisiana, USA: M.S. thesis, Louisiana State University.

Hubbard, S. M., D. G. Smith, H. Nielsen, D. A. Leckie, M. Fustic, R. J. Spencer, and L. Bloom, 2011, Seismic geomorphology and sedimentology of a tidally influenced river deposit, Lower Cretaceous Athabasca oil sands, Alberta, Canada. AAPG bulletin, **95**, no. 7, 1123-1145.

Ikeda, T., T. Tsuji, and T. Matsuoka, 2013, Window-controlled CMP crosscorrelation analysis for surface waves in laterally heterogeneous media. Geophysics, **78**, no. 6, EN95-EN105.

Ikelle, L. T., and L. Amundsen, 2005, Introduction to petroleum seismology. 1st Ed. Edited by M. Cooper. **12**, Investigations in Geophysics: Society of Exploration Geophysicists.

Inazaki, T., 2007, Integrated geophysical investigation for the vulnerability assessment of earthen levee. 20th EEGS Symposium on the Application of Geophysics to Engineering and Environmental Problems.

Inazaki, T., and K. Hayashi, 2011, Utilization of integrated geophysical surveying for the safety assessment of levee systems. Symp. Appl. Geophys. Engin. Environ. Problems.

IPET, Interagency Performance Evaluation Task-force., 2007, Performance evaluation of the New Orleans and Southeast Louisiana Hurricane Protection System: Final Report of the Interagency Performance Evaluation Task Force. Washington, D.C.: U.S. Army Corps of Engineers.

Karl, L., T. Fechner, M. Schevenels, S. François, and G. Degrande, 2011, Geotechnical characterization of a river dyke by surface waves. Near Surface Geophysics, **9**, no. 6, 515 - 527. doi: 10.3997/1873-0604.2011030.

Kolb, C., F. Smith, and R. Silva, 1975, Pleistocene sediments of the New Orleans-Lake Pontchartrain area. US Army Corps Technical Report, No. S-75-6, 56p.

Kolb, C. R., and R. T. Saucier, 1982, Engineering geology of New Orleans. Reviews in Engineering Geology, **5**, 75-93.

Kolb, C. R., and J. R. Van Lopik, 1958, Geology of the Mississippi River deltaic plain, southeastern Louisiana. In U.S. Army Engineer Waterways Experiment Station. Vicksburg, MS: United States Army Corps of Engineers.

Kuras, O., D. Beamish, P. Meldrum, and R. Ogilvy, 2006, Fundamentals of the capacitive resistivity technique. Geophysics, **71**, no. 3, G135-G152. doi: 10.1190/1.2194892.

Labrecque, P. A., S. M. Hubbard, J. L. Jensen, and H. Nielsen, 2011, Sedimentology and stratigraphic architecture of a point bar deposit, Lower Cretaceous McMurray Formation, Alberta, Canada. Bulletin of Canadian Petroleum Geology, **59**, no. 2,147-171.

Lane, J. W. J., J. Ivanov, F. Day-Lewis, D., Clemens Drew, R. Patev, and R. Miller, D, 2008, Levee evaluation using MASW: Preliminary findings from the Citrus Lakefront levee, New Orleans, Louisiana. Symposium on the Application of Geophysics to Engineering and Environmental Problems, **21**, no. 1,703-712.

Lay, T., and T. C. Wallace, 1995, Modern global seismology: Academic Press.

Liner, C, 2013, Suphasevel 1.5. SeismicUnix. Colorado School of Mines, Golden, CO.

Lorenzo, J. M., J. Hicks, and E. E. Vera, 2014, Integrated seismic and cone penetration test observations at a distressed earthen levee: Marrero, Louisiana, USA. Engineering Geology, **168**, 59-68. doi: 10.1016/j.enggeo.2013.10.019.

Lunne, T., P. K. Robertson, and J. J. M. Powell, 1997, Cone penetration testing in geotechnical practice: Routledge.

Maillet, R., 1947, The fundamental equations of electrical prospecting. Geophysics, **12**, no. 4,529-556. doi: 10.1190/1.1437342.

Malischewsky, P. G., and F. Scherbaum, 2004, Love's formula and H/V-ratio (ellipticity) of Rayleigh waves. Wave Motion, **40**, no. 1, 57-67.

Mavko, G., T. Mukerji, and J. Dvorkin, 2009, The rock physics handbook: Tools for seismic analysis of porous media: Cambridge university press.

Mayne, P. W., and G. J. Rix, 1995, Correlations between shear wave velocity and cone tip resistance in natural clays. Soils and Foundations, no. 35,107-110.

Milliman, J. D., and J. P. M. Syvitski, 1992, Geomorphic/tectonic control of sediment discharge to the ocean: The Importance of Small Mountainous Rivers. The Journal of Geology, **100**, no. 5,525-544. doi: 10.2307/30068527.

Mindlin, R., 1949, Compliance of elastic bodies in contact. Journal of Applied Mechanics, **16**,259-268.

Molle, J., 2005, The accuracy of the interpretation of CPT-based soil classification methods in soft soils, Delft University of Technology.

Montgomery, R. L., 1974, Correlation of engineering properties of cohesive soils bordering the Mississippi River from Donaldsonville to Head of Passes, LA. edited by U.S. Army Corps of Engineers. New Orleans, LA.

Nazarian, S., I. Stokoe, H. Kenneth, and W. Hudson, 1983, Use of spectral analysis of surface waves method for determination of moduli and thicknesses of pavement systems.

Park, C. B., R. D. Miller, and J. Xia, 1998, Imaging dispersion curves of surface waves on multi-channel record. SEG Expanded Abstracts.

Park, C. B., R. D. Miller, and J. Xia, 1999, Multichannel analysis of surface waves. Geophysics, **64**, no. 3, 800-808.

Park, C. B., R. D. Miller, and J. Xia, 2001, Offset and resolution of dispersion curve in multichannel analysis of surface waves (MASW). Proceedings of the SAGEEP.

Richart, F. E., J. R. Hall, and R. D. Woods, 1970, Vibrations of soils and foundations: Prentice-Hall.

Rix, G. J., and E. A. Leipski, 1991, Accuracy and resolution of surface wave inversion. Recent Advances in Instrumentation, Data Acquisition and Testing in Soil Dynamics, at Orlando, FL.

Roberts, H. H., 1997, Dynamic changes of the Holocene Mississippi River delta plain: The delta cycle. Journal of Coastal Research, **13**, no. 3, 605-627. doi: 10.2307/4298659.

Robertson, P. K., 1990, Soil classification using the cone penetration test. Canadian Geotechnical Journal, **27**, no. 1, 151-158.

Robertson, P. K., 2009, Interpretation of cone penetration tests; a unified approach. Canadian Geotechnical Journal, **46**, no. 11, 1337-1355. doi: 10.1139/T09-065.

Robertson, P. K., R. G. Campanella, D. Gillespie, and J. Grieg, 1986, Use of piezometer cone data. In-situ '86, ASCE Specialty Conference: On use of In site tests in geotechnical engineering, at Blacksburg, VA.

Rogers, J. D., G. Boutwell, D. Schmitz, D. Karadeniz, C. Watkins, A. Athanasopoulos-Zekkos, and D. Cobos-Roa, 2008, Geologic conditions underlying the 2005 17th Street canal levee failure in New Orleans. Journal of geotechnical and geoenvironmental engineering, **134**, no. 5,583-601.

Sambridge, M., 1999, Geophysical inversion with a neighbourhood algorithm—I. Searching a parameter space. Geophysical Journal International, **138**, no. 2,479-494.

Samouëlian, A., I. Cousin, A. Tabbagh, A. Bruand, and G. Richard, 2005, Electrical resistivity survey in soil science: a review. Soil and Tillage Research, **83**, no. 2,173-193. doi: 10.1016/j.still.2004.10.004.

Saucier, R. T., 1994a, Geomorphology and Quaternary geologic history of the Lower Mississippi Valley. **1**: U.S. Army Corps of Engineers, Waterways Experiment Station.

Saucier, R. T., 1994b, Geomorphology and Quaternary geologic history of the Lower Mississippi Valley. **2**: U.S. Army Corps of Engineers, Waterways Experiment Station.

Scholte, J. G., 1947, The range of existence of Rayleigh and Stoneley Waves. Geophysical Journal International, **5**, no. 5.

Scruton, P., 1960, Delta building and the deltaic sequence. Edited by F. P. Shepard, Recent Sediments, Northwest Gulf of Mexico: American Association of Petroleum Geologists.

Seed, R. B., R. G. Bea, R. I. Abdelmalak, A. G. Athanasopoulos, G. P. Boutwell, J. D. Bray, J. L. Briaud, C. Cheung, D. Cobos-Roa, J. Cohen-Waeber, B. D. Collins, L. Ehrensing, D. Farber, M. Hanemann, L. F. Harder, K. S. Inkabi, A. M. Kammerera, D. Karadeniz, R. E. Kayen, R. E. Moss, J. Nicks, S. Nimmala, J. M. Pestana, J. Porter, K. Rhee, M. F. Riemer, K. Roberts, J. D. Rogers, R. Storesund, A. V. Govindasamy, X. Vera-Grunauer, J. E. Wartman, C. M. Watkins, E. W. Jr., and S. C. Yim, 2006, Investigation of the performance of the New Orleans flood protection systems in Hurricane Katrina on August 29, 2005. Berkeley, CA: University of California Berkeley.

Smith, A. F. M., and G. O. Roberts, 1993, Bayesian computation via the Gibbs sampler and related Markov Chain Monte Carlo methods. Journal of the Royal Statistical Society. Series B (Methodological), **55**, no. 1,3-23.

Stockwell, J. W., 1999, The CWP/SU: Seismic Unix package. Computers & Geosciences, **25**, no. 4, 415-419.

Stokoe, K. H., S. Wright, J. Bay, and J. Roesset, 1994, Characterization of geotechnical sites by SASW method. Edited by Richard Woods, Geophysical characterization of sites: Oxford Publishers.

Strutt, J. W, 1885, On waves propagated along the plane surface of an elastic solid. Proceedings of the London Mathematical Society, **17**, 4-11.

Taggart, M. S., Jr., and A. D. Kaiser, Jr, 1960, Clay mineralogy of Mississippi River deltaic sediments. Geological Society of America Bulletin, **71**, no. 5, 521-530. doi: 10.1130/0016-7606(1960)71[521:CMOMRD]2.0.CO;2.

Timofeev, V. M., A. W. Rogozinski, J. A. Hunter, and M. Douma, 1994, A new ground resistivity method for engineering and environmental geophysics, Symposium on the Application of Geophysics to Engineering and Environmental Problems. 701-715.

USACE, 1989a, London Avenue Outfall Canal: Design Memorandum No. 19A. **1,** edited by United States Army Corps of Engineers. New Orleans.

USACE, 1989b, London Avenue Outfall Canal: Design Memorandum No. 19A. **2,** edited by United States Army Corps of Engineers. New Orleans.

USACE, 2010, Lake Pontchartrain and Vicinity Hurricane Protection Project. London Avenue Canal Cone Penetration Test: LECPT-46PT. Savannah District.

Veatch, B., and R. Martin, 2011, Lake Pontchartrain and Vicinity Hurricane Protection Project: MOWL for London Avenue Canal. New Orleans: U.S. Army Corps of Engineers Hurricane Protection Office.

Wang, Z., H. Wang, and M. E. Cates, 2001, Effective elastic properties of solid clays. Geophysics, **66**, no. 2, 428-440. doi: 10.1190/1.1444934.

Wathelet, M., 2008, An improved neighborhood algorithm: Parameter conditions and dynamic scaling. Geophys. Res. Lett., **35**, no. 9, L09301. doi: 10.1029/2008gl033256.

Wathelet, M., D. Jongmans, and M. Ohrnberger, 2004, Surface-wave inversion using a direct search algorithm and its application to ambient vibration measurements. Near Surface Geophysics, **2**, no. 4, 211-221.

Whiteley, R. J., and P. Caffi, 2014, Evaluating the effectiveness of rolling impact compaction at a brownfield site with high and low frequency seismic surface waves and geotechnical testing. Near Surface Geophysics, **12**, no. 3, 405-414.

Xia, J., R. D. Miller, and C. B. Park, 1999, Estimation of near-surface shear-wave velocity by inversion of Rayleigh waves. Geophysics, **64**, no. 3, 691-700. doi: 10.1190/1.1444578.

Xia, J., R. D. Miller, C. B. Park, and G. Tian, 2003, Inversion of high frequency surface waves with fundamental and higher modes. Journal of Applied Geophysics, **52**, no. 1, 45-57.

Yamashita, Y., D. Groom, T. Inazaki, and K. Hayashi, 2004, Rapid near surface resistivity survey using the capacitvely-coupled resistivity system: OhmMapper. Proceeding of the 7th SEGJ International Symposium.

Zimmer, M., M. Prasad, and G. Mavko, 2002, Pressure and porosity influences on V_P-V_S ratio in unconsolidated sands. The Leading Edge, **21**, no. 2, 178-183.

APPENDIX A: SEISMIC PROCESSING PROGRAMS

The following appendix details the seismic processing programs used to generate the dispersion curves at the London Avenue Canal study area. The processing objectives can be lumped into 5 main steps (Figure A1), each with discrete steps (Table A1). The processing steps are unique to the data acquisition at LAC levee toe, and should be adapted depending on the method used to collect and store the seismic data.

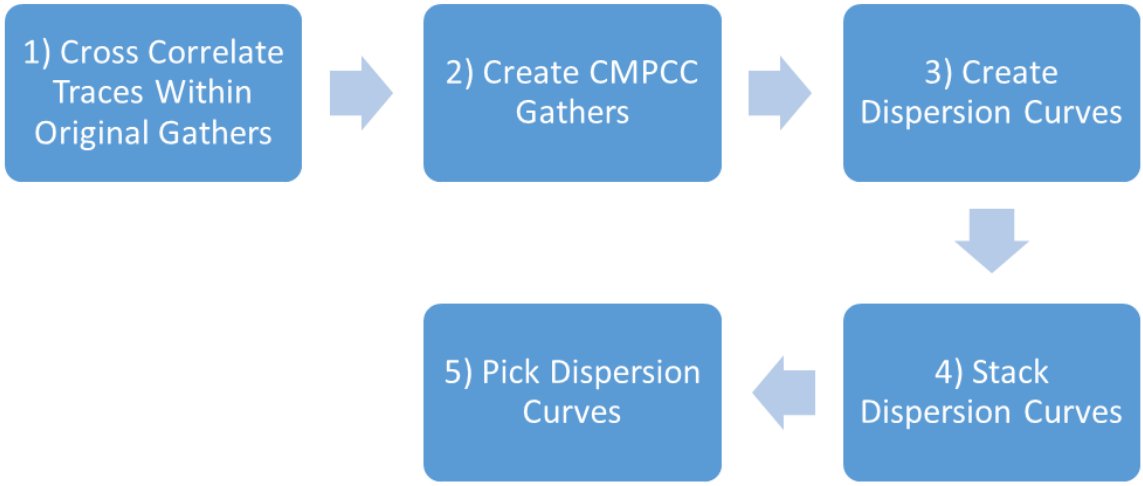

Figure A1: The five main processing objectives to create dispersion curves to use for inversion

Table A1: Seismic Processing for Dispersion Curves of Surface Waves

OBJECTIVE	STEPS
1) Cross Correlation	• Define geometry of acquisition array for the file containing all data (Make_header_geometry.pl) • Separate each trace into individual files (Xccwin.pl) • Cross Correlate all traces from within the same original gather (Xxcor_v1.pl)
2) Generate CMPCC Gathers	• Horizontally sum CC pairs with the same CMP and spacing • Group stacked CC pairs with the same CMP into new CMPCC gathers, organized by smallest to largest spacing (create_gathers.pl)
3) Calculate Dispersion Curves	• Perform a phase-shift wavefield transformation on each CMPCC gather, calculating a dispersion curve for each (makedispfile.pl).
4) Stack Dispersion Curves	• Create temp files of neighboring CMPs to stack • Horizontally sum temp files of dispersion curves (Xstackdisp.pl)
5) Pick Dispersion Curves	• Manually pick dispersion curves along the peak of the dispersion curves (iphasevel_wstack.pl)

Make_header_geometry.pl

The following program set the geometry for the raw seismic data in “1_4.5Hz.su”. The units of distance between geophones and shotpoints are set in decimeters. The later calculation of midpoints forces the use of decimeters due to SeismicUnix only accepting integers within the header files.

```
=pod

  1. Instantiate classes
      Create a new version of the package
      Personalize to give it a new name if you wish
    Use classes:
    flow
    log
    message
    sufilter
    sugain
    suspecfx
    suxwigb

=cut

  my $log                               = new message();
  my $run                               = new flow();
  my $setheader                                 = new sushw();

  my ($DATA_SEISMIC_SU) = System_Variables::DATA_SEISMIC_SU();

=pod

  3. Declare local variables

=cut
  my (@flow);

=pod

  4. Declare file names

=cut

          #All_clean_rev_kill
   $file_in[1]                      = '1_4.5Hz';
   $sufile_in[1]              = $file_in[1].$suffix_su;
   $inbound[1]                        = $DATA_SEISMIC_SU.'/'.$sufile_in[1];
   $outbound[1]                               =
$DATA_SEISMIC_SU.'/'.$file_in[1].'_geom'.$suffix_su;
```

```
#
=pod

=pod

  setheader
  set header values

=cut

 $setheader      ->clear();
 $setheader      ->first_val(450,0,450,-100,1001,1,1);
 $setheader      ->intra_gather_inc(300,0,300,0,0,1,0);
 $setheader      ->inter_gather_inc(300,300,0,0,1,0,1);
 $setheader      ->gather_size(24,24,24,24,24,24,120);
 $setheader      ->name('gx','sx','offset','scalco','fldr','tracf',’ep’);
 $setheader[1]   = $setheader ->Step();

=pod

  Standard:
  1. DEFINE FLOW(S)

=cut

 @items   = ($setheader[1],$in,$inbound[1],$out,$outbound[1]);
 $flow[1] = $run->modules(\@items);

=pod

  2. RUN FLOW(S)
=cut

 $run->flow(\$flow[1]);

=pod

  3. LOG FLOW(S)TO SCREEN AND FILE

=cut
 print  "$flow[1]\n";
#$log->file($flow[1]);

=pod
```

Individual Traces—make_raw_gathers.pl & Xccwin.pl

Before we place traces into individual files, the shotpoints need to be grouped, the traces which did not acquire data need to be expunged from the files, and gathers separated. The command line code to separate each trace for seismic unix is as follows:

Shotpoints are grouped using N as the shotpoint number, 1 through 16 with the prompt:

suwind < 1_4.5Hz_geom.su key=ep max=N min=N > SP"N"_4.5Hz_geom.su

Data feed traces are then rejected using the "tracf" header and the prompt:

suwind < SP"N"_4.5Hz_geom.su key=tracf reject=1 > SPN_4.5Hz_geom_cl.su

Finally, the shotpoints are split into the component gathers using "make_raw_gathers.pl". Since SeismicUnix rewrites or erases the offset and cdp headers during processing, metadata information is carried within the filename for redundancy. The code for "make_raw_gathers.pl":

```
#! /usr/bin/perl

=pod
=head1 DOCUMENTATION
=head2 SYNOPSIS
 Program Name:      make_raw_gathers.pl
 Purpose:       Separate Shot Gathers
 Author:        Derek Goff
 Depends:       Seismic Unix modules from CSM
=cut
#global

 use Moose;
 use suwind;
 use SeismicUnix qw ($in $out $on $go $to $suffix_ascii $off $suffix_su);
 use SU;

 my $log                                = new message();
 my $run                                = new flow();
 my $suwind                             = new suwind();

 my ($DATA_SEISMIC_SU) = System_Variables::DATA_SEISMIC_SU();

#local

 my (@flow, @items);
 my (@file_in, @sufile_in, @inbound, @file_out, @outbound, @sufile_out);
 my (@suwind);

=pod

Declare file names
```

```
Start SP for loop

=cut

for my $spn (1..16) {

=pod

Start gather for loop

=cut


 $file_in[1]     = 'SP'.$spn.'_4.5Hz_go_cl';
 $sufile_in[1]  = $file_in[1].$suffix_su;
 $inbound[1]   = $DATA_SEISMIC_SU.'/'.$sufile_in[1];



 for my $gn (1..5) {

  $file_out[1]   = 'SP'.$spn.'_G'.$gn.'_go_cl';
  $sufile_out[1]          = $file_out[1].$suffix_su;
  $outbound[1]            = $DATA_SEISMIC_SU.$sufile_out[1];

=pod

Establish Min and Max tracl to use from $spn and $gn
Declare traces to select based on key

=cut

#Min
  my $mn = 120*($spn-1)+24*($gn-1)+1;

#Max
  my $mx = 120*($spn-1)+24*($gn-1)+24;

  $suwind-> clear();
  $suwind-> key('tracl');
  $suwind-> min($mn);
  $suwind-> max($mx);
  $suwind[1] = $suwind->Step();

=pod
```

Define Flows

=cut

```
 @items = ($suwind[1],$in,$inbound[1],$out,$outbound[1],$go);
 $flow[1] = $run -> modules(\@items);
```

=pod

Run Flows

=cut

```
 $run->flow(\$flow[1]);
 print $flow[1]."\n";

 }#close for $gn
}#close for $spn
```

Xccwin.pl
After defining header values in order, "Xccwin.pl" takes the input from the separated gathers and individualizes each trace. Since the SU program *suxcor* erases all header information during cross-correlation, the geometry of each trace will be contained in the name, as shown in the code below:

```
#! /usr/bin/perl

=pod

=head1 DOCUMENTATION

=head2 SYNOPSIS

 Program Name:        Xccwin.pl
 Purpose:       Separate Shot Gathers
 Author:        Derek Goff
 Depends:       Seismic Unix modules from CSM
 Date:          8/21/2014
 Description:

=head2 USES

 (for subroutines)
    manage_files_by
    System_Variables (for subroutines)
```

```
    (for variable definitions)
    SeismicUnix (Seismic Unix modules)

=cut

#global

 use Moose;
 use suwind;
 use SeismicUnix qw ($in $out $on $go $to $suffix_ascii $off $suffix_su);
 use SU;

 my $log                                = new message();
 my $run                                = new flow();
 my $suwind                             = new suwind();

 my ($DATA_SEISMIC_SU) = System_Variables::DATA_SEISMIC_SU();

#local

 my (@flow, @items);
 my (@file_in, @sufile_in, @inbound, @file_out, @outbound, @sufile_out);
 my (@suwind);

=pod

Declare file names

Start SP for loop

=cut

for my $spn (1..16) {

=pod

Start gather for loop

=cut
for my $gn (1..5) {

 $file_in[1]      = 'SP'.$spn.'_G'.$gn.'_go_cl';
 $sufile_in[1]  = $file_in[1].$suffix_su;
 $inbound[1]   = $DATA_SEISMIC_SU.'/'.$sufile_in[1];
=pod
```

Start reciever for loop

=cut

for my $rn (2..24) {

$file_out[1]   = 'SP'.$spn.'_G'.$gn.'_R'.$rn;
$sufile_out[1]= $file_out[1].$suffix_su;
$outbound[1] = $DATA_SEISMIC_SU.'/xcor/'.$sufile_out[1];

=pod

Declare traces to select based on key

=cut

$suwind-> clear();
$suwind-> key('tracf');
$suwind-> min($rn);
$suwind-> max($rn);
$suwind[1] = $suwind->Step();

=pod

Define Flows

=cut

@items = ($suwind[1],$in,$inbound[1],$out,$outbound[1],$go);
$flow[1] = $run -> modules(\@items);

=pod

Run Flows

=cut

$run->flow(\$flow[1]);
print $flow[1]."\n";

} #close rec. for loop

} #close gather for loop

} #close SP for loop

Cross Correlate Traces—Xxcor_v1.pl

The cross correlation of the two seismic traces, $X(t)$ and $Y(t)$, containing signal from surface waves provides a measure of similarity, $m_{X,Y}(\tau)$, over all recorded times (Ikelle and Amundsen, 2005):

$$m_{X,Y}(\tau) = \sum_{t=-\infty}^{+\infty} X(t)Y(t-\tau) \tag{A1}$$

The SeismicUnix (Stockwell, 1999) program *suxcor* applies (A1) to two supplied traces. First, it multiplies the amplitude of a the filter trace, $Y(t)$, at a time, t with the amplitude of a sample trace $X(t)$. The products for all times are then summed together. The initial time of $Y(t)$ time can be manipulated, such that the amplitudes chosen from $Y(t)$ to multiply with $X(t)$ are shifted in the time domain to smaller or larger values. This shift is the time lag, τ. For our 26 second traces, the filter trace is shifted backwards 26s $\tau = 26s$ and forwards $\tau = -26s$ resulting in 52 seconds of amplitude similarities, $m_{X,Y}(\tau)$, being generated. However, output trace restarts with a new t=0, such that t=26s is equivalent to $\tau = 0$.

With the traces separated into individual files, each trace is correlated with every trace in the original gather. We produce 253 unique cross correlations per gather. Finally, the position of the common mid-point, halfway between the two receivers, is set in the cdp header. Likewise, the spacing between the receivers is set in the offset header. The naming format established in the previous code must be used in order to set the headers. The code below performs both tasks:

```
#! /usr/bin/perl

=pod

=head1 DOCUMENTATION

=head2 SYNOPSIS

 Program Name:      Xxcor_v1.pl
 Purpose:       Cross Correlate Traces
 Author:        Derek Goff
 Depends:       Seismic Unix modules from CSM
 Date:          8/21/2014
 Version:       1.0
 Description:

=head2 USES

 (for subroutines)
    manage_files_by
    System_Variables (for subroutines)

    (for variable definitions)
```

```
    SeismicUnix (Seismic Unix modules)

FILE NAME FORMAT:
        Files need to be in format
        SPshotpointnumber_Ggathernumber_Rreceivernumber.su

=cut

#global

 use Moose;
 use suxcor;
 use sugethw_moose;
 use sushw;
 use SeismicUnix qw ($in $out $on $go $to $suffix_ascii $off $suffix_su);
 use SU;

 my $log                        = new message();
 my $run                        = new flow();
 my $suxcor                     = new suxcor();
 my $sugethw                    = new sugethw_moose();
 my $sushw                      = new sushw();

 my ($DATA_SEISMIC_SU) = System_Variables::DATA_SEISMIC_SU();

#local

 my (@flow, @items);
 my (@file_in, @sufile_in, @inbound, @file_out, @outbound, @sufile_out);
 my (@suxcor, @sugethw, @sushw);
 my (@fgpath, @dgpath);
=pod

Define geometry temp file paths

Start SP for loop

=cut

 $fgpath[1] = $DATA_SEISMIC_SU.'/xcor2/fgtemp.dat';
 $dgpath[1] = $DATA_SEISMIC_SU.'/xcor2/dgtemp.dat';

for my $spn (13..16) {

=pod
```

```
=head2 DEFINITIONS

suxcor < (Data trace) sufile=(Filter Trace) > (OUTPUT {xcor} Trace)

Start gather for loop
Start filter trace for loop
 - Trace used to cross correlate
 - Hangs out in for loop for a while
Start data trace for loop
 - Data trace changes for every loop

Ranges define which traces to use

=cut
#Not Set for full loop
for my $gn (1..5) {

for my $rn (2..24) {

for my $j ($rn+1..24) {


#Define file names
#filter trace input
#USED FOR SUXCOR
 $file_in[1]      = 'SP'.$spn.'_G'.$gn.'_R'.$rn;
 $sufile_in[1]  = $file_in[1].$suffix_su;
 $inbound[1]   = $DATA_SEISMIC_SU.'/xcor/'.$sufile_in[1];

#data trace input
#USED FOR FLOW
 $file_in[2]      = 'SP'.$spn.'_G'.$gn.'_R'.$j;
 $sufile_in[2]  = $file_in[2].$suffix_su;
 $inbound[2]   = $DATA_SEISMIC_SU.'/xcor/'.$sufile_in[2];

#output filname
#USED FOR FLOW
 $file_out[1]    = 'SP'.$spn.'_G'.$gn.'_R'.$rn.'_R'.$j;
 $sufile_out[1]= $file_out[1].$suffix_su;
 $outbound[1] = $DATA_SEISMIC_SU.'/xcor'.$spn.'/'.$sufile_out[1];

=pod

=head1 Set Subroutines

=head2 Cross Correlate traces based on above loop
```

```
=cut

 $suxcor-> clear();
 $suxcor-> sufile($inbound[1]);
 $suxcor[1] = $suxcor->Step();

=pod

=head1 Set Geometry for each trace

=head2 Create temporary files holding geometry information

=cut

#Geometry for Filter Trace
 $sugethw-> clear();
 $sugethw-> setheaderword("gx");
 $sugethw-> output("geom");
 $sugethw[1] = $sugethw->Step();

#Geometry for Data Trace
 $sugethw-> clear();
 $sugethw-> setheaderword("gx");
 $sugethw-> output("geom");
 $sugethw[2] = $sugethw->Step();

=pod

Define and run Flows

=cut

#Set Geometry of filter
 @items = ($sugethw[1],$in,$inbound[1],$out,$fgpath[1],$go);
 $flow[1] = $run -> modules(\@items);
  $run->flow(\$flow[1]);
    my $fgtemp = $DATA_SEISMIC_SU.'/xcor2/fgtemp.dat';
           open (my $ffh, "<", "$fgtemp") or die "fgtemp failed";
            my $fgeo = <$ffh>;
             close $ffh;

#Set Geometry of data
 @items = ($sugethw[2],$in,$inbound[2],$out,$dgpath[1],$go);
 $flow[2] = $run -> modules(\@items);
  $run->flow(\$flow[2]);
```

```
   my $dgtemp = "$DATA_SEISMIC_SU"./xcor2/dgtemp.dat';
         open (my $dfh, "<", "$dgtemp") or die "dgtemp failed";
          my $dgeo = <$dfh>;
           close $dfh;

#define cmp value in cdp header
#CDP Will be Set in DECIMETERS
         my $cdp                  = ($fgeo+$dgeo)*10/2;
#define spacing between rcvrs in offset header
#SPACING/OFFSET Set in DECIMETERS
         my $space      = abs($fgeo-$dgeo)*10;

#Geometry of output
 $sushw-> clear();
 $sushw-> name('cdp','offset');
 $sushw-> first_val($cdp,$space);
 $sushw[1] = $sushw->Step();

#Run Cross Correlation and set Geometry
 @items = ($suxcor[1],$in,$inbound[2],$to,$sushw[1],$out,$outbound[1],$go);
 $flow[3] = $run -> modules(\@items);
  $run->flow(\$flow[3]);

print $flow[1]."\n\n";
print $flow[2]."\n\n";
print $flow[3]."\n\n";

} #close data in loop

} #close rec. for loop

} #close gather for loop

} #close SP for loop
```

Create CMPCC Gathers—create_gathers.pl

The next step in the process is to create the CMPCC gathers from the individualized traces. We organize traces using the "cdp" header value and spacing assigned from Xxcor_v1.pl to stack traces with the same "cdp" header value and spacing. Stacked traces are then grouped according to CMP, as outlined by Hayashi and Suzuki (2004).

```
#!/usr/bin/perl

=pod

=head1 DOCUMENTATION

=head2 SYNOPSIS
```

```
 Program Name:        create_gathers.pl
 Purpose:       Create CMPCC Gathers
 Author:        Derek Goffd
 Depends:       Seismic Unix modules from CSM
 Date:          12/9/2014
 Version:       1.0
 Description:   Place the stacked CMP+Offset
                                traces into a CMPCC gather

=head2 USES

 (for subroutines)
    manage_files_by
    System_Variables (for subroutines)

    (for variable definitions)
    SeismicUnix (Seismic Unix modules)

FILE NAME FORMAT:
        Input files are expected to be cross correlated
        Files need to be in format
        SPshotpointnumber_Ggathernumber_Rreceivernumber_Rreceivernumber.su
PREREQUISITES
        A directory named /all/ must exist at the filepath
        /seismics/data/.../su/all in the local directory


=cut

#global

 use Moose;
 use suxcor;
 use sugethw_moose;
 use sushw;
 use sustack;
 use SeismicUnix qw ($in $out $on $go $to $suffix_ascii $off $suffix_su);
 use SU;
 use manage_dirs_by_num;
 use File::Path qw (make_path remove_tree);

 my $log                        = new message();
 my $run                        = new flow();
 my $suxcor                     = new suxcor();
 my $sugethw                    = new sugethw_moose();
```

```
 my $sushw                          = new sushw();
 my $cat                            = new cat();
 my $sustack                        = new sustack();

 my ($TEMP_DATA_SEISMIC_SU) = System_Variables::TEMP_DATA_SEISMIC_SU();

 my ($DATA_SEISMIC_SU) = System_Variables::DATA_SEISMIC_SU();

#local

 my (@flow, @items);
 my ($rows,$rowsA);
 my (@file_in, @sufile_in, @inbound, @file_out, @outbound, @sufile_out);
 my (@file_inbound, @file_outbound);
 my (@suxcor, @sugethw, @sushw, @cat, @sustack);
 my (@ref_key1_array, @ref_key1_arrayA);
 my ($ref_key1_array, $ref_key1_arrayA);

=pod

Define geometry temp file paths

Start Shotpoint for loop

Create filepath for the output files to enter into

=cut

######

remove_tree($DATA_SEISMIC_SU.'/all/'); #removes directory if exists
make_path($DATA_SEISMIC_SU.'/all/'); #creates new directory

for my $spn (1..16) {
####
=pod

=head2 DEFINITIONS

Start gather for loop
Start filter trace for loop
 - Trace used to cross correlate
 - Hangs out in for loop for a while
Start data trace for loop
 - Data trace changes for every loop
```

Ranges define which traces to use

=cut

```
 for my $gn (1..5) {

  for my $rn (2..24) {

   for my $j ($rn+1..24) {

#set the formula for the spacing/offset
# 3=rcvr space
# could create variables for this outside the for loops
 my $space = (3*abs($rn-$j))*10; #Units are now decimeters

# set formula for the cmp
# 12 = sp spread; 9 represents distance to 1st rcvr
 my $cmp = (12*$spn-(3/2)*($rn+$j)-9)*10; #Units are now decimeters

#inbound
 $file_in[1]      = 'SP'.$spn.'_G'.$gn.'_R'.$rn.'_R'.$j;
 $sufile_in[1]  = $file_in[1].$suffix_su;
 $inbound[1]   = $DATA_SEISMIC_SU.'/xcor'.$spn.'/'.$sufile_in[1];

#outbound
 $file_out[1]    = 'SP'.$spn.'_G'.$gn.'_R'.$rn.'_R'.$j.'_cmp'.$cmp.'_off'.$space;
 $sufile_out[1]= $file_out[1].$suffix_su;
 $outbound[1] = $DATA_SEISMIC_SU.'/all/'.$sufile_out[1];


 $sushw-> clear();
 $sushw-> first_val($space,$cmp);
 $sushw-> name('offset','cdp');
 $sushw[1] = $sushw->Step();

 @items = ($sushw[1],$in,$inbound[1],$out,$outbound[1]);
 $flow[1] = $run -> modules(\@items);
  $run->flow(\$flow[1]);

# print "$flow[1]\n"

   } #close data in loop

  } #close rec. for loop

 } #close gather for loop
```

```
} #close SP for loop

=pod

=head1 Create gathers for cmp

Know the mininum and maximum values (applied respectively to the for loops)
for the cmp's and spacing between geophones

Gathers are created for each offset-cmp pairs consisting of all cross-correlations with those pairs

=cut

#cmp =-675
#cmp <= 1785

for ( my $cmp=-675; $cmp <= 1785; $cmp+=15) { #units are decimeters


#Remove Directory MASTER OVERWRITE OF DIRECTORY
 remove_tree($DATA_SEISMIC_SU.'/cmp'.$cmp.'/');
#Forcibly Create a file path if it does not exist
 make_path($DATA_SEISMIC_SU.'/cmp'.$cmp, {
          verbose=> 1,
          });

#space <= 700
 for ( my $space=30; $space <= 700; $space+=30 ) { #units are decimeters


 my $pattern                    = '_cmp'.$cmp.'_off'.$space.$suffix_su;
# print "$pattern\n";

 my $dir = '/home/dereg/LondonAvenueCanal/seismics/data/060112/Z/su/all/';
 my @files = <$dir/*$pattern>;
 my $count = @files;

 if ($count==0){
  next
 } else {


  print "\nCMP= $cmp\n";
  print "Spacing= $space\n";
```

```
 $file_inbound[1]       = $DATA_SEISMIC_SU.'/all/'.'.lsc1_grep';

 $file_outbound[1]     =
$DATA_SEISMIC_SU.'/cmp'.$cmp.'/cmp'.$cmp.'_off'.$space.$suffix_su;

 manage_dirs_by::lsc1_grep_dir_files($DATA_SEISMIC_SU.'/all/',$pattern);
 (@ref_key1_array,$rows)               = manage_files_by::read_1col(\$file_inbound[1]);

#concatenate traces into single files

 $cat-> clear();
 $cat-> first(1);
        #Defines which file to start with in the array
 $cat-> last($count);
        #Defines the last file to keep concatenate in the string
 $cat-> list($DATA_SEISMIC_SU.'/all/',@ref_key1_array);
 $cat[1] = $cat->Step();

 @items = ($cat[1],$out,$file_outbound[1]);
 $flow[2] = $run->modules(\@items);

        $run->flow(\$flow[2]);

 print "$flow[2]\n";



=pod

Stack gathers of same cmp and offset

=cut



 print "\nStack\n";
#CHANGE _off -> _off_
#gathers will look at 3rd column separated by "_"
 $file_outbound[2]     =
$DATA_SEISMIC_SU.'/cmp'.$cmp.'/cmp'.$cmp.'_off_'.$space.'_stack'.$suffix_su;

 $sustack-> clear ();
 $sustack-> key('offset');
 $sustack[1] = $sustack->Step();

 @items = ($sustack[1],$in,$file_outbound[1],$out,$file_outbound[2]);
```

```
$flow[3] = $run->modules(\@items);

        $run->flow(\$flow[3]);

print "$flow[3]\n";


 }
}



=pod

Create gathers of the stacked traces
Stacked traces need to be in format:
cmp1111_off_11_stack.su

=cut

 print "\nGathers\n";

 $file_inbound[3]       = $DATA_SEISMIC_SU.'/cmp'.$cmp.'/'.'lsc1_grep';

 $file_outbound[3]      = $DATA_SEISMIC_SU.'/cmp'.$cmp.'/G_cmp'.$cmp.$suffix_su;

 my $patternA                           = 'stack'.$suffix_su;

 my $dirA = '/home/dereg/LondonAvenueCanal/seismics/data/060112/Z/su/cmp'.$cmp.'/';
 my @filesA = <$dirA/*$patternA>;
 my $countA = @filesA;

 if ($countA==0){
  next
 } else {

  manage_dirs_by_num::lsc1_grep_dir_files($DATA_SEISMIC_SU.'/cmp'.$cmp.'/',$patternA);

  ($ref_key1_arrayA,$rowsA)                     = manage_files_by::read_1col(\$file_inbound[3]);

 $cat-> clear();
 $cat-> first(1);
        #Defines which file to start with in the array
 $cat-> last($countA);
        #Defines the last file to keep concatenate in the string
 $cat-> list($DATA_SEISMIC_SU.'/cmp'.$cmp.'/',$ref_key1_arrayA);
```

```
$cat[2] = $cat->Step();

@items = ($cat[2],$out,$file_outbound[3]);
$flow[4] = $run->modules(\@items);

        $run->flow(\$flow[4]);

print "$flow[4]\n";


 }
}
```

Create Dispersion Curves—makedispfile.pl

Once the CMPCC gathers created, the dispersion images can be generated. However, due to the odd spacings where a cmp can exist either at the site of a geophone or between two geophones, the dispersion images are stacked. In order to do this, files containing the dispersion images are first created. The code below utilizes suphasevel (Liner, 2013) from SeismicUnix (Stockwell, 1999) in a perl script.

Calculation of Dispersion

A wavefield transformation method generates a dispersion image of each CMPCC gather using the suphasvel program (Liner, 2013) within SeismicUnix (Stockwell, 1999). The transformation of a CMPCC gather into a dispersion curve follows the steps outlined in 4.1.2. The following code uses the methodology from Park et al. (1999) to calculate the dispersion curves and place each CMPCC into individual files.

```
#!/usr/bin/perl

=pod

=head1 Documentation

=head2 Synopsis

        Program:        makedispfile.pl
        Purpose:        Creation of a Dispersion Curve
        Author:         Derek S. Goff
        Date:           November 17 2013 V1.1
        Description:    Implements  suphasevel.pm
                        Creates phase velocity dispersions
                        12/17/2014 V1.2 Made Interactive
                        3/16/2015  V2.0 View Old Picks, Window Gathers

=head2 Uses

    Subroutines:
        manage_files_by
```

```
        System_Variables (for subroutines)

    Varibale Definitions:
        SeismicUnix (Seismic Unix modules)

=cut

 use Moose;
 use SeismicUnix qw ($in $out $on $go $to $suffix_ascii $off $suffix_su);
 use SU;
 use suphasevel;
 use suamp;
 use suifft;
 use suflip;
 use File::Path qw (make_path remove_tree);


=head2 Steps For Running a Mute

 1. Instanitiate Classes
        Create a new version of a package
        Give it a new name if desired
   Use classes:
        flow
        log
        message
        sufilter
        suximage

=cut

 my $log                    = new message();
 my $run                    = new flow();
 my $suximage                       = new suximage();
 my $suxwigb                = new suxwigb();
 my $suamp                  = new suamp();
 my $suphasevel                     = new suphasevel();
 my $suifft                 = new suifft();
 my $sufilter               = new sufilter();
 my $sugain                 = new sugain();
 my $suflip                 = new suflip();
 my $suwind                 = new suwind();
 my $sushw                  = new sushw();
 my $suchw                  = new suchw();
```

```
=pod

 2. Utilize lgc10.geol.lsu.edu directory navigation system

=cut

 my ($DATA_SEISMIC_SU) = System_Variables::DATA_SEISMIC_SU();

remove_tree($DATA_SEISMIC_SU.'/disp/');
make_path($DATA_SEISMIC_SU.'/disp/', {
        verbose=> 1,
        });

=pod

 3. Declare local variables

=cut

 my (@flow, @items);
 my (@suamp, @suximage, @suxwigb, @suphasevel, @sufilter, @sugain, @suflip);
 my (@suwind, @sushw, @suchw);
 my (@file_in, @sufile_in, @inbound, @file_out, @outbound, @outpicks);

 my $start_cmp=-675;

for ( my $cmp=$start_cmp; $cmp <= 1785; $cmp+=15) {

=pod

Define inbound files

=cut

  $file_in[1]                   = 'G_cmp'.$cmp;
  $sufile_in[1]                 = $file_in[1].$suffix_su;
  $inbound[1]                   = $DATA_SEISMIC_SU.'/cmp'.$cmp.'/'.$sufile_in[1];

  $file_out[1]                  = $file_in[1].'_phvel';
  $file_out[2]                  = 'G_cmp_'.$cmp.'_phvel'; #Changed from using $file_in
#output file
  $outbound[1]                  = $DATA_SEISMIC_SU.'/disp/'.$file_out[2].'.su';
#output pick file into data directory
  $outpicks[1]                  = $DATA_SEISMIC_SU.'/'.$file_out[1].'_picks';
#output pick file into subset picks directory
#WARNING, PICK DIRECTORY MAY NOT EXIST
```

```
 $outpicks[2]                = $DATA_SEISMIC_SU.'/picks/'.$file_out[2].'_picks';
 $outpicks[3]                = $DATA_SEISMIC_SU.'/picks/'.$file_out[2].'_newpicks';

# $file_in[2] = eval ($outbound[2]);
# print ($file_in[2]);


#INITIATE PHASEVEL PROCESSING

 $suphasevel   -> clear();
 $suphasevel   -> fv("500");
 $suphasevel   -> nv("300");
 $suphasevel   -> dv("25");
 $suphasevel   -> fmax("40");
 $suphasevel   -> norm($on);
 $suphasevel   -> verb($on);
 $suphasevel[1]        = $suphasevel->Step();

 $suamp-> clear();
 $suamp-> mode("real");
 $suamp[1] = $suamp->Step();

 $suwind       -> clear();
 $suwind       -> tmin(26);
 $suwind       -> tmax(28);
 $suwind[1] = $suwind->Step();

 $suchw                -> clear();
 $suchw                -> key1('cdp');
 $suchw                -> key2('tracl');
 $suchw[1] = $suchw->Step();

 @items =
($suwind[1],$in,$inbound[1],$to,$suphasevel[1],$to,$suamp[1],$to,$suchw[1],$out,$outbound[1
],$go);
 $flow[1]       = $run -> modules(\@items);

 $run->flow(\$flow[1]); #Execute Original Trace
 print $flow[1]."\n";

} #close for
```

Stack Dispersion Curves—Xstackdisp.pl

Now with the initial dispersion created, adjacent dispersion images are stacked in order to obtain the information contained at the unique spacings between the 1.5m cmps. This essentially combines the phase velocity data at each frequency, and boosts the zones were signal is captured.

The tradeoff is that 3m spacing between each 1D shear wave velocity model will be generated instead of the original 1.5m spacing. The stacking code is seen below:

```
#!/usr/bin/perl

=pod

=head1 DOCUMENTATION

=head2 SYNOPSIS

 Program Name:        create_gathers.pl
 Purpose:        Create CMPCC Gathers
 Author:         Derek Goffd
 Depends:        Seismic Unix modules from CSM
 Date:           12/9/2014
 Version:        1.0
 Description:    Place the stacked CMP+Offset
                                 traces into a CMPCC gather

=head2 USES

 (for subroutines)
    manage_files_by
    System_Variables (for subroutines)

    (for variable definitions)
    SeismicUnix (Seismic Unix modules)

FILE NAME FORMAT:
        Input files are expected to be cross correlated
        Files need to be in format
        SPshotpointnumber_Ggathernumber_Rreceivernumber_Rreceivernumber.su
PREREQUISITES
        A directory named /all/ must exist at the filepath
        /seismics/data/.../su/all in the local directory


=cut

#global

 use Moose;
# use suxcor;
# use sugethw_moose;
 use sushw;
 use Sustack;
```

```
 use susort;
 use SeismicUnix qw ($in $out $on $go $to $suffix_ascii $off $suffix_su);
 use SU;
# use manage_dirs_by_num;
 use File::Path qw (make_path remove_tree);
 use File::Temp qw (tempfile);

 my $log                         = new message();
 my $run                         = new flow();
# my $suxcor                      = new suxcor();
# my $sugethw                             = new sugethw_moose();
 my $sushw                       = new sushw();
 my $suchw                       = new suchw();
 my $cat                         = new cat();
 my $sustack                     = new Sustack();
 my $susort                      = new susort();
 my $suximage                            = new suximage();

 my ($TEMP_DATA_SEISMIC_SU) = System_Variables::TEMP_DATA_SEISMIC_SU();

 my ($DATA_SEISMIC_SU) = System_Variables::DATA_SEISMIC_SU();

#local

 my (@flow, @items);
 my ($rows,$rowsA);
 my (@file_in, @sufile_in, @inbound, @file_out, @outbound, @sufile_out);
 my (@file_inbound, @file_outbound);
 my (@suxcor, @sugethw, @sushw, @cat, @sustack, @susort, @suximage);
 my (@ref_key1_array, @ref_key1_arrayA);
 my ($ref_key1_array, $ref_key1_arrayA);
 my (@temp, @tempout);


#cmp =-675
#cmp <= 1785

for ( my $cmp=660; $cmp <= 690; $cmp+=30) { #units are decimeters

my $stackcmp=$cmp+15;

=pod

Define inbound files

=cut
```

```
 $file_in[1]                    = 'G_cmp_'.$cmp.'_phvel';
 $sufile_in[1]                  = $file_in[1].$suffix_su;
 $inbound[1]                    = $DATA_SEISMIC_SU.'/disp/'.$sufile_in[1];
 $file_in[2]                    = 'G_cmp_'.$stackcmp.'_phvel';
 $sufile_in[2]                  = $file_in[2].$suffix_su;
 $inbound[2]                    = $DATA_SEISMIC_SU.'/disp/'.$sufile_in[2];

 $temp[1]                       = $TEMP_DATA_SEISMIC_SU.'1.su';
 $temp[2]                       = $TEMP_DATA_SEISMIC_SU.'2.su';
 $tempout[1]                    = $TEMP_DATA_SEISMIC_SU.'out.su';

 $file_out[1]                   = $file_in[1].'_phvel';
 $file_out[2]                   = 'G_cmp_'.$cmp.'_'.$stackcmp.'_phvel'; #Changed from using
$file_in
#output file
 $outbound[1]                   = $DATA_SEISMIC_SU.'/dispstack/'.$file_out[2].'.su';


if (-e $DATA_SEISMIC_SU.'/cmp'.$cmp.'/') {
#Do nothing
}
else {
#Forcibly Create a file path if it does not exist
 make_path($DATA_SEISMIC_SU.'/cmp'.$cmp, {
        verbose=> 1,
        });
}


 $sushw                 -> clear();
 $sushw                 -> key('offset');
 $sushw                 -> a(1);
 $sushw[1] = $sushw->Step();

 $sushw                 -> clear();
 $sushw                 -> key('offset');
 $sushw                 -> a(2);
 $sushw[2] = $sushw->Step();

        system($sushw[1].$in.$inbound[1].$out.$temp[1]);

        system($sushw[2].$in.$inbound[2].$out.$temp[2]);

        system("cat $temp[1] $temp[2] $out $tempout[1]");
```

```
$susort          ->clear();
$susort          ->key1('cdp');
$susort          ->key2('offset');
$susort[1] = $susort->Step();

$sustack         ->clear();
$sustack         ->key('cdp');
$sustack[1] = $sustack->Step();

$suximage-> clear();
$suximage-> title($file_out[2]);
$suximage-> xlabel("Phase_Velocity_dm/s");
$suximage-> ylabel("Frequency_Hz");
$suximage-> box_width(700);
$suximage-> box_height(600);
$suximage-> cmap("hsv6");
$suximage-> box_X0(0);
$suximage-> box_Y0(0);
$suximage-> legend($on);
$suximage-> windowtitle("Phase_Velocity_Dispersion_Map_NoPicks");
$suximage[1]  = $suximage->Step();

@items = ($susort[1],$in,$tempout[1],$to,$sustack[1],$out,$outbound[1]);
 $flow[1]        = $run -> modules(\@items);

@items = ($suximage[1],$in,$outbound[1]);
 $flow[2]        =$run -> modules(\@items);

$run->flow(\$flow[1]);
print $flow[1]."\n";

$run->flow(\$flow[2]);
print $flow[2]."\n";

}
```

Pick Dispersion Curves—iphasevel_wstack.pl

Iphasevel_wstack.pl is an interactive program to pick dispersion images, view those picks, and repick as needed. The program uses the seismic unix code within a perl wrapper, allowing for the picks to be saved as a separate ASCII file.

```
#!/usr/bin/perl

=pod

=head1 Documentation
```

=head2 Synopsis

Program: Xphasevel_wstack.pl
Purpose: Creation of a Dispersion Curve
Stack Dispersion Images
Make Pick
Author: Derek S. Goff
Date: November 17 2013 V1.1
Description: Implements suphasevel.pm
Creates phase velocity dispersions
12/17/2014 V1.2 Made Interactive
3/16/2015 V2.0 View Old Picks, Window Gathers
4/20/2015 V3.0 Add option to stack dispersions
Subroutines Sustack, Suximage, and Susort are NOT
located in main liball directory

=head2 Uses

Subroutines:
manage_files_by
System_Variables (for subroutines)

Varibale Definitions:
SeismicUnix (Seismic Unix modules)

=cut

```
use Moose;
use SeismicUnix qw ($in $out $on $go $to $suffix_ascii $off $suffix_su);
use SU;
use suphasevel;
use Suamp;
use suifft;
use suflip;
use Sustack;
use lib '/home/dereg/LondonAvenueCanal/seismics/pl/060112/Z';
use Susort;
use Suximage;
```

=head2 Steps For Running a Mute

1. Instanitiate Classes
Create a new version of a package
Give it a new name if desired

```
   Use classes:
        flow
        log
        message
        sufilter
        suximage

=cut

 my $log                    = new message();
 my $run                    = new flow();
 my $suximage                       = new Suximage();
 my $suxwigb                = new suxwigb();
 my $suamp                  = new Suamp();
 my $suphasevel                     = new suphasevel();
 my $suifft                 = new suifft();
 my $sufilter               = new sufilter();
 my $sugain                 = new sugain();
 my $suflip                 = new suflip();
 my $suwind                 = new suwind();
 my $sushw                  = new sushw();
 my $suchw                  = new suchw();
 my $sustack                = new Sustack();
 my $susort                 = new Susort();

=pod

 2. Utilize lgc10.geol.lsu.edu directory navigation system

=cut

 my ($DATA_SEISMIC_SU) = System_Variables::DATA_SEISMIC_SU();
 my ($TEMP_DATA_SEISMIC_SU) = System_Variables::TEMP_DATA_SEISMIC_SU();

=pod

 3. Declare local variables

=cut

 my (@flow, @items);
 my (@suamp, @suximage, @suxwigb, @suphasevel, @sufilter, @sugain, @suflip);
 my (@sushw, @suchw);
 my (@suwind,@sustack,@susort);
 my (@file_in, @sufile_in, @inbound, @file_out, @outbound, @outpicks);
 my (@temp, @tempout);
```

```
#SET UNIVERSAL SU PARAMETERS

#INITIATE PHASEVEL PROCESSING

=pod

 5. suphasevel
        fv = The starting phase velocity (pv) to process
            -> Not always in (m/s)
            -> Depends on units in geometry (header)
        nv = How many steps to take
            -> Number of velocities to test
        dv = Step Size
            -> How large a gap between
                -> test velocities
        fmax = Maximum frequency to process

        fv+nv*dv = largest velocity tested


=cut

 $suphasevel   -> clear();
 $suphasevel   -> fv("500");
 $suphasevel   -> nv("300");
 $suphasevel   -> dv("25");
 $suphasevel   -> fmax("60");
 $suphasevel   -> norm($on);
 $suphasevel   -> verb($on);
 $suphasevel[1]          = $suphasevel->Step();

=pod

 7. Set type of traces to output
        amp gives amplitude traces
        phase gives phase traces...
        see suamp.pm for further instruction
   -> None are really neccessary
   -> amp is default

=cut

 $suamp-> clear();
 $suamp-> mode("real");
```

```
$suamp[1] = $suamp->Step();

=pod

 10.  Window time value of traces
          For a 52 long second CMPCC gather
          where the two cross correlated traces
          were 26s each, zero lag time is at 26s.
          A 2 sec window extends to 28s, hopfully
          before a shot is CC'd with different
          shot other than itself.

=cut

 $suwind        -> clear();
 $suwind        -> tmin(26);
 $suwind        -> tmax(28);
 $suwind[1] = $suwind->Step();


################################################################################
#START STACKING PROGRAM
################################################################################

=pod

Output a question to ask if dispersion
curves should be stacked.

=cut

my $qstack;
$qstack = 'y';

  print("Would you like to stack dispersion curves?\n");
  print("Not reccommended if you haven't viewed unstacked curves yet.\n");
  print("Stack Dispersion Curves...     'y'\n");
  print("Continue Without Stacking...   'n'\n");
  print("\%");
  $qstack = <STDIN>;
  chomp ($qstack);

if ($qstack eq 'y') {

################################################################################
#CHECK IF DISPERSION DIRECTORY AND FILES EXIST
```

```
##############################################################################
use File::Path qw (make_path remove_tree);
if (-e $DATA_SEISMIC_SU.'/disp/') {

print "Dispersion image directory found\n";
print "Did not confirm dispersion files exist\n";

} #close if
#MAKE DISPERSION FILES IF NOT
else {
	print "Directory $DATA_SEISMIC_SU/disp/ not found";

	make_path($DATA_SEISMIC_SU.'/disp/', {
		verbose=> 1,
		});

	my $start_cmp=-675;
	for ( my $cmp=$start_cmp; $cmp <= 1785; $cmp+=15) {

=pod

Define inbound files for creating original dispersion images

=cut
	#SET FILE STRUCTURE FOR MAKING ORIGINAL DISPERSION CURVES

		$file_in[1]			= 'G_cmp'.$cmp;
		$sufile_in[1]			= $file_in[1].$suffix_su;
		$inbound[1]			=
$DATA_SEISMIC_SU.'/cmp'.$cmp.'/'.$sufile_in[1];
		$file_out[1]			= 'G_cmp_'.$cmp.'_phvel'; #Changed from using
$file_in
		#output file
		$outbound[1]			= $DATA_SEISMIC_SU.'/disp/'.$file_out[1].'.su';

	#MAKE ORIGINAL DISPERSION CURVES TO $DATA../disp/

		$suchw		-> clear();
		$suchw		-> key1('cdp');
		$suchw		-> key2('tracl');
		$suchw[1] = $suchw->Step();

		@items =
($suwind[1],$in,$inbound[1],$to,$suphasevel[1],$to,$suamp[1],$to,$suchw[1],$out,$outbound[1
],$go);
		$flow[1]	= $run -> modules(\@items);
```

```
                $run->flow(\$flow[1]); #Execute Original Trace
                print $flow[1]."\n";

                }; #End for loop of orignial dispersions
        } #Close off else

################################################################################
#AFTER ORIGINAL FILE TEST: CREATE STACKS
################################################################################
#PROMPT OLD VS NEW PICKS

my $response;
my $start_cmp;

$response = 'n' ;
  print("View/Modify old (o) pick files or create new (n) ones \n");
  print("\%");
  $response = <STDIN>;
  chomp ($response);

 if ($response ne 'n') {

        if ($response eq 'o') {
         print("\n Set cmp to start with\n");
        } #close $response eq 'o'
        else {
         print("Sorry, command not recognized.\n");
         print("Please enter the cmp you would like to view\n");
        } #close else

 print("cmp=");

 $start_cmp = <STDIN>;
 chomp ($start_cmp);
 $response = 'n' ;
 chomp ($response);

} #close $response ne 'n'

 else { $start_cmp = -675

} #close else $start_cmp

print("\nThe starting cmp will be $start_cmp\n");
```

```
#SET WHILE, FOR LOOP TO CREATE FILES

        #FOR LOOP TO ADJUST WHICH CMPS ARE VIEWED

  while (($response eq 'n') || ($response eq 'q')) {
#start -675 end 1785
    for ( my $cmp=$start_cmp; $cmp <= 1785; $cmp+=30) {
          my $stackcmp=$cmp+15;

          if ($response eq 'n') {

#DEFINE FILE STRUCTURE FOR STACKING
  $file_in[1]                   = 'G_cmp_'.$cmp.'_phvel';
  $sufile_in[1]                 = $file_in[1].$suffix_su;
  $inbound[1]                   = $DATA_SEISMIC_SU.'/disp/'.$sufile_in[1];
  $file_in[2]                   = 'G_cmp_'.$stackcmp.'_phvel';
  $sufile_in[2]                 = $file_in[2].$suffix_su;
  $inbound[2]                   = $DATA_SEISMIC_SU.'/disp/'.$sufile_in[2];

  $temp[1]                      = $TEMP_DATA_SEISMIC_SU.'1.su';
  $temp[2]                      = $TEMP_DATA_SEISMIC_SU.'2.su';
  $tempout[1]                   = $TEMP_DATA_SEISMIC_SU.'out.su';

  $file_out[1]                  = $file_in[1].'_phvel';
  $file_out[2]                  = 'G_cmp_'.$cmp.'_'.$stackcmp.'_phvel'; #Changed from using
$file_in
#output file
  $outbound[1]                  = $DATA_SEISMIC_SU.'/dispstack/'.$file_out[2].'.su';
  $outpicks[1]                  = $DATA_SEISMIC_SU.'/'.$file_out[1].'_picks';
#output pick file into subset picks directory
#WARNING, PICK DIRECTORY MAY NOT EXIST
  $outpicks[2]                  = $DATA_SEISMIC_SU.'/dispstack/picks/'.$file_out[2].'_picks';
  $outpicks[3]                  =
$DATA_SEISMIC_SU.'/dispstack/picks/'.$file_out[2].'_newpicks';

#CREATE STACKABLE TEMP FILES
  $sushw                -> clear();
  $sushw                -> key('offset');
  $sushw                -> a(1);
  $sushw[1] = $sushw->Step();

  $sushw                -> clear();
  $sushw                -> key('offset');
  $sushw                -> a(2);
  $sushw[2] = $sushw->Step();
```

```
        system($sushw[1].$in.$inbound[1].$out.$temp[1]);
#       print($sushw[1].$in.$inbound[1].$out.$temp[1]."\n");

        system($sushw[2].$in.$inbound[2].$out.$temp[2]);
#       print($sushw[2].$in.$inbound[2].$out.$temp[2]."\n");

        system("cat $temp[1] $temp[2] $out $tempout[1]");
#       print ("cat $temp[1] $temp[2] $out $tempout[1]\n");

#SET PARAMETERS
 #SUSORT PARAMETERS
 $susort        ->clear();
 $susort        ->key1('cdp');
 $susort        ->key2('offset');
 $susort[1] = $susort->Step();

 #SUSTACK PARAMETERS
 $sustack       ->clear();
 $sustack       ->key('cdp');
 $sustack[1] = $sustack->Step();

=pod

 6. Set suximage parameters for the input
        traces that will be used.  This is a
        viewing of the CMPCC gather.

=cut

 #Input data Image
 $suxwigb-> clear();
 $suxwigb-> title($file_in[1]);
 $suxwigb-> xlabel("Offset");
 $suxwigb-> ylabel("TWTT_s");
 $suxwigb-> box_width(800);
 $suxwigb-> box_height(700);
 $suxwigb-> box_X0(0);
 $suxwigb-> box_Y0(0);
 $suxwigb-> windowtitle("Original_Data");
 $suxwigb[2]  = $suxwigb->Step();



=pod

 8. Set Filtering Parameters
```

```
=cut

 $sufilter-> clear();
 $sufilter-> freq("0,60,80,300");
 $sufilter-> amplitude("1,1,0.5,0");
 $sufilter[1]  =  $sufilter->Step();

=pod

 9. Add Gain to traces
        Primarily used for the view of the
        CMPCC gather.

=cut


 $sugain         -> clear();
 $sugain         -> pbal($on);
# $sugain        -> width(.1);
 $sugain[1]   =    $sugain->Step();

my $newcnt = 30;

 if (-e $outpicks[2]) {


        my $cnt;
        open(FH,$outpicks[2]) or die "open old pick file failed";
        $cnt++ while <FH>;
        close FH;
        print "\nOld pick file found with $cnt picks\n";
        #COUNTING FOR VIEWING NEW PICKS DOESNT WORK
        #NEED TO REARRANGE FLOW AND SUXIMAGE PARAMATERS


#VIEW DISPERSION WITH OLD PICKS
 $suximage-> clear();
 $suximage-> title($file_out[2]);
 $suximage-> xlabel("Phase_Velocity_dm/s");
 $suximage-> ylabel("Frequency_Hz");
 $suximage-> box_width(700);
 $suximage-> box_height(600);
 $suximage-> cmap("hsv6");
 $suximage-> box_X0(0);
 $suximage-> box_Y0(0);
```

```
 $suximage-> legend($on);
 $suximage-> curvefile($outpicks[2]);
 $suximage-> npair($cnt);
 $suximage-> curvecolor("black");
 $suximage-> windowtitle("Phase_Velocity_Dispersion_Map_NoPicks");
 $suximage[4]  = $suximage->Step();

#MAKE PICKS
 $suximage-> clear();
 $suximage-> title($file_out[2]);
 $suximage-> xlabel("Phase_Velocity_dm/s");
 $suximage-> ylabel("Frequency_Hz");
 $suximage-> box_width(700);
 $suximage-> box_height(600);
 $suximage-> cmap("hsv6");
 $suximage-> box_X0(0);
 $suximage-> box_Y0(0);
 $suximage-> legend($on);
 $suximage-> picks($outpicks[2]);
 $suximage-> curvefile($outpicks[2]);
 $suximage-> npair($cnt);
 $suximage-> curvecolor("black");
 $suximage-> windowtitle("Phase_Velocity_Dispersion_Map_Picks");
 $suximage[5]  = $suximage->Step();

#VIEW CREATED PICKS
 $suximage-> clear();
 $suximage-> title($file_out[2]);
 $suximage-> xlabel("Phase_Velocity_dm/s");
 $suximage-> ylabel("Frequency_Hz");
 $suximage-> box_width(700);
 $suximage-> box_height(600);
 $suximage-> cmap("hsv6");
 $suximage-> box_X0(0);
 $suximage-> box_Y0(0);
 $suximage-> legend($on);
 $suximage-> curvefile($outpicks[2]);
 $suximage-> npair($newcnt);
 $suximage-> curvecolor("black");
 $suximage-> windowtitle("Phase_Velocity_Dispersion_Map_NewPicks");
 $suximage[6]  = $suximage->Step();

 } #close if (-e $outpicks[1])

 else { print "\nNo old picks found for cmp=$cmp"."_$stackcmp!\n";
```

```
#VIEW DISPERSION (NO OLD PICKS)
 $suximage-> clear();
 $suximage-> title($file_out[2]);
 $suximage-> xlabel("Phase_Velocity_dm/s");
 $suximage-> ylabel("Frequency_Hz");
 $suximage-> box_width(700);
 $suximage-> box_height(600);
 $suximage-> cmap("hsv2");
 $suximage-> box_X0(0);
 $suximage-> box_Y0(0);
 $suximage-> legend($on);
 $suximage-> windowtitle("Phase_Velocity_Dispersion_Map_NoPicks");
 $suximage[4]  = $suximage->Step();

#MAKE PICKS
 $suximage-> clear();
 $suximage-> title($file_out[2]);
 $suximage-> xlabel("Phase_Velocity_dm/s");
 $suximage-> ylabel("Frequency_Hz");
 $suximage-> box_width(700);
 $suximage-> box_height(600);
 $suximage-> cmap("hsv6");
 $suximage-> box_X0(0);
 $suximage-> box_Y0(0);
 $suximage-> legend($on);
 $suximage-> picks($outpicks[2]);
 $suximage-> windowtitle("Phase_Velocity_Dispersion_Map_Picks");
 $suximage[5]  = $suximage->Step();

#VIEW CREATED PICKS
 $suximage-> clear();
 $suximage-> title($file_out[2]);
 $suximage-> xlabel("Phase_Velocity_dm/s");
 $suximage-> ylabel("Frequency_Hz");
 $suximage-> box_width(700);
 $suximage-> box_height(600);
 $suximage-> cmap("hsv6");
 $suximage-> box_X0(0);
 $suximage-> box_Y0(0);
 $suximage-> legend($on);
 $suximage-> curvefile($outpicks[2]);
 $suximage-> npair($newcnt);
 $suximage-> curvecolor("black");
 $suximage-> windowtitle("Phase_Velocity_Dispersion_Map_NewPicks");
 $suximage[6]  = $suximage->Step();
```

```
} #close else

=pod

 11B. Set suximage parameters
 These default settings will generate an image of
 the dispersion curve for viewing

=cut

 #For Original Dispersion Curve
 $suximage-> clear();
 $suximage-> title($cmp.$temp[1]);
 $suximage-> xlabel("Phase_Velocity");
 $suximage-> ylabel("Frequency");
 $suximage-> box_width(700);
 $suximage-> box_height(600);
 $suximage-> cmap("hsv2");
 $suximage-> box_X0(0);
 $suximage-> box_Y0(0);
 $suximage-> legend($on);
 $suximage-> windowtitle("Phase_Velocity_Dispersion_Map");
 $suximage[1]  = $suximage->Step();

 #For actual data output
 $suximage-> clear();
 $suximage-> title($stackcmp.$temp[2]);
 $suximage-> xlabel("Phase_Velocity");
 $suximage-> ylabel("Frequency");
 $suximage-> box_width(700);
 $suximage-> box_height(600);
 $suximage-> cmap("hsv2");
 $suximage-> box_X0(0);
 $suximage-> box_Y0(0);
 $suximage-> legend($on);
 $suximage-> windowtitle("Phase_Velocity_Dispersion_Map");
 $suximage[2]  = $suximage->Step();

 #For gained/filtered data output
 $suximage-> clear();
 $suximage-> title("filtered_gained_".$file_out[1]);
 $suximage-> xlabel("Phase_Velocity_\(dm/s\)");
 $suximage-> ylabel("Frequency");
 $suximage-> box_width(700);
 $suximage-> box_height(600);
 $suximage-> cmap("hsv6");
```

```
 $suximage-> box_X0(0);
 $suximage-> box_Y0(0);
 $suximage-> windowtitle("Phase_Velocity_Dispersion_Map");
 $suximage[3]  = $suximage->Step();


#DEFINE FLOWS TO RUN

=pod

 12. Define Flows

=cut

#Create a window to pick values for cmps, Windowed Data
 @items = ($susort[1],$in,$tempout[1],$to,$sustack[1],$to,$suximage[4],$go);
  $flow[1]       = $run -> modules(\@items);

#Phasevel dispersion image w/o filter or gain, Windowed, NO PICKS
  @items = ($susort[1],$in,$tempout[1],$to,$sustack[1],$to,$suximage[5]);
  $flow[2]       = $run -> modules(\@items);
#,$to,$suflip[1]

#Phasevel dispersion image w/o filter or gain, Windowed, VIEW PICKS
  @items = ($susort[1],$in,$tempout[1],$to,$sustack[1],$to,$suximage[6],$go);
  $flow[3]       = $run -> modules(\@items);

#Phasevel dispersion image w/o filter or gain, Not Windowed
#  @items = ($suphasevel[1],$in,$inbound[1],$to,,$suamp[1],$to,$suximage[4]);
#  $flow[4]      = $run -> modules(\@items);
#,$to,$suflip[1]

#Create outbound file
 @items = ($susort[1],$in,$tempout[1],$to,$sustack[1],$out,$outbound[1],$go);
 $flow[5]       = $run -> modules(\@items);

#Produce Original Dispersion Curves
 @items = ($suximage[1],$in,$temp[1],$go);
 $flow[6]       = $run -> modules(\@items);

 @items = ($suximage[2],$in,$temp[2],$go);
 $flow[7]       = $run -> modules(\@items);

=pod

 13. Run Flows
```

```
=cut

#$run->flow(\$flow[6]); #Execute Original Disp Image
# print $flow[6]."\n";

#$run->flow(\$flow[7]); #Execute Original Disp Image
# print $flow[7]."\n";

#CONTINUATION PROMPTS

#Run Real Stuff
# View Dispersion Curve Windowed
 print $flow[1]."\n";
 $run->flow(\$flow[1]);
 print ("\n Would you like to make new picks along the dispersion curve? \n");
 print ("Your picks will be saved to $outpicks[2]\n");
 print ("\n Yes (y) or No (n) \n");
 print ("\%");
 my $pickq;
 $pickq=<STDIN>;
 chomp ($pickq);

if ($pickq eq 'y') {

  if ( -e $DATA_SEISMIC_SU.'/dispstack/picks/') {
          #Do Nothing
          } #Close if
  else {
          print "Directory $DATA_SEISMIC_SU/dispstack/picks not found";

          make_path($DATA_SEISMIC_SU.'/dispstack/picks', {
                  verbose=> 1,
                  });
          } #Close else

#Make Picks for Windowed Dispersion Curve
 print $flow[2]."\n";
 print ("\n Press s in xwindow to save point of dispersion curve \n");
 print ("\n Don't Press ctrl c to close the window \n");
 $run->flow(\$flow[2]); #Execute Dispersion Curve Window
 print ("\n Would you like to see your new picks?\n");
 print ("Yes (y) or No (n)\n\%");
 my $viewq;
 $viewq=<STDIN>;
 chomp ($viewq);
```

```
  if ( $viewq eq 'y') {
   $run->flow(\$flow[3]);
   } #close if ( $viewq eq 'y')
  else {
   print "\nI'll take that as a no\n";
  } #close else
 } #close if ($pickq eq 'y')
else {
 print "\nI'll take that as a no\n";
 }

# $run->flow(\$flow[3]);
# print $flow[3]."\n";

#Dispersion Curve not Windowed
# print $flow[4]."\n";
# print ("\n Press s in xwindow to save point of dispersion curve \n");
# print ("\n Press ctrl c to close the window \n");
# $run->flow(\$flow[4]);

=pod

14. Select which cmp to view next
        Or exit

=cut

my $response2; #Set Options for what to do
my $next_cmp = $cmp+30;
print(" \n Continue with next cmp=$next_cmp... (n) \n");
print(" Choose different cmp?... (d)\n");
print(" Exit?.... (q)\n ");
print("\%");
$response2=<STDIN>;
chomp ($response2);

        my $quitkey='a'; #Set option to carry through or quit
        my $diffcmp; #use to jump to new cmp
        while (($quitkey eq 'a')||($quitkey eq 'z')) {

         if ($quitkey eq 'a') {             #Enter Exectuables
#JUMP TO NEW CMP
                if ($response2 eq 'd') {
                        print("\nWhich CMP would you like to jump to?\n");
                        print("cmp=");
                        $diffcmp=<STDIN>;
```

```
                chomp ($diffcmp);
                $cmp=$diffcmp-30;
                $response='n';
                $quitkey='z';
                chomp($quitkey);
                print ($quitkey);
                last;
        } #close if ($response2 eq 'd')

#JUMP TO NEXT CMP
        if ($response2 eq 'n') {
                $response='n';
                $quitkey='z';
                chomp($quitkey);
        } #close if ($response2 eq 'n')

#CONFIRM TO QUIT
        else {
                my $exitkey;
                print("Are you sure you want to quit?... (0)\n");
                print("Remain... (1)\%");
                $exitkey=<STDIN>;
                chomp($exitkey);
                if ($exitkey ne '1') {
                        $response='q';
                        $quitkey='z';
                        } #close if
                else {
                        print(" \n Continue with next cmp=$next_cmp... (n) \n");
                        print(" Choose different cmp?... (d)\n");
                        print(" Exit?.... (q)\n ");
                        print("\%");
                        $response2=<STDIN>;
                        chomp ($response2);
                        }       #close nested else
                } #close else
         } #close if quitkey=1
         elsif ($quitkey eq 'z') {

        last;
         } #close else quitkey

        } #close while $quitkey

    } #close if $response='n'
```

```
            elsif ($response eq 'q') {

print("Closing Program\n\n");
unlink $temp[1]; #delete file from system
unlink $temp[2]; #delete file from system
unlink $tempout[1]; #delete file from system
exit;

            } #close elsif $response='q'
          } # close for
  } # Close While



} #if $qstack eq 'y'


################################################################################
#FINISH STACKED PROGRAM
#BEGIN ORIGNIAL PROGRAM
################################################################################
else { #Run Original Code

print "I'll take that as a no\n\n";

=pod

Output a question to ask if new pick
files should be create or old ones changed.

=cut
my $response;
my $start_cmp;

$response = 'n' ;
  print("View/Modify old (o) pick files or create new (n) ones \n");
  print("\%");
  $response = <STDIN>;
  chomp ($response);

 if ($response ne 'n') {

          if ($response eq 'o') {
           print("\n Set cmp to start with\n");
```

```
        } #close $response eq 'o'
        else {
         print("Sorry, command not recognized.\n");
         print("Please enter the cmp you would like to view\n");
        } #close else

 print("cmp=");

 $start_cmp = <STDIN>;
 chomp ($start_cmp);
 $response = 'n' ;
 chomp ($response);

} #close $response ne 'n'

 else { $start_cmp = -675

} #close else $start_cmp

print("\nThe starting cmp will be $start_cmp\n");

=pod

 4. Define the file name of the shot record to be used to
    compute a multi-mode phase velocity dispersion map

   IMPORTANT
  ->Please note that output files will be amped
  ->They will not be complex frequency data!!

=cut

#Set cmp spacing
my $cmpspacing=15;

#FOR LOOP TO ADJUST WHICH CMPS ARE VIEWED

  while (($response eq 'n') || ($response eq 'q')) {
#start -675 end 1785
    for ( my $cmp=$start_cmp; $cmp <= 1785; $cmp+=15) {

          if ($response eq 'n') {



=pod
```

Define inbound files

=cut

```
  $file_in[1]                   = 'G_cmp'.$cmp;
  $sufile_in[1]                 = $file_in[1].$suffix_su;
  $inbound[1]                   = $DATA_SEISMIC_SU.'/cmp'.$cmp.'/'.$sufile_in[1];

  $file_out[1]                  = $file_in[1].'_phvel';
  $file_out[2]                  = 'G_cmp_'.$cmp.'_phvel'; #Changed from using $file_in
#output file
  $outbound[1]                  = $DATA_SEISMIC_SU.'/disp/'.$file_out[1].'.su';
#output pick file into data directory
  $outpicks[1]                  = $DATA_SEISMIC_SU.'/'.$file_out[1].'_picks';
#output pick file into subset picks directory
#WARNING, PICK DIRECTORY MAY NOT EXIST
  $outpicks[2]                  = $DATA_SEISMIC_SU.'/picks/'.$file_out[2].'_picks';
  $outpicks[3]                  = $DATA_SEISMIC_SU.'/picks/'.$file_out[2].'_newpicks';

# $file_in[2] = eval ($outbound[2]);
# print ($file_in[2]);
```

=pod

6. Set suximage parameters for the input
   traces that will be used. This is a
   viewing of the CMPCC gather.

=cut

```
 #Input data Image
 $suxwigb-> clear();
 $suxwigb-> title($file_in[1]);
 $suxwigb-> xlabel("Offset");
 $suxwigb-> ylabel("TWTT_s");
 $suxwigb-> box_width(800);
 $suxwigb-> box_height(700);
 $suxwigb-> box_X0(0);
 $suxwigb-> box_Y0(0);
 $suxwigb-> windowtitle("Original_Data");
 $suxwigb[2]  = $suxwigb->Step();
```

```
=pod

 8. Set Filtering Parameters

=cut

 $sufilter-> clear();
 $sufilter-> freq("0,60,80,300");
 $sufilter-> amplitude("1,1,0.5,0");
 $sufilter[1]  =  $sufilter->Step();

=pod

 9. Add Gain to traces
        Primarily used for the view of the
        CMPCC gather.

=cut


 $sugain         -> clear();
 $sugain         -> pbal($on);
# $sugain        -> width(.1);
 $sugain[1]   =    $sugain->Step();

=pod

 11. Create Windows for picking and viewing

=cut

=pod

 11A. Check if old picks exist

=cut

my $newcnt = 30;

 if (-e $outpicks[1]) {


        my $cnt;
        open(FH,$outpicks[1]) or die "open old pick file failed";
        $cnt++ while <FH>;
```

```
        close FH;
        print "\nOld pick file found with $cnt picks\n";
        #COUNTING FOR VIEWING NEW PICKS DOESNT WORK
        #NEED TO REARRANGE FLOW AND SUXIMAGE PARAMATERS


#VIEW DISPERSION WITH OLD PICKS
 $suximage-> clear();
 $suximage-> title($file_out[1]);
 $suximage-> xlabel("Phase_Velocity_dm/s");
 $suximage-> ylabel("Frequency_Hz");
 $suximage-> box_width(700);
 $suximage-> box_height(600);
 $suximage-> cmap("hsv6");
 $suximage-> box_X0(0);
 $suximage-> box_Y0(0);
 $suximage-> legend($on);
 $suximage-> curvefile($outpicks[1]);
 $suximage-> npair($cnt);
 $suximage-> curvecolor("black");
 $suximage-> windowtitle("Phase_Velocity_Dispersion_Map_NoPicks");
 $suximage[4]  = $suximage->Step();

#MAKE PICKS
 $suximage-> clear();
 $suximage-> title($file_out[1]);
 $suximage-> xlabel("Phase_Velocity_dm/s");
 $suximage-> ylabel("Frequency_Hz");
 $suximage-> box_width(700);
 $suximage-> box_height(600);
 $suximage-> cmap("hsv6");
 $suximage-> box_X0(0);
 $suximage-> box_Y0(0);
 $suximage-> legend($on);
 $suximage-> picks($outpicks[2]);
 $suximage-> curvefile($outpicks[1]);
 $suximage-> npair($cnt);
 $suximage-> curvecolor("black");
 $suximage-> windowtitle("Phase_Velocity_Dispersion_Map_Picks");
 $suximage[5]  = $suximage->Step();

#VIEW CREATED PICKS
 $suximage-> clear();
 $suximage-> title($file_out[1]);
 $suximage-> xlabel("Phase_Velocity_dm/s");
 $suximage-> ylabel("Frequency_Hz");
```

```
 $suximage-> box_width(700);
 $suximage-> box_height(600);
 $suximage-> cmap("hsv6");
 $suximage-> box_X0(0);
 $suximage-> box_Y0(0);
 $suximage-> legend($on);
 $suximage-> curvefile($outpicks[2]);
 $suximage-> npair($newcnt);
 $suximage-> curvecolor("black");
 $suximage-> windowtitle("Phase_Velocity_Dispersion_Map_NewPicks");
 $suximage[6]  = $suximage->Step();

 } #close if (-e $outpicks[1])

 else { print "\nNo old picks found for cmp=$cmp!\n";

#VIEW DISPERSION (NO OLD PICKS)
 $suximage-> clear();
 $suximage-> title($file_out[1]);
 $suximage-> xlabel("Phase_Velocity_dm/s");
 $suximage-> ylabel("Frequency_Hz");
 $suximage-> box_width(700);
 $suximage-> box_height(600);
 $suximage-> cmap("hsv6");
 $suximage-> box_X0(0);
 $suximage-> box_Y0(0);
 $suximage-> legend($on);
 $suximage-> windowtitle("Phase_Velocity_Dispersion_Map_NoPicks");
 $suximage[4]  = $suximage->Step();

#MAKE PICKS
 $suximage-> clear();
 $suximage-> title($file_out[1]);
 $suximage-> xlabel("Phase_Velocity_dm/s");
 $suximage-> ylabel("Frequency_Hz");
 $suximage-> box_width(700);
 $suximage-> box_height(600);
 $suximage-> cmap("hsv6");
 $suximage-> box_X0(0);
 $suximage-> box_Y0(0);
 $suximage-> legend($on);
 $suximage-> picks($outpicks[2]);
 $suximage-> windowtitle("Phase_Velocity_Dispersion_Map_Picks");
 $suximage[5]  = $suximage->Step();

#VIEW CREATED PICKS
```

```
$suximage-> clear();
$suximage-> title($file_out[1]);
$suximage-> xlabel("Phase_Velocity_dm/s");
$suximage-> ylabel("Frequency_Hz");
$suximage-> box_width(700);
$suximage-> box_height(600);
$suximage-> cmap("hsv6");
$suximage-> box_X0(0);
$suximage-> box_Y0(0);
$suximage-> legend($on);
$suximage-> curvefile($outpicks[2]);
$suximage-> npair($newcnt);
$suximage-> curvecolor("black");
$suximage-> windowtitle("Phase_Velocity_Dispersion_Map_NewPicks");
$suximage[6]  = $suximage->Step();

} #close else

=pod

 11B. Set suximage parameters
 These default settings will generate an image of
 the dispersion curve for viewing

=cut

 #For actual data output
 $suximage-> clear();
 $suximage-> title($file_in[1]);
 $suximage-> xlabel("Phase_Velocity");
 $suximage-> ylabel("Frequency");
 $suximage-> box_width(700);
 $suximage-> box_height(600);
 $suximage-> cmap("hsv2");
 $suximage-> box_X0(0);
 $suximage-> box_Y0(0);
 $suximage-> legend($on);
 $suximage-> windowtitle("Phase_Velocity_Dispersion_Map");
 $suximage[1]  = $suximage->Step();

 #For gained/filtered data output
 $suximage-> clear();
 $suximage-> title("filtered_gained_".$file_out[1]);
 $suximage-> xlabel("Phase_Velocity_\(dm/s\)");
 $suximage-> ylabel("Frequency");
 $suximage-> box_width(700);
```

```
 $suximage-> box_height(600);
 $suximage-> cmap("hsv2");
 $suximage-> box_X0(0);
 $suximage-> box_Y0(0);
 $suximage-> windowtitle("Phase_Velocity_Dispersion_Map");
 $suximage[3]  = $suximage->Step();

=pod

 12. Define Flows

=cut

#Produce phasevel dispersion image for viewing (Not Pretty)
# - Reestablish flow Number if want to use again
# @items =
($sufilter[1],$in,$inbound[1],$to,$sugain[1],$to,$suphasevel[1],$to,$suamp[1],$to,$suximage[3]
,$go);
# $flow[]        = $run -> modules(\@items);

#Create a window to pick values for cmps, Windowed Data
 @items =
($suwind[1],$in,$inbound[1],$to,$suphasevel[1],$to,$suamp[1],$to,$suximage[4],$go);
  $flow[1]       = $run -> modules(\@items);

#Phasevel dispersion image w/o filter or gain, Windowed, NO PICKS
  @items = ($suwind[1],$in,$inbound[1],$to,$suphasevel[1],$to,$suamp[1],$to,$suximage[5]);
  $flow[2]       = $run -> modules(\@items);
#,$to,$suflip[1]

#Phasevel dispersion image w/o filter or gain, Windowed, VIEW PICKS
  @items =
($suwind[1],$in,$inbound[1],$to,$suphasevel[1],$to,$suamp[1],$to,$suximage[6],$go);
  $flow[3]       = $run -> modules(\@items);

#Phasevel dispersion image w/o filter or gain, Not Windowed
#  @items = ($suphasevel[1],$in,$inbound[1],$to,,$suamp[1],$to,$suximage[4]);
#  $flow[4]      = $run -> modules(\@items);
#,$to,$suflip[1]

#Create outbound file
 @items = ($suphasevel[1],$in,$inbound[1],$to,$suamp[1],$out,$outbound[1],$go);
 $flow[5]       = $run -> modules(\@items);

#Produce image of input shot record
 @items = ($sugain[1],$in,$inbound[1],$to,$suxwigb[2],$go);
```

```
 $flow[6]        = $run -> modules(\@items);


=pod

 13. Run Flows

=cut

 $run->flow(\$flow[6]); #Execute Original Trace
 print $flow[6]."\n";

#Run Real Stuff
# View Dispersion Curve Windowed
 print $flow[1]."\n";
 $run->flow(\$flow[1]);
 print ("\n Would you like to make new picks along the dispersion curve? \n");
 print ("Your picks will be saved to $outpicks[2]\n");
 print ("\n Yes (y) or No (n) \n");
 print ("\%");
 my $pickq;
 $pickq=<STDIN>;
 chomp ($pickq);

if ($pickq eq 'y') {

#Make Picks for Windowed Dispersion Curve
 print $flow[2]."\n";
 print ("\n Press s in xwindow to save point of dispersion curve \n");
 print ("\n Don't Press ctrl c to close the window \n");
 $run->flow(\$flow[2]); #Execute Dispersion Curve Window
 print ("\n Would you like to see your new picks?\n");
 print ("Yes (y) or No (n)\n\%");
 my $viewq;
 $viewq=<STDIN>;
 chomp ($viewq);
  if ( $viewq eq 'y') {
   $run->flow(\$flow[3]);
   } #close if ( $viewq eq 'y')
  else {
   print "\nI'll take that as a no\n";
  } #close else
 } #close if ($pickq eq 'y')
else {
 print "\nI'll take that as a no\n";
 }
```

```
# $run->flow(\$flow[3]);
# print $flow[3]."\n";

#Dispersion Curve not Windowed
# print $flow[4]."\n";
# print ("\n Press s in xwindow to save point of dispersion curve \n");
# print ("\n Press ctrl c to close the window \n");
# $run->flow(\$flow[4]);

=pod

14. Select which cmp to view next
        Or exit

=cut

my $response2; #Set Options for what to do
my $next_cmp = $cmp+15;
print(" \n Continue with next cmp=$next_cmp... (n) \n");
print(" Choose different cmp?... (d)\n");
print(" Exit?.... (q)\n ");
print("\%");
$response2=<STDIN>;
chomp ($response2);

        my $quitkey='a'; #Set option to carry through or quit
        my $diffcmp; #use to jump to new cmp
        while (($quitkey eq 'a')||($quitkey eq 'z')) {

         if ($quitkey eq 'a') {             #Enter Exectuables
#JUMP TO NEW CMP
                if ($response2 eq 'd') {
                        print("\nWhich CMP would you like to jump to?\n");
                        print("cmp=");
                        $diffcmp=<STDIN>;
                        chomp ($diffcmp);
                        $cmp=$diffcmp-15;
                        $response='n';
                        $quitkey='z';
                        chomp($quitkey);
                        print ($quitkey);
                        last;
                } #close if ($response2 eq 'd')

#JUMP TO NEXT CMP
```

```
                if ($response2 eq 'n') {
                        $response='n';
                        $quitkey='z';
                        chomp($quitkey);
                } #close if ($response2 eq 'n')

#CONFIRM TO QUIT
                else {
                        my $exitkey;
                        print("Are you sure you want to quit?... (0)\n");
                        print("Remain... (1)\%");
                        $exitkey=<STDIN>;
                        chomp($exitkey);
                        if ($exitkey ne '1') {
                                $response='q';
                                $quitkey='z';
                                } #close if
                        else {
                                print(" \n Continue with next cmp=$next_cmp... (n) \n");
                                print(" Choose different cmp?... (d)\n");
                                print(" Exit?.... (q)\n ");
                                print("\%");
                                $response2=<STDIN>;
                                chomp ($response2);
                                }       #close nested else
                        } #close else
                 } #close if quitkey=1
                 elsif ($quitkey eq 'z') {

                last;
                 } #close else quitkey

                } #close while $quitkey

           } #close if $response='n'


           elsif ($response eq 'q') {

print("Closing Program\n\n");
exit;

           } #close elsif $response='q'
         } # close for
  } # Close While
```

```
} #else original code
```

APPENDIX B: INVERSION CODE

The ASCII files containing the picks for the dispersion curve must be turned into target files that the inversion software, Dinver, can interpret. ASCII files are imported into Dinver and converted to a target file. The following steps in Dinver convert the files:

1) Select the "Targets" tab
2) Set Dispersion
3) Load ASCII file in Dispersion target window
4) Select appropriate domain for each "Type" column
5) Apply conversion factor to convert decimeter/s to m/s
6) Resample curve from the minimum pick to the maximum pick 25 times, scaling by frequency
7) Save as a target file

The resampling of the dispersion curve is necessary to gain a relatively consistent distribution of samples along the frequency axis. Scaling by frequency weights the sample points similarly across all CMPs. This allows the inversion to treat each experimental curve equally, without shifting the weighting between high and low frequencies based on the number of manual picks made. The newly saved target files are then ready for an automated inversion process.

Dispersion Curve Inversion—Xdinver.pl

Shear wave velocity inversions are conducted using a direct search process of the dispersion curves within a neighborhood algorithm. The neighborhood algorithm allows a full search through parameter space, and optimizes each tested dispersion curve to search for the smallest misfit to the original dispersion curve. The parameters searched are p-wave velocity, s-wave velocity, Poisson's ratio, and density. The code below automates the inversion process for the dispersion targets. Just as with the programs used in Appendix A, perl packages specifically written for use with the inversion process are used by these programs and are not contained in this appendix.

```
#!/usr/bin/perl

=pod

=head1 Documentation

=head2 Synopsis

        Program:        Xdinver.pl
        Purpose:        Inversion of Dispersion Curve
        Author:         Derek S. Goff
        Date:           May 1 2015
        Description:    Implements  suphasevel.pm
                        Inverts Dispersion Curve using
                        Geopsy's dinver program
                More information at http://www.geopsy.org
```

```
=head2 Uses

    Subroutines:
        manage_files_by
        System_Variables (for subroutines)

    Varibale Definitions:
        SeismicUnix (Seismic Unix modules)

=cut

 use Moose;
 use SeismicUnix qw ($in $out $on $go $to $suffix_ascii $off $suffix_su);
 use SU;
 use Dinver;
 use File::Path qw(make_path remove_tree);

 my $log                    = new message();
 my $run                    = new flow();
 my $dinver                 = new Dinver();

=pod

 2. Utilize zamin.lsu.edu directory navigation system

=cut

 my ($DATA_SEISMIC_SU) = System_Variables::DATA_SEISMIC_SU();
 my ($GEOPSY) = System_Variables::GEOPSY();


=pod

 Set Geopsy Directory File System

=cut

 my ($GEOPSY_PARAM)    = $GEOPSY.'param/';
 my ($GEOPSY_TARGET)   = $GEOPSY.'target/';
 my ($GEOPSY_ENV)      = $GEOPSY.'env/';
 my ($GEOPSY_REPORTS) = $GEOPSY.'reports/';

=pod

 Create Geopsy Directory system if it doesnt exist
```

```
=cut

if (-e $GEOPSY_PARAM) {#do nothing
}
else { make_path("$GEOPSY_PARAM", "$GEOPSY_TARGET", "$GEOPSY_ENV",
"$GEOPSY_REPORTS",
                { verbose => 1, mode => 0771 });
}

my (@flow, @items);
my (@dinver,@parameters);
my (@file_in, @target_in, @inbound, @file_out, @outbound);

my $t_suffix = '.target';
my $p_suffix = '.param';
my $r_suffix = '.report';
my $start_cmp = -495;


for ( my $cmp=$start_cmp; $cmp <= 1720; $cmp+=30) {
          my $stackcmp=$cmp+15;

        $file_in[1] = $GEOPSY_TARGET.$cmp.'_'.$stackcmp;
        $target_in[1] = $file_in[1].$t_suffix;
        $inbound[1] = $target_in[1];
        $parameters[1] = $GEOPSY_PARAM."5lay_rev".$p_suffix;
        $file_out[1] = $GEOPSY_REPORTS."5lay_rev_".$cmp.'_'.$stackcmp;
        $outbound[1] = $file_out[1].$r_suffix;
=pod

 Set Dispersion Curve Inversion options
 See Dinver.pm for more information

=cut

 $dinver        -> clear();
 $dinver        -> plug("DispersionCurve");
 $dinver        -> target($inbound[1]);
 $dinver        -> param($parameters[1]);
 $dinver        -> itmax("200"); # 0 iterations = Pure Monte Carlo
 $dinver        -> ns0("5000"); # Initial Models to create
 $dinver        -> ns("1000"); # Models per iteration
 $dinver        -> nr("500"); # Best Models to consider
 $dinver        -> output($outbound[1]);
# $dinver       -> force();
# $dinver       -> resume();
```

```
$dinver[1] = $dinver->Step();

print ($dinver[1]."\n");
system ($dinver[1]);
print ("\n\nMoving to next target\n");

} #close for loop
```

Extract Reports—Xgrepreport.pl

The reports generated by the inversion are used to create the 1D shear wave velocity profile for each CMP. The code below extracts the median profile of the best 1000 models generated of 205000 models, and produces the deviation of that model based on the range of velocities observed by the best 1000 models. The amount of models used is an estimate of how many models are needed to create a 10% misfit range from the best matching model. The median profile is extracted every 1 meter in depth. The extraction code is shown below:

```
!/usr/bin/perl

=pod

=head1 Documentation

=head2 Synopsis

        Program:        Xgreport.pl
        Purpose:        Extract Vs Profiles from inversion
        Author:         Derek S. Goff
        Date:           May 1 2015
        Description:    Implements  Gpdcreport.pm
                        Extracts information from geopsy .report files
                        using Geopsy's gpdcreport program
                    More information at http://www.geopsy.org

        Fully implement the following bash code into a perl program:
        gpdcreport /home/dereg/LondonAvenueCanal/seismics/geopsy/060112/Z/reports/5lay_-495_-480.report -gm -best 10 | gpprofile -vs -resample -d 25 -n 25 | grep -v "#" | awk ‘{print $2,$1}'|gphistogram -x-count 25 -mean

        Version 0.2 to use | gphistogram -x-count -x-min...

=head2 Uses

    Subroutines:
        manage_files_by
        System_Variables (for subroutines)

    Varibale Definitions:
```

```
        SeismicUnix (Seismic Unix modules)

=head2 Output Data

        col1: depth (m)
        col2: Vs (m/s)
        col3: Standard deviation (m/s)
        col4: ? Probably number of samples in bin (like fold)
        col5: cmp

=cut

 use Moose;
 use SeismicUnix qw ($in $out $on $go $to $suffix_ascii $off $suffix_su);
 use SU;
 use Gpdcreport;
 use Gpprofile;
 use Gphistogram;
 use Gpviewdcreport;
 use File::Path qw(make_path remove_tree);
 use Data::Dumper;

 my $log                    = new message();
 my $run                    = new flow();
 my $gpdc                   = new Gpdcreport();
 my $gpprof                 = new Gpprofile();
 my $gphist                 = new Gphistogram();
 my $gpview                 = new Gpviewdcreport();
=pod

 2. Utilize zamin.lsu.edu directory navigation system

=cut

 my ($DATA_SEISMIC_SU) = System_Variables::DATA_SEISMIC_SU();
 my ($GEOPSY) = System_Variables::GEOPSY();


=pod

 Set Geopsy Directory File System

=cut

 my ($GEOPSY_PARAM)    = $GEOPSY.'param/';
 my ($GEOPSY_TARGET)   = $GEOPSY.'target/';
```

```
 my ($GEOPSY_ENV)          = $GEOPSY.'env/';
 my ($GEOPSY_REPORTS) = $GEOPSY.'reports/';


my (@flow, @items);
my (@gpdc,@parameters, @report_in, @temp_out);
my (@file_in, @target_in, @inbound, @file_out, @outbound);
my (@gpprof, @gphist, @gpview);

my $t_suffix = '.target';
my $p_suffix = '.param';
my $r_suffix = '.report';
my $start_cmp = -495;


 print("\n You may need to clear the output profile \n");

#1720
for ( my $cmp=$start_cmp; $cmp <= 1720; $cmp+=30) {
           my $stackcmp=$cmp+15;

          $file_in[1] = $GEOPSY_REPORTS.'5lay_rev_'.$cmp.'_'.$stackcmp;
                    #Set the input file name
          $report_in[1] = $file_in[1].$r_suffix;
          $inbound[1] = $report_in[1];
#         $parameters[1] = $GEOPSY_PARAM."5lay".$p_suffix;
          $temp_out[1] = $GEOPSY."\.temp_prof";
          $temp_out[2] = $GEOPSY."\.temp_prof2";
          $file_out[1] = $GEOPSY."New_Profile_5lay_rev_best1000_median_highres.txt";
          $outbound[1] = $file_out[1].$r_suffix;


=pod

Use this section to define several common variables
1)Number of models to use
2)What depth of investigation to look at
3)How often to sample along the profile according to depth

=cut

 my $models            = "1000"; # Number of models to use from report
 my $depth             = "25";   # Depth of investigation for the bins
 my $depth_interval    = ".5";   # Sample interval you would like to use in meters
 my $start_depth       = "0";  #Depth to start profile at
 my $grid_population = "25";   # Pertains to number of samples in each bin
```

```
#############################################################
 my $x_int      = (($depth/$depth_interval)+(1-($start_depth/$depth_interval)));
 my $xk_limit = ($x_int-1);
#my $x_int      = (($depth/$depth_interval));
#my $xk_limit= ($x_int-1);

$gpdc            -> clear();
$gpdc            -> gm();
$gpdc            -> best($models);
$gpdc            -> file($inbound[1]);
$gpdc[1] = $gpdc->Step();

$gpprof                  ->clear();
$gpprof                  ->vs();
$gpprof                  ->resample();
$gpprof                  ->depth($depth);
$gpprof                  ->samples($grid_population); #Grid Population (number each bin)
$gpprof[1] = $gpprof->Step();

$gphist          ->clear();
$gphist          ->xcount($x_int);
$gphist          ->xmin($start_depth);
$gphist          ->median(); # mean() = mean ; median() = median
$gphist[1] = $gphist->Step();


 @items = ($gpdc[1],$to,$gpprof[1],$to,"grep -v \"#\" $to awk \{print
\$2,\$1}\'",$to,$gphist[1],"$to grep -v \"#\"",$out,$temp_out[1]);
  $flow[1]       = $run -> modules(\@items);

 $run->flow(\$flow[1]);
# print $flow[1]."\n";

=pod

Create an array from the temp file
Append the cmp number onto the array
Create new file that is appended with each profile

=cut



 #Create an array of arrays to handle the profile
 my @aoa;
 for my $i (0..$xk_limit) {
```

```
        open my $FH, "<" ,"$temp_out[1]" or die "Couldn't open file";
        while (<$FH>) {
                chomp $_;
                push @aoa, [ split(' ')];
        }
        close $FH;
        #Create new column populated by the cmp of the profile
        push @{ $aoa[$i] }, "$cmp";
 } # close for my $i

 #Output the array of array profile to a text file
 open my $OUT, ">>", "$file_out[1]" or die "Couldn't write file";
        for my $j (0..$xk_limit) {
          for my $k (0..4) {
        print $OUT " $aoa[$j][$k]";
          } #$k
        print $OUT "\n";
        } #$j
        close $OUT;


} # close for

print ("$file_out[1] \n");
```

VITA

Derek S. Goff, a native of Texas, graduated from Durango High School in Colorado. His love for the outdoors kept him in Colorado, where he graduated from the University of Colorado Boulder in 2012 with a Bachelor's in Geology and a minor in physics. Desiring to further his understanding of geology and physics, Derek attended Louisiana State University in the Department of Geology & Geophysics. Upon completion of his degree requirements, Derek will go to work for Houston Energy.